Identification and functional characterization of the E2-conjugating enzyme UBE2QL1 in endolysosomal damage response

Inaugural-Dissertation

zur

Erlangung des Doktorgrades

Dr. rer. nat.

Der Fakultät für

Biologie

an der

Universität Duisburg-Essen

vorgelegt von

Lisa Körver

aus Bonn

März 2021

Die der vorliegenden Arbeit zugrunde liegenden Experimente wurden in der Abteilung für Molekularbiologie I am Zentrum für Medizinische Biotechnologie der Universität Duisburg-Essen durchgeführt.

1. Gutachter: Herr Prof. Dr. Hemmo Meyer
2. Gutachter: Frau Prof. Dr. Perihan Nalbant
3. Gutachter: Herr Prof. Dr. David Teis, Universität Innsbruck
Vorsitzende des Prüfungsausschusses: Frau Prof. Dr. Shirley Knauer

Tag der mündlichen Prüfung: 10. Juni 2021

DOI: 10.17185/duepublico/81246
URN: urn:nbn:de:hbz:465-20231130-113737-8

Table of contents

List of figures

List of tables

Summary

Lysosomes represent the cell's most important degradative organelles and take over essential functions in sensing the nutrient status. Damaging lysosomal membranes for example by oxidative stress, chemicals or invading pathogens, leads to lysosomal membrane permeabilization (LMP) with fatal consequences for the cells. The cell counteracts this stress situation by the so-called endolysosomal damage response (ELDR) with the ultimate goal to clear damaged lysosomes by autophagy (also called lysophagy).

One hallmark of this response is the extensive ubiquitination of lysosomal membrane proteins with K48 and K63-linked polyubiquitin chains. Among the many critical elements of ELDR, the ubiquitin-directed AAA^+-ATPase p97 stands out because it is, together with a specified set of co-factors, recruited to K48-linked polyubiquitin on lysosomal membranes. Removal of these ubiquitin chains by p97 occurs in cooperation with the recruitment of the autophagic machinery, which is mediated by K63-chains. Together, this allows for the initiation of the autophagic clearance of the damaged organelles. Although ELDR has become an important research topic over the last years, it has remained unclear what enzymes are involved in building these specific and highly important ubiquitin chains on damaged lysosomes.

In this study, we established a siRNA-based systematic screening approach with the aim to identify E2-conjugating enzymes responsible for the vigorous ubiquitination in response to lysosomal damage (in this case induced by the lysosomotropic chemical L-leucyl-L-leucine methyl ester (LLOMe)). We identified UBE2QL1 to drive mainly K48-linked ubiquitination on lysosomal membranes. Correspondingly, UBE2QL1 translocated to lysosomes upon damage induction. We found that upon siRNA-mediated depletion of UBE2QL1, p97 and proteins of the autophagic machinery were no longer recruited to damaged membranes, leading to inefficient autophagic clearance. In line with this, UBE2QL1 was also required for HeLa cells to survive long treatments with LLOMe.

Furthermore, this work showed that UBE2QL1 is also important for lysosomal homeostasis in otherwise unchallenged cells, as its depletion led to LMP, dissociation of Mechanistic Target of Rapamycin (mTOR) from lysosomal membranes and consequent Transcription Factor EB (TFEB) dephosphorylation, which is associated

with activation of genes for lysosomal biogenesis. Indeed, this resulted in a higher number of lysosomes. This indicates a potential role for UBE2QL1 in pathologies with LMP and upregulated lysosome biogenesis as hallmarks.

Thus, we identified UBE2QL1 as a key regulator of lysophagy and lysosomal homeostasis and this contributes majorly to the understanding of the signaling processes during ELDR.

Zusammenfassung

Lysosomen stellen die wichtigsten Zellorganellen zum Abbau von Zellkomponenten dar. Darüber hinaus besitzen sie essenzielle Funktionen bei der Beobachtung der zellulären Nährstoffsituation. Die lysosomale Membran kann z.B. durch oxidativen Stress, Chemikalien oder eindringende Pathogene geschädigt werden, was zu ihrer Permeabilisierung (engl.: Lysosomal membrane permeabilization, LMP) führt. Dies kann fatale Folgen für die Zelle haben. Die Zelle wirkt dieser Stresssituation mit einem speziellen Signalweg (engl.: Endolysosomal Damage Response, ELDR) entgegen, der die Autophagie der geschädigten Lysosomen einleitet (auch Lysophagie genannt).
Ein Merkmal dieser zellulären Antwort ist die extensive Ubiquitinierung von lysosomalen Membranproteinen mit K48- und K63-verknüpften Ubiquitinketten. Neben den vielen wichtigen Elementen von ELDR sticht die Ubiquitin-gesteuerte AAA^+-ATPase p97 heraus, da sie zusammen mit einem spezifizierten Set aus Kofaktoren zu den K48-Ketten rekrutiert wird. Die Entfernung dieser Ketten durch p97 geschieht in Zusammenarbeit mit der Rekrutierung der Autophagie Proteine, was wiederum von den K63-Ketten vermittelt wird. Diese Geschehnisse initiieren zusammen den autophagischen Abbau der geschädigten Organellen. Obwohl ELDR in den letzten Jahren zu einem wichtigen Forschungsgebiet wurde, ist noch nicht geklärt, welche Enzyme diese speziellen und sehr wichtigen Ubiquitinketten auf geschädigten Lysosomen katalysieren.
In dieser Studie etablierten wir einen systematischen siRNA Screen mit dem Ziel, E2-konjugierende Enzyme zu finden, die für die starke Ubiquitinierung nach den lysosomalen Schäden verantwortlich sind (hier hervorgerufen durch die der lysosomotrophischen Chemikalie L-leucyl-L-leucine methyl ester (LLOMe)). Wir identifizierten UBE2QL1 als E2-Enzym, das hauptsächlich K48-verknüpfte Ubiquitinketten auf lysosomalen Membranen katalysierte. Dementsprechend lokalisierte UBE2QL1 zu den Lysosomen, sobald diese geschädigt wurden. Wir fanden heraus, dass p97 und die Autophagie Proteine nicht länger zu geschädigten lysosomalen Membranen rekrutiert wurden wenn UBE2QL1 mittels siRNA verringert wurde. Das führte zu einem unvollständigen Abbau der Organellen mittels Autophagie. Ebenfalls zeigten wir, dass HeLa während langer Behandlungen mit LLOMe UBE2QL1 zum Überleben benötigten.

Diese Arbeit machte darüber hinaus deutlich, dass UBE2QL1 auch für die lysosomale Homöostase in nicht gestressten Zellen wichtig ist; die Verringerung von UBE2QL1 führte zu LMP, Dissoziation von Mechanistic Target of Rapamycin (mTOR) von der lysosomalen Membran und folglich zur Dephosphorylierung von Transcription Factor EB (TFEB). Dies wird mit der Aktivierung von Genen für die lysosomale Biogenese in Verbindung gebracht. Tatsächlich resultierte dies in einer höheren Anzahl an Lysosomen, was auf eine potenzielle Rolle von UBE2QL1 in Pathologien hinweist, zu deren Merkmalen LMP und die Hochregulierung der lysosomalen Biogenese gehören. Folglich identifizierten wir hier UBE2QL1 als Schlüsselregulator der Lysophagie und der lysosomalen Homöostase, was maßgeblich zum Verständnis der Signalwege während ELDR beiträgt.

1 Introduction

1.1 The ubiquitin system

As cells synthesize new proteins for plenty of different purposes, they also possess sophisticated mechanisms for their degradation in order to ensure protein homeostasis (proteostasis) (Harper and Bennett 2016). This is especially important during external or internal cellular stresses. Additionally, targeted degradation of misfolded or short-lived proteins takes place routinely. In the case of stress harming certain organelles, the cell is also able to degrade whole organelles (such as mitochondria, ribosomes or lysosomes) in order to oppose this situation (Dikic 2017).

There are two cellular pathways specified for protein degradation. Firstly, a large multimeric protease, the 26S-proteasome, recognizes and unfolds proteins to process them through its translocation channel. This pathway is called the ubiquitin-proteasome system (UPS) (Finley 2009). Secondly, proteins can be degraded in lysosomes by their specified hydrolases. This takes place for example during endocytosis of membrane receptors, which are then sorted to lysosomes for degradation in a process called vesicular sorting (Mukhopadhyay and Riezman 2007; Clague and Urbe 2010). During autophagy, substrates from the cytosol and whole organelles are recognized and engulfed by autophagosomal membranes. These new vesicles eventually fuse with lysosomes, leading to the digestion of their content (Clague and Urbe 2010) (autophagy is described in section 1.2).

A common feature of both degradation pathways is the labelling of their substrates. They are post-translationally marked with a small, highly conserved molecule – ubiquitin (Dikic 2017). Ubiquitin is a 76-amino acid protein that is conjugated via its terminal glycine to mostly lysine residues in the designated target proteins. (Pickart and Eddins 2004). It constitutes the model member of the family of Ubiquitin-like proteins (UBLs). They are all structurally related to ubiquitin and posttranslationally conjugated to their substrates by similar enzymatic cascades (Pickart and Eddins 2004). For example, Neural-precursor-cell-expressed developmentally down-regulated 8 (NEDD8) is the UBL which is closest related to ubiquitin. It modifies the ubiquitin machinery itself by regulation of activity of almost all cullins, the scaffold proteins of CRLs, by mono-neddylation. Also, the Small-Ubiquitin-related Modifier (SUMO) is added to SUMO consensus motifs in proteins. There are four different

families of SUMO and distinct polymerization variances, similar to polyubiquitin. Hence, SUMOylation has diverse roles in cellular pathways, specifically in cellular responses to different stresses (van der Veen and Ploegh 2012). Furthermore, during autophagy, the UBLs autophagy-related genes (ATG)8 and 12 are conjugated to other components of the autophagy machinery in order to ensure autophagosome biogenesis (described in section 1.2) (van der Veen and Ploegh 2012).

1.2 The ubiquitin-conjugation cascade

A three-step cascade of interacting enzymes carries out ubiquitination: E1 (ubiquitin-activating) enzymes, E2 (ubiquitin-conjugating) enzymes and E3 (ubiquitin) ligases (Fig. 1.1) (Scheffner, Nuber, and Huibregtse 1995). E1 enzymes are composed of an adenylation domain, a catalytic domain with an active cysteine and a Ubiquitin Fold Domain (UFD) (Schulman and Harper 2009). The E1 enzyme binds ATP and ubiquitin, leading to acyl-adenylation at its C-terminus of ubiquitin. The activated ubiquitin molecule is attacked by the catalytic cysteine of the E1 enzyme to form a thioester bond (Lake et al. 2001; Schulman and Harper 2009). Upon binding of ubiquitin, structural rearrangements in the E1 enzyme reveal a specific binding site for E2 enzymes in the UFD to build a stable E1~E2 complex (Ye and Rape 2009). This allows the transfer of the ubiquitin-thioester of the E2 (Schulman and Harper 2009) (Fig.1.1). Eight human E1 enzymes are responsible for activation of particular UBLs, with Ubiquitin-like modifier-Activating enzyme 1 (UBA1) and the later identified UBA6 providing specificity for ubiquitin itself (Jin et al. 2007; Schulman and Harper 2009). UBA1 is known to interact with a vast number of the approximately 40 human E2 enzymes, while UBA6 transfers ubiquitin to UBA6 specific E2 enzyme 1 (USE1) only, with yet unknown substrates (Jin et al. 2007).

E2 enzymes contain a highly conserved Ubiquitin-Conjugating Domain (UBC) of about 150 amino acids composed of four α-helices and a four-stranded β-sheet. It comprises overlapping binding sites for all types of E3 ligases and E1 enzymes and the catalytic cysteine to bind ubiquitin. Additionally, many E2 enzymes possess N- or C-terminal extensions with diverse individual functions (Stewart et al. 2016) (Fig. 1.2 A). Once E2 enzymes are loaded with an ubiquitin molecule, they cooperate with E3 ligases in the ubiquitination of target proteins. E3 ligases are the final players in this enzymatic cascade and catalyze the transfer of ubiquitin from the E2 enzyme to the target protein (Scheffner, Nuber, and Huibregtse 1995). Depending on the type of E3 ligase, ubiquitin

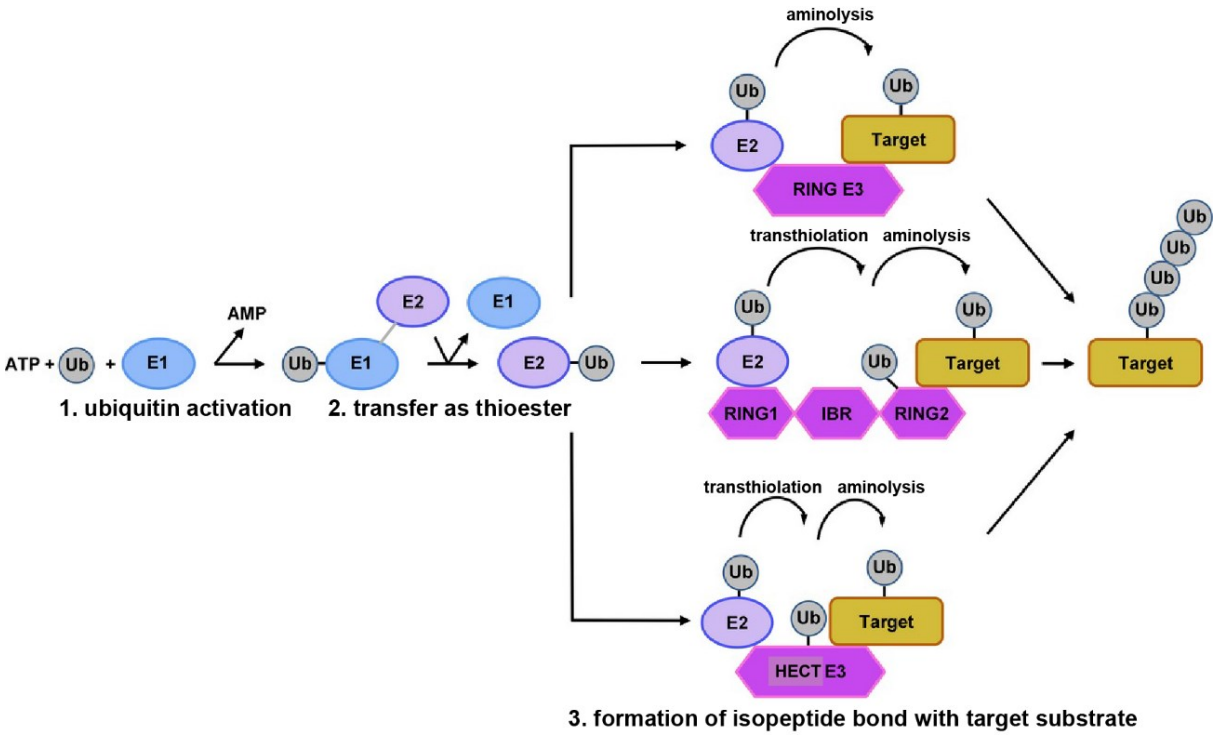

Figure 1.1: Ubiquitin is conjugated to substrates in a three-step enzymatic cascade.
A ubiquitin molecule is activated by an E1 activating enzyme using ATP and bound with a thioester bond (1.). Binding of E1~Ub to an E2 conjugating enzyme leads to structural rearrangements in the E2 enzyme and transfer of the ubiquitin molecule to its UBC domain (2.). E2 enzymes cooperate with three types of E3 ligases. Multimeric RING type E3 ligases provide a binding site for the E2 enzyme and the substrate. Binding leads to structural activation of the E2 enzyme and transfer of the ubiquitin molecule in an aminolysis reaction to mostly lysines in the designated substrate. In contrast, RBR and HECT E3 ligases possess binding sites for the loaded E2 enzyme and additional active site cysteines, to which the ubiquitin molecule is transferred in a transthiolation reaction to form an E3~Ub intermediate. Conjugation to substrates is mediated by the E3 ligase in this case (3.). Modified after (Elton et al. 2015).

is transferred to the substrate directly from the E2 enzyme or in an intermediate step to the catalytic center of the E3 ligase. Transfer to an active site cysteine of a E3 ligase occurs in a transthiolation reaction, whereas aminolysis reactions take place on lysine residues (Fig. 1.1). Atypical E2 enzymes that react with e.g. hydroxylgroups in serines and threonines, are also known (Stewart et al. 2016) (Fig. 1.2 B).

Around 700 human E3 ligases of three different families are known so far. The Really Interesting New Gene (RING) and RING-related E3 ligases account for the largest group (Metzger et al. 2014). These enzymes often form homo or heterodimers or multi-subunit complexes, which is also typical for the Cullin RING ligase (CRL) superfamily. CRLs are composed of a specific cullin scaffold protein, a small RING protein for binding the E2 enzyme and an adaptor protein that interacts with the specific substrate (Metzger et al. 2014). RING-type E3 ligases do not possess a catalytic center and need

an E2 enzyme to transfer the ubiquitin molecule to target proteins. They are considered as enhancers of E2 enzyme reactivity towards aminolysis (Pruneda et al. 2012). RING domains hold two loop regions with conserved cysteine and histidine residues in the core that bind Zn^{2+} atoms. Together with a central, connecting helix they form the binding cleft for E2 enzymes (Deshaies and Joazeiro 2009). Due to the flexibility of the ubiquitin molecule bound to the active site of the E2 enzyme, they can have only little contact (open state) or contacts between the hydrophobic patch in the ubiquitin and the crossover helix in the E2 enzyme (closed state) (Stewart et al. 2016) (Fig. 1.2 C). A hydrogen bond between a conserved side chain in the RING-type E3 ligase and an E2 enzyme backbone carbonyl pushes the equilibrium towards the closed state, thereby enhancing its reactivity towards aminolysis. This is essential for E3 ligase-mediated ubiquitin transfer (Pruneda et al. 2012).

In contrast, homologous to E6AP C-terminus (HECT) domain containing E3 ligases comprise a binding site for ubiquitin. The catalytic HECT domain at their C-terminus consists of an N-lobe for binding the E2 enzyme, and a C-lobe. Both are connected by a flexible hinge region (Weber, Polo, and Maspero 2019). This requires an additional step during ubiquitination of substrates. The E2 enzyme transfers the ubiquitin molecule to the HECT domain to form an intermediate thioester bond. Only binding of ubiquitin-loaded E2 enzymes leads to structural rearrangements of the HECT domain lobes, allowing for ubiquitin transfer to the target protein (Sluimer and Distel 2018). The interaction with HECT E3 ligases requires solely the transthiolation reactivity of E2 enzymes, which they are able to undergo even without an assisting E3 ligase. It is therefore assumed that HECT E3 ligases do not need E2 enzymes in closed states for ubiquitination of substrates (contrary to RING-type E3 ligases) (Stewart et al. 2016). The distinct N-terminal domains of HECT E3 ligases categorize them into two families: The NEDD4 family E3 ligases comprise a WW domain for substrate recognition and C2 domains for targeting them to phospholipid membranes, binding substrates or regulating their activity. In contrast, the HECT and RLD Domain Containing E3 Ubiquitin Protein Ligase (HERC) subfamily E3 ligases are characterized by one or several Regulator of Chromatin Condensation-1 (RCC) like domains (RLDs) and most often interact with chromatin (Sluimer and Distel 2018).

A third family of E3 ligases are the RING-between-RING (RBR) ligases consisting of a RING1, an in-between-RING (IBR) and a RING2 domain, each of them with Zn^{2+}

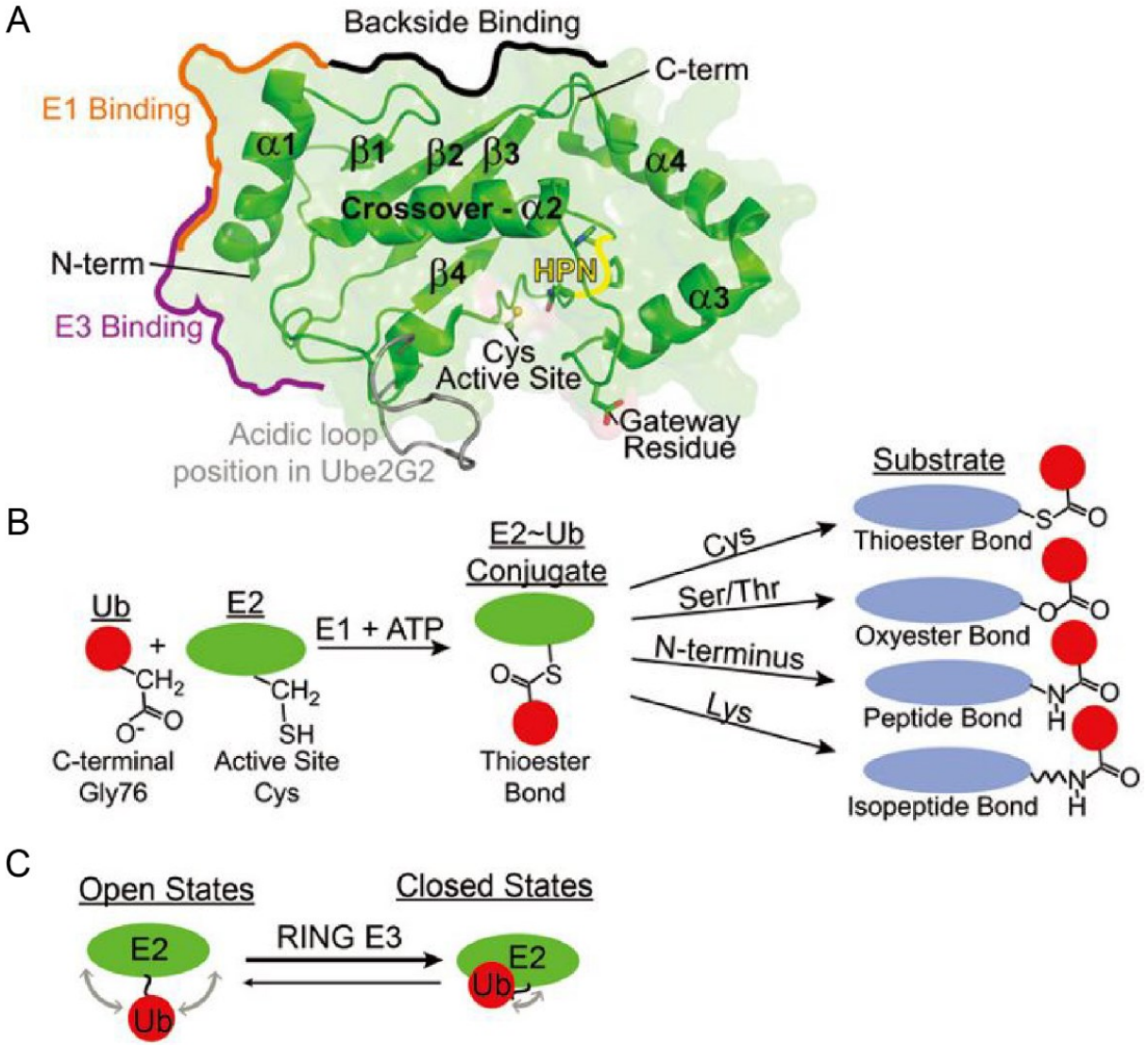

Figure 1.2: Structure and reactivity of E2-conjugating enzymes.

(A) Representative structure of E2 enzymes shown for UBE2D3. The UBC domain with the active site cysteine is shown in green and other structural features (for example binding sites for E1 enzymes and E3 ligases and for regulation of activity by backside binding) are labeled. The acidic loop of UBE2G2, when aligned with UBE2D3 is shown in gray. **(B)** The C-terminal carboxylate of ubiquitin is conjugated to the E2 enzyme active site cysteine by an E1 enzyme resulting in a thioester bond. The E2~Ub can react with side chains of cysteines, serines, threonines, lysines or the N-terminus of proteins to form different types of bonds. **(C)** Binding of E2~Ub to a RING E3 ligase shifts its conformation from an open state towards a closed, more reactive state. Modified after (Stewart et al. 2016).

binding activity. The E2~Ub intermediate binds to RING1 followed by formation of a thioester bond between the ubiquitin and the catalytic cysteine in RING2 (Walden and Rittinger 2018). The feature of binding the E2~Ub via a RING domain but also possessing an active cysteine defines RBR ligases as RING-HECT hybrids (Dove and Klevit 2017). In contrast to the interaction with RING-type E3 ligases, RING1 interaction with E2 enzymes keeps them in an open state. This is due to a shorter

second Zn^{2+}-binding domain in RING1 and is essential for preventing the E2 enzyme from performing aminolysis itself. This was structurally shown for the human homolog of Ariadne (HHARI)I and ubiquitin-conjugating enzyme 2 (UBE2)L3 Ubiquitin-Conjugating Enzyme H7 (UbcH7)~Ub (Dove et al. 2017; Yuan et al. 2017).

1.2.1 The relevance of E2 enzymes in human pathologies

Due to the importance in a multitude of cellular signaling events, aberrations or mutations in all parts of the ubiquitination machinery can lead to severe pathologies, including cancer or neurodegenerative disorders (Rape 2018). This study focusses on E2 enzymes. Therefore, in the following, examples of misregulated E2 enzymes in three types of pathologies (cancer, neurodengerative diseases and autoimmune disease) will be discussed.

Many E2 enzymes act in Deoxyribonucleic Acid (DNA) repair, apoptosis and cell cycle regulation, and are hence associated with diverse types of cancer (Hormaechea-Agulla et al. 2018). For example, a specific mutation and loss of function is reported for UBE2T in the Fanconi anemia syndrome. This disorder is characterized by misfunctional DNA repair mechanisms, leading to genomic instability. Monoubiquitination of key proteins of this DNA repair pathway by UBE2T is essential and its disruption has been reported in patients (Machida et al. 2006; Hira et al. 2015). Furthermore, elevated levels of UBE2T have been reported for several types of cancer, hence it is a potential oncogene. This is linked to its function in targeting the E3 ligase Breast Cancer Gene 1 (BRCA1), an important tumor suppressor, for proteasomal degradation (Alpi, Chaugule, and Walden 2016).

Another well-studied example for E2 enzyme-related diseases are neurological disorders such as Parkinson's disease, where the E3 ligase Parkin plays a major role. In fact, several E2 enzymes (UBE2D2, UBE2D3, UBE2L3, UBE2N, UBE2R1 and UBE2A) were identified to regulate Parkin's activity in mitophagy and could therefore influence the mechanism of development of Parkinson's disease (Hormaechea-Agulla et al. 2018). Due to its cooperation with Heme-Oxidized Iron-Responsive Element-Binding Protein (IRP2) Ubiquitin Ligase (HOIL) in the Linear Ubiquitin Chain Assembly Complex (LUBAC) complex, UBE2L3 is involved in the Nuclear Factor 'kappa-light-chain-enhancer' of Activated B-Cells (NF-κB) immune response and elevated levels are associated with autoimmune disorders and blood cancers (Alpi, Chaugule, and Walden 2016).

Attempts to target ubiquitinating enzymes with drugs has not been very successful until now (Huang and Dixit 2016). Given their broad functions and important role in determining ubiquitination, it has become clear that E2 enzymes are promising drug targets in human disease. They could provide more specificity than the already explored inhibitors of E1 enzymes (Huang and Dixit 2016). Small molecule inhibitors that inhibit E2 enzymes target for example UBE2N and UBE2R1, although none of them reached clinical trials yet (Huang and Dixit 2016; Stewart et al. 2016).

1.2.2 The ubiquitin code

Beyond the addition of a single ubiquitin molecule lysines in a target protein, so called mono-ubiquitination, all seven lysines (K) in the same ubiquitin molecule (K6, 11, 27, 29, 33, 48 and 63), as well as the N-terminal methionine (M1) are targets for ubiquitination. This leads to more or less complex diubiquitin or polyubiquitin chains with a multitude of divergent signaling properties (Komander and Rape 2012) (Fig. 1.3). The way of assembly of several ubiquitin molecules determines the structure of polyubiquitin chains. In homotypic chains, the same residue in all ubiquitin molecules is used to add the next ubiquitin. In contrast, in heterotypic polyubiquitin, several different residues are used within the same polymer, resulting in mixed or branched chains (Akutsu, Dikic, and Bremm 2016). Ubiquitin linked via K48 was the first identified polyubiquitin and its signaling function towards proteasomal degradation is well studied (Chau et al. 1989). In principle, all homotypic chain types, except for K63-linked ubiquitin, can target proteins to the proteasome, as for example K11-linked chains act in Endoplasmatic Reticulum-Associated Degradation (ERAD) (Xu et al. 2009). K63-linked polyubiquitin chains and mono-ubiquitination play a role in several other pathways, such as endolysosomal sorting of receptors (Duncan et al. 2006). Additionally and similar to K27-linked ubiquitin, they are important signals in autophagy-mediated digestion of cellular contents (Clague and Urbe 2010).

1.2.3 Ubiquitin chain type specificity of ubiquitinating enzymes

As a general rule, the last enzyme that carries the ubiquitin molecule is thought to determine the target residue on a proximal ubiquitin and thereby the chain type that is being synthesized (Stewart et al. 2016). In the case of reactions catalyzed by HECT and RBR E3 ligases that form an E3~Ub intermediate, it is the E3 enzyme that determines the chain type (Sluimer and Distel 2018; Walden and Rittinger 2018) (described in section 1.1.1). For some of the HECT E3 ligases, ubiquitin chain

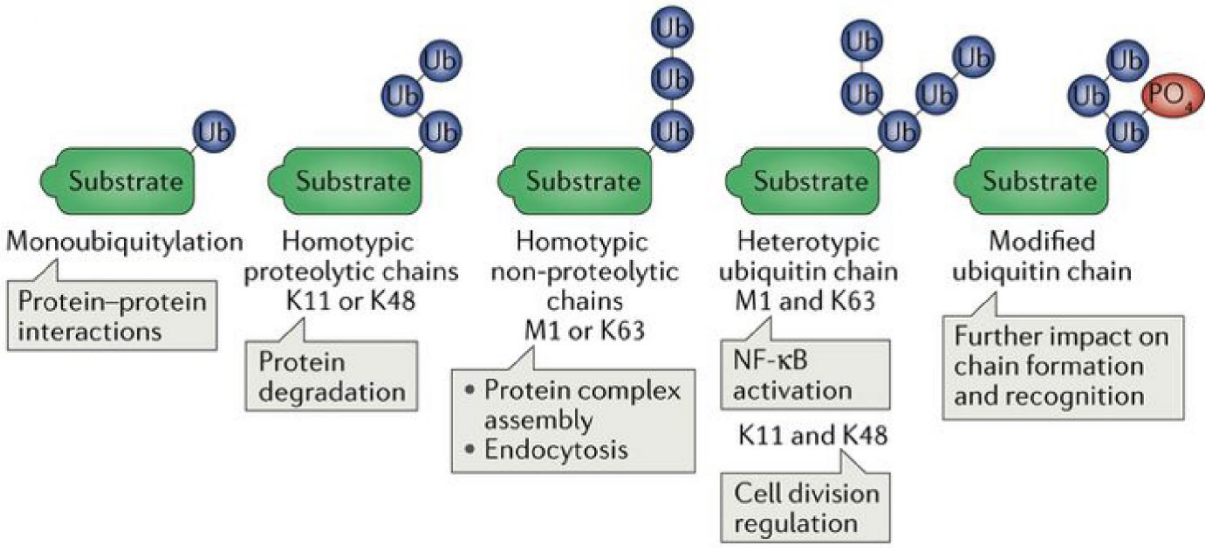

Figure 1.3: The diversity of ubiquitin-conjugates.

Ubiquitin can be conjugated to substrates as monoubiquitin or polyubiquitin. All of the seven lysines and the N-terminal methionine (M1) of ubiquitin serve as targeting sites for the formation of polyubiquitin chains. Homotypic chains are characterized by using the same residue in all conjugated ubiquitin molecules. K11 and K48 conjugates often signal towards proteasomal degradation, whereas polyubiquitin linked via M1 or K63 plays roles in complex assembly and endocytosis. Heterotypic ubiquitin chains can lead to branched structures with distinct cellular signaling roles. Ubiquitin can be posttranslationally modified itself. Phosphorylation at S65 is for example important during autophagic clearance of mitochondria. Adopted from (Rape 2018).

specificities are known. For example, NEDD4-1 and Reverses Suppressor of Ty (SPT)-phenotype Protein 5 (RSP5) assemble K63-linked ubiquitin, while E6AP prefers K48-linked chains (Sluimer and Distel 2018). For RBR ligases, it is well studied for HOIP, a subunit of the LUBAC complex that it provides a specificity towards linear chains linked to M1 (Smit et al. 2012; Walden and Rittinger 2018). Additionally, it was recently shown that Two RING Fingers And Double RING Finger Linked (DRIL) (TRIAD)3/RNF216 specifically conjugates ubiquitin linked via K63 to substrates *in vitro* (Schwintzer, Aguado Roca, and Broemer 2019).

In contrast, E2-conjugating enzymes determine the chain type in the case of ubiquitination carried out by RING-type E3 ligases (Stewart et al. 2016). This is the largest of the E3 ligase families, which emphasizes the importance of E2 enzymes in the ubiquitination cascade. In fact, E2 enzymes can either perform ubiquitin chain initiation on substrates (priming E2 enzymes) or chain elongation on ubiquitin molecules (or both). Often, both types cooperate with the same E3 ligase (Stewart et al. 2016). Several mechanisms for E2 enzyme chain type specificity are known so far. For example, UBE2K uses a region within the UBC domain to recognize a tyrosine

near K48 in the ubiquitin molecule, thereby dictating the designated binding site (Stewart et al. 2016). Other K48-specific E2 enzymes (UBE2R1, UBE2R2, UBE2G1 and UBE2G2) possess a short, flexible acidic loop proximal to the active site (Fig. 1.2 A) (Stewart et al. 2016). In the case of UBE2G2, so called backside binding to the UBC domain of a non-RING region of the E3 ligase gp78 results in unwinding of the acidic loop. This enhances the aminolysis reactivity of the E2 towards the K48 residue in ubiquitin (Das et al. 2013). UBE2N is known to assemble K63 chains and requires the E2 variants UBE2V1 or UBEV2 as subunits to ensure the specific chain elongation (Eddins et al. 2006). Some E2 enzymes display low specificity, as for example the UBE2D (UbcH5) family, which is often used for *in vitro* studies because it reacts with any lysine in ubiquitin (Stewart et al. 2016).

1.2.3.1 Structure of polyubiquitin chains

Among the homotypic chains, K6, K11 and K48-linked ubiquitin adopt rather compact conformations, while linear ubiquitin linked via M1 or K63 chains display a more open assembly (Komander and Rape 2012). In the recent years, evidence for the importance of heterotypic ubiquitin chains has emerged, thanks to advanced methods to dissect the ubiquitination landscape. Indeed, 10-20 % of ubiquitin polymers are present as branched chains (Swatek et al. 2019; Haakonsen and Rape 2019). Several residues in the same ubiquitin can be ubiquitinated in branched chains, resulting the characteristic structure. For example, K11/K48-linked polyubiquitin displays a strong degradative signal, as it leads to extraction of proteins from membranes and recognition by the proteasome (Yau and Rape 2016). Heterotypic chains can be built by several cooperating E3 ligases, as in the case of Interleukin-1 (IL-1) receptor binding where Tumor Necrosis Factor (TNF) Receptor Associated Factor (TRAF)6 induces the formation of K63-linked chains and LUBAC adds linear ubiquitin chains (Emmerich et al. 2013). Also, the use of multiple E2 enzymes by one E3 ligase can lead to formation of heterotypic ubiquitin chains. For proteasomal degradation of cell cycle regulators, the Anaphase Promoting Complex/Cyclosome (APC/C) interacts with UBE2C for the initiation of ubiquitination and UBE2S for chain elongation, resulting in K11/K48-branched chains (Grice et al. 2015).

Another level of complexity in the ubiquitin code is added by the posttranslational modification of ubiquitin itself that provides inhibiting and activating functions (Fig. 1.3). Reversible acetylation of ubiquitin on K6 and K48 by Histone Acetyltransferases

(HATs) (and Histone Deacetylases (HDACs)) neutralizes the lysine's positive charge and thereby blocks the interaction with E2 enzymes and formation of polyubiquitin chains (Herhaus and Dikic 2015). Phosphorylation of ubiquitin occurs most frequently on S57 and S65 with different outcomes. The best-studied example is the activation of the E3 ligase Parkin by PTEN-Induced Kinase 1 (PINK1) mediated phosphorylation of ubiquitin at S65 and Parkin itself on the Mitochondrial Outer Membrane (MOM). Through an efficient feed-forward mechanism, Parkin is recruited and retained. It efficiently ubiquitinates proteins on the MOM in order to recruit autophagy adaptors in the process of autophagic clearance of depolarized mitochondria (also called mitophagy) (Shiba-Fukushima et al. 2012; Herhaus and Dikic 2015).

1.2.3.2 Deubiquitinating Enzymes (DUBs)

Ubiquitination is reversible and the ubiquitin code is completed by deubiquitinating enzymes (DUBs) that antagonize ubiquitinating enzymes and thereby stabilize proteins (Komander and Rape 2012). DUBS take over essential housekeeping functions, as for example at the proteasome, where they cleave off ubiquitin from target proteins and thereby ensure sufficient levels of free ubiquitin in the cell (Komander and Rape 2012). Most of the around 99 human DUBs are cysteine proteases, while the Jab1/Mov34/Mpr1 Pad1 N-terminal+ (MPN+) (JAMM) family is characterized by their Zn^{2+}-dependent metalloproteinase activity (Clague, Urbe, and Komander 2019). They act in cleaving isopeptide or amide bonds after the terminal carbonyl of the last residue (Gly76) of the ubiquitin molecule. Thereby they contribute to regulation of protein degradation and trafficking, processing of inactive ubiquitin precursors and removal of ubiquitin from proteins during their degradation at the proteasome itself (Amerik and Hochstrasser 2004). DUBs provide also a wide range of specificities, which further adds complexity to the ubiquitin code. DUBs can have preferences for distinct polyubiquitin linkage types and some are able to cleave them at the end (exo-DUB activity) or within the chain (endo-DUB activity). Other DUBs favor certain lengths of polyubiquitin or possess specificities for ubiquitin linked to certain substrates (Clague, Urbe, and Komander 2019). DUBs are important for a multitude of cellular processes. Many play roles in DNA repair, cell cycle regulation or immune signaling, indicating their importance for diseases. Other DUBs control important signaling during autophagy, as for example in clearance of mitochondria and peroxisomes, where USP30 localizes to and cleaves K6-linked ubiquitin to limit selective autophagy.

(Clague, Urbe, and Komander 2019). Furthermore, the Ovarian Tumor (OTU) DUB YOD1 assists the Adenosine Triphosphatases (ATPases) Associated with diverse cellular Activities $(AAA)^{+}$-ATPase p97 (also called VCP) in directing it and other co-factors to polyubiquitinated proteins in order to extract them from membranes during processes such as ERAD and autophagic clearance of lysosomes (lysophagy) (Papadopoulos et al. 2017; Ernst et al. 2009).

1.2.4 The p97 and cofactor protein system

Many ubiquitinated proteins require downstream processing by the hexameric AAA+-type ATPase Valosin containing protein (VCP)/p97 (hereafter called p97). As a segregase it binds and extracts ubiquitinated proteins from complexes or membranes in order to facilitate their proteasomal degradation or to retain their functions in a multitude of cellular processes (van den Boom and Meyer 2018).

Each p97 protomer is composed of a globular N-domain and two ATPase domains, D1 and D2. While D1 is more involved in stabilization of the hexameric structure, D2 is the major domain for the ATPase activity (Ye et al. 2017). p97 uses energy from ATP hydrolysis to structurally remodel its ubiquitinated substrates in order to release them from membranes or binding partners and to deliver them to the proteasome (van den Boom and Meyer 2018). Depending on the cellular pathway, p97 cooperates with alternative sets of about 30 different cofactor proteins (Fig. 1.4). Cofactors act as substrate adapters, targeting factors or regulators of p97. Most cofactors bind via the N-domain, while some use the C-terminal part of p97 (Ye et al. 2017). Most of these cofactor proteins have a direct relation to the UPS, as they functionally bind the polyubiquitinated substrates within the respective p97 complex (Meyer and Weihl 2014).

p97 has a pivotal role in cellular homeostasis and functions in a multitude of protein quality control pathways. This is best-studied ERAD, where unfolded proteins of the ER are tagged with polyubiquitin on the cytosolic site. ERAD substrates are recognized, extracted from the membrane and delivered to the proteasome by p97 and its substrate adaptor Ubiquitin Fusion Degradation 1 (Ufd1)- Nuclear Protein Localization 4 (Npl4) (Buchberger, Schindelin, and Hanzelmann 2015). Similar extraction mechanisms involving p97 play essential roles in Ribosome-Associated Quality Control (RQC), Mitochondria-Associated Degradation (MAD) and chromatin-associated degradation. Furthermore, p97 has critical roles in cell cycle progression

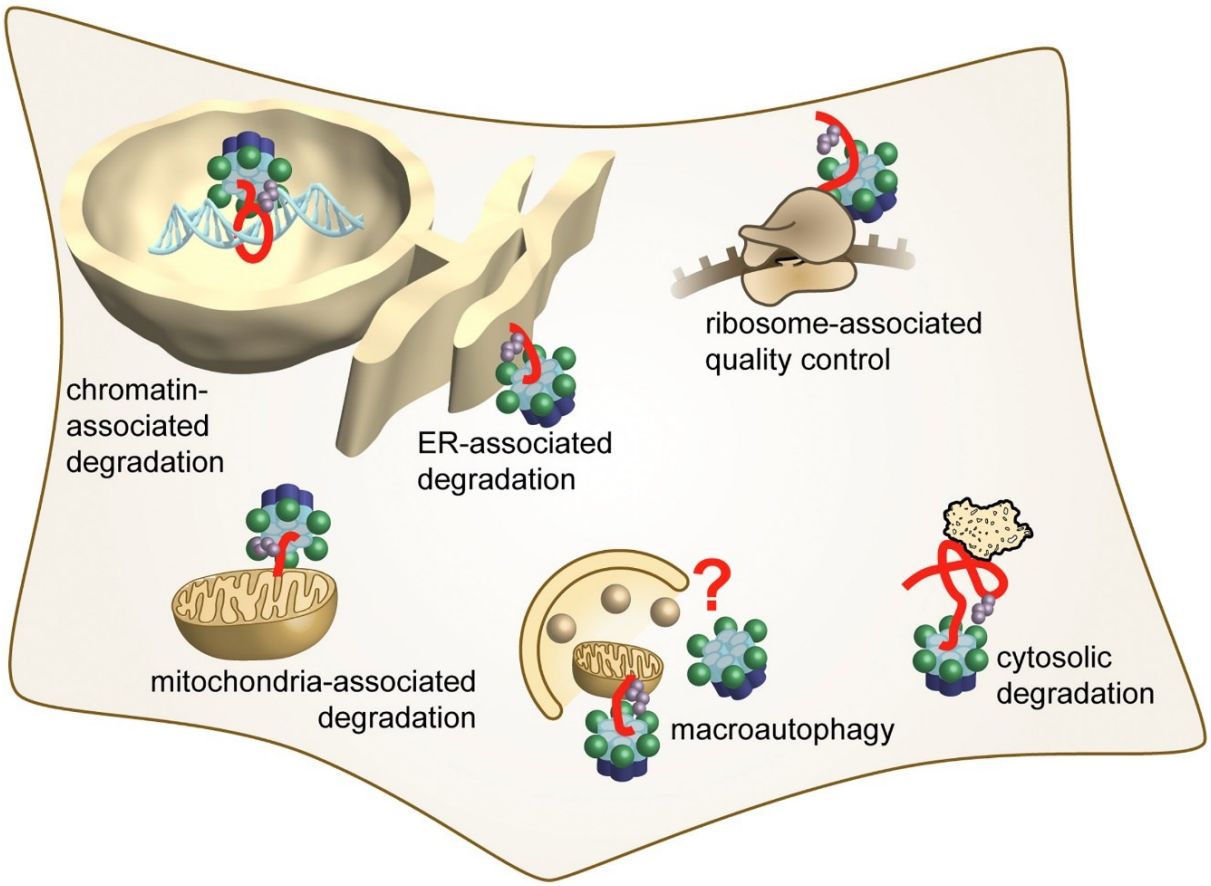

Figure 1.4: Roles of p97 in protein quality control.
p97 binds and extracts ubiquitinated substrates (in red, ubiquitin in violet) from membranes or protein complexes in a vast number of cellular processes. The retrotranslocation of unfolded proteins in the ER to the proteasome (ERAD) is well studied. Similar mechanisms apply for mitochondria-associated degradation (MAD) and ribosome-associated quality control (RQC), where p97 removes nascent polypeptide chains from stalled ribosomes. On chromatin, p97 removes proteins in general quality control mechanisms and in DNA damage response. Furthermore, p97 functions in macroautophagy and targets yet unknown ubiquitinated substrates on lysosomal membranes to ensure their autophagic degradation. Adopted from (van den Boom and Meyer 2018).

and DNA damage response, thereby contributing to genomic stability (Fig. 1.4) (van den Boom and Meyer 2018).

Additionally to proteasomal degradation, p97 has also been connected to endosomal sorting and autophagy (Bug and Meyer 2012). Well-studied roles emerged in selective autophagy of organelles, namely mitophagy and lysophagy (Karbowski and Youle 2011; Papadopoulos and Meyer 2017). Mitochondria are highly dynamic and are able to adapt their shape to several cellular conditions. Organelle fusion is mediated by Mitofusins (Mfn1 and Mfn2) and Optic Atrophy 1 (OPA1) while Dynamin-Related Protein 1 (Drp1) regulates fission events (Escobar-Henriques and Anton 2020). Mitochondrial proteostasis in the MOM is maintained by the UPS involving p97

(Karbowski and Youle 2011). p97, in cooperation with its adaptors Ufd1-Npl4 and UBXD1, acts in extraction proteasomal degradation of OMM proteins, as for example mitofusins, This ensures segregation of depolarized mitochondria and facilitates the engulfment by autophagosomes (Papadopoulos and Meyer 2017). More recently, a similar function for p97 was described for the autophagic clearance of damaged lysosomes. The relevant p97 cofactors in this pathway are Ubiquitin Regulatory X Domain containing protein 1 (UBXD1), Phospholipase A-2-Activating Protein (PLAA) and YOD1, which, probably similar as in mitophagy, extract yet unknown substrates targeted with K48-linked polyubiquitin from lysosomes as a prerequisite for autophagy (see section 1.4) (Papadopoulos and Meyer 2017; Papadopoulos et al. 2017).

Autosomal dominant mutations in the interface between the N- and D1-domains of p97 can lead to severe late onset diseases with different phenotypes. Affected patients suffer from one or any mixture of the four described pathologies: Inclusion Body Myopathy (IBM), Paget's Disease of the Bone (PDB), Frontotemporal Dementia (FTD) and Amyotrophic Lateral Sclerosis (ALS) (summarized as VCP/p97-associated disease or IBMPFD/ALS) (Meyer and Weihl 2014). More recently, the name Multisystem Proteinopathy 1H(MSP1) was introduced (Taylor 2015). While p97-knockout mice are embryonic lethal, the disease-relevant mutations do not lead to complete, but rather partial loss of p97 functions. Intriguingly, all phenotypes display degenerative characteristics without developmental impairments. Common features in affected tissues (mostly muscles and neurons) are inclusions containing ubiquitinated proteins and accumulation of non-degradative autophagosomes, underlining the role of p97 in autophagy and protein homeostasis (Meyer and Weihl 2014). More recent studies link p97-associated effects in MSP1 to defects in lysophagy and lysosomal homeostasis (Johnson et al. 2015; Papadopoulos et al. 2017; Arhzaouy et al. 2019) (see section 1.3.1).

1.3 Autophagy

Cellular autophagy is the process of degradation of proteins or cellular organelles in lysosomes. Three main autophagic pathways are distinguished, namely macroautophagy, microautophagy and chaperone-mediated autophagy. During macroautophagy (hereafter referred to as autophagy), portions of the cytoplasm and organelles are engulfed by an isolation membrane, the phagophore. Upon the closure of autophagophore and its subsequent fusion with a lysosome, the cargo is degraded

by lysosomal hydrolases. In contrast, in mircoautophgay, smaller cytoplasmic portions are invaginated directly by lysosomal membranes for degradation. Lastly, proteins comprising a specific KFERQ-like pentapeptic sequence are recognized by the Heat Shock Cognate 70 kDa (Hsc70) chaperone. This mediates binding to Lysosome-Associated Membrane Protein 2A (LAMP-2A) on lysosomal membranes and translocation into their lumen during chaperone-associated autophagy (Mizushima and Komatsu 2011). Degradation of cellular contents by autophagy is an essential way of recycling and providing new building blocks for the cell during starvation but also under basal conditions. Hence, defects in autophagy are hallmarks of diverse human pathologies and components of the autophagy machinery have become attractive and extensively studied drug targets (Schneider and Cuervo 2014).

1.3.1 Autophagosome biogenesis

The basis of autophagic degradation is the engulfment of the target cellular content by a newly synthesized membrane, the phagophore. It engulfes the cargo by elongation and, after closure of the remaining pore, forms a double-membrane vesicle, termed the autophagosome, which eventually fuses with a lysosome for degradation of the content (Rubinsztein, Shpilka, and Elazar 2012) (Fig. 1.5A). Formation of autophagosomal membranes is coordinated by ATG that where first extensively studied in yeast but are highly conserved (Weidberg, Shvets, and Elazar 2011).

The first active protein complex promoting autophagosome biogenesis is the Uncoordinated-51 (Unc-51) Like Kinase 1 (ULK1) complex. It consists of ULK1 and ATG13, ATG101 and Focal Adhesion Kinase (FAK) family-Interacting Protein of 200 kDa (FIP200), which stabilize the complex and support the translocation of ULK1. Regulation of ULK1 is mediated by the Mechanistic Target of Rapamycin Complex 1 ((mTORC1), hereafter called mTOR) and Adenosine Monophosphate (AMP) activated Kinase (AMPK) (Fig 1.5B). During nutrient-rich conditions, active mTOR on lysosomal membranes phosphorylates and inhibits ULK1. Upon cellular starvation, AMPK in turn inactivates mTOR, leading to its dissociation from lysosomes (Mercer, Gubas, and Tooze 2018). Activation of the ULK complex results in its translocation to specified ER sites, so called omegasomes, that serve as platforms for the nucleation of the phagophore (Karanasios et al. 2013) (Fig 1.5A). Here, the ULK1 complex activates the Phosphoinosite 3-Kinase (PI3K) complex 1 consisting of Vacuolar Protein Sorting 34(VPS34), Beclin 1 (BECN1), the pseudokinase p150 and ATG14 (Kim et al. 2013),

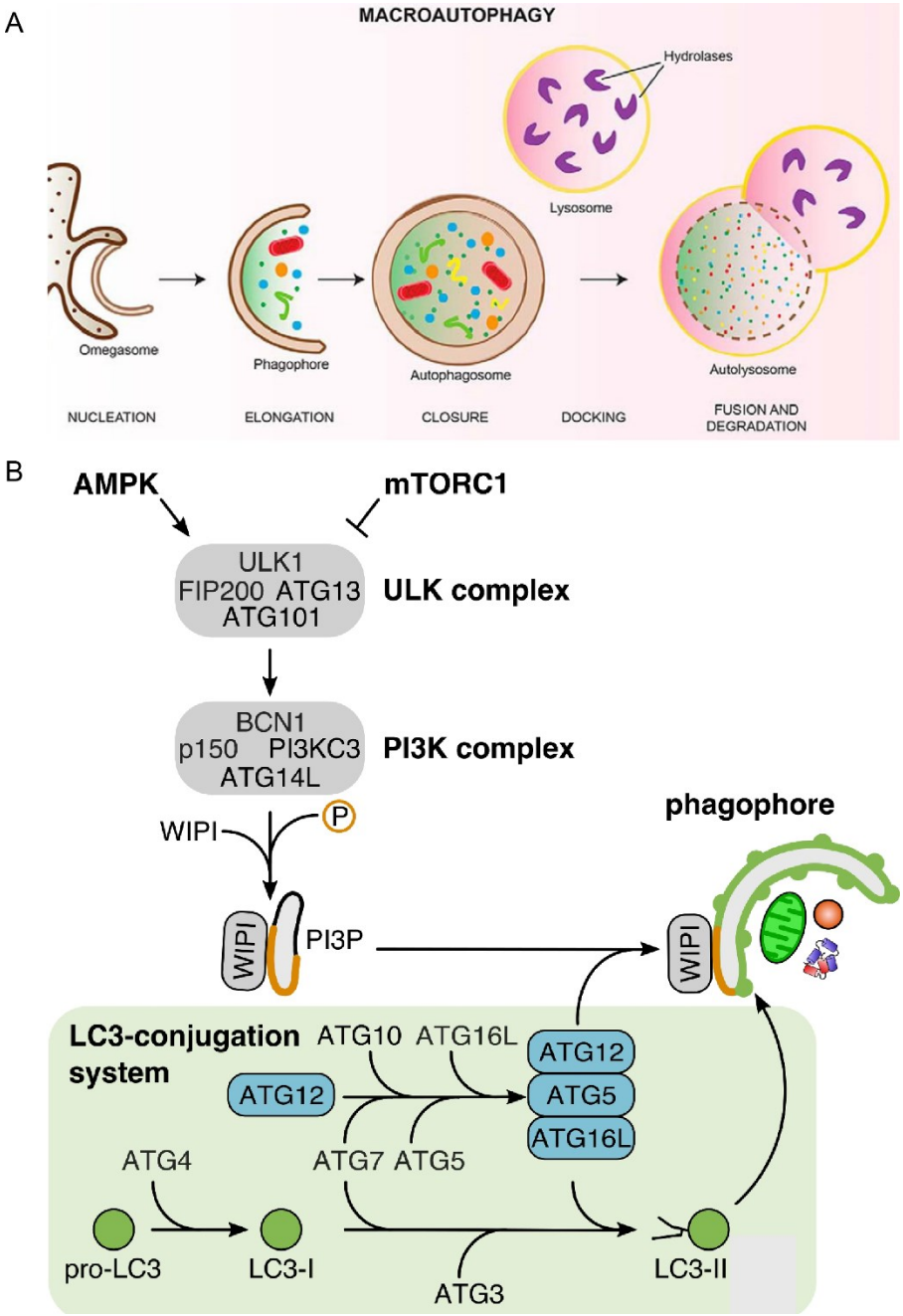

Figure 1.5: Steps in mammalian autophagy.

(A) Autophagosome formation. Nucleation of the phagophore starts at the ER at so called omegasomes to form a phagophore which is then elongated. After membrane closure, the autophagosome fuses with a lysosome to form the autolysosome and degrade the cellular content. Adopted from (Mercer, Gubas, and Tooze 2018). **(B)** Molecular mechanisms of phagophore formation. The initiating ULK1 complex is regulated by kinases itself. Activation leads to its translocation to omegasomes and downstream activation of the PI3K complex 1. Formation of PI3P on membranes leads to recruitment of effectors such as WIPIs that promote phagophore nucleation. Elongation of the phagophore is ensured by two ATG conjugation systems. Pro-LC3 is cleaved by ATG4 to LC3-I that is then conjugated to PE on phagophores (LC3-II). For this, the E1-like ATG7 activates and binds the C-terminus of LC3-I and transfers it to the E2-like ATG3. ATG7 additionally works with another E2-like enzyme, ATG10, to ensure the conjugation of ATG12 to ATG5. They interact with ATG16L to form an E3-like enzyme that accomplishes conjugation of LC3 to PE. Adopted after (Agop-Nersesian et al. 2018).

leading to the production of Phosphatidylinositol 3-Phosphate (PI3P) on the ER membrane. This is important for the recruitment of downstream effectors responsible for membrane rearrangements to initiate nucleation, such as WD-repeat Domain phosphoinositide-Interacting Proteins (WIPIs) (Fig 1.5B) (Mercer, Gubas, and Tooze 2018).

After nucleation from the omegasome, the elongation of the phagophore is ensured by two ubiquitin-like conjugation systems and the recruitment of further ATG8-family members (Rubinsztein, Shpilka, and Elazar 2012). In humans, two ATG8 families exist, the Light Chain 3 (LC3) (with splice variants LC3A, LC3B, LC3B2 and LC3C) and the γ-aminobutyric Acid Receptor Associated Proteins (GABARAB) (with splice variants (GABARAP, GABARAPL1 and GAPARAPL2) family (hereafter referred to as LC3/ATG8 family) that contain an ubiquitin fold and two additional N-terminal α-helices (Lystad and Simonsen 2019). During autophagy, pro-LC3 needs first to be cleaved to LC3-I at its C-terminus by the ATG4 protease to expose a C-terminal glycine. For LC3 conjugation to Phosphatidylethanolamine (PE) on immature autophagic membranes, an E1-like enzyme (ATG7), an E2-like enzyme (ATG3) and an E3-like complex (ATG12-ATG5-ATG16L) are required (Fig. 1.5B). ATG7 activates and binds the C-terminal glycine of LC3-I and transfers it to the membrane-bound ATG3. At the same time, it helps in formation of the ATG12-ATG5-ATG16L complex, where it transfers ATG12 to the E2-like enzyme ATG10. This results in conjugation of ATG12 to ATG5, allowing interaction with a dimer of ATG16L. The complex recruits and activates the E2 enzyme-like ATG3 and thereby ensures the transfer of LC3-I to PE on autophagosomal membranes. Conjugated LC3, called LC3-II, remains on these membranes being responsible for the recruitment of LC3-Interacting Region (LIR) containing proteins that act in autophagosome biogenesis (Fig. 1.5B) (Lystad and Simonsen 2019).

The final closure of the autophagosome is not yet completely understood and it remains unclear how ATG8 proteins contribute to fusion with the lysosome. It was shown however that the lipid transfer protein ATG2 and the Endosomal Sorting Complexes Required for Transport (ESCRT) III localize to closing membranes and have important roles (Lystad and Simonsen 2019). Furthermore, the ATG conjugation system (consisting of ATG3, ATG5 and ATG7) is essential for closure but not for fusion with lysosomes. In contrast, the ATG8 proteins LC3 and GABARAB are not required

for closure but initiate an essential step towards fusion by recruitment of Pleckstrin Homology And RUN Domain Containing M1 (PLEKHM1) (Nakamura and Yoshimori 2017). PLEKHM1 is an important adaptor at the fusion sites, interacting with the small Guanosine Triphosphate (GTP)ases Ras-related protein 7 (Rab7) and Adenosine Diphosphate (ADP) Ribosylation Facto Like GTPase 8b (Arl8b) that in turn recruit tethering factors of the Homotypic fusion and Protein Sorting (HOPS) complex. Membrane fusion is finally accomplished by interaction of HOPS with N-ethylmaleimide Sensitive factor Attachment protein Receptors (SNARE) complexes on both, the phagophore and lysosomal membranes (Yim and Mizushima 2020). For fusion, autophagosomes are transported to the perinuclear region where lysosomes accumulate. This occurs along microtubules in a LC3-dependent manner (Kimura, Noda, and Yoshimori 2008). Additionally, the small GTPase Rab7 connects autophagosomes, as well as lysosomes to microtubules and thereby ensures the correct positioning of both (Nakamura and Yoshimori 2017).

1.3.2 Selective autophagy

During cellular nutrient deprivation (and in low rates even under basal, nutrient-rich conditions) the cell randomly recycles cytoplasmic components in order to provide amino acids to build new proteins using non-selective autophagy. In contrast, selective autophagy requires ubiquitinated proteins as starting signals. (Mizushima and Komatsu 2011). Specified autophagy adapters contain a ubiquitin binding domain and a LIR domain. They recognize ubiquitinated target proteins and initiate the accumulation of the autophagic machinery by recruiting the LC3/ATG8 family via the LIR domain (Sharma et al. 2018). The main autophagy adaptors are Sequestome-1 (SQSTM1)/p62 (hereafter called p62), Calcium-Binding And Coiled-Coil Domain-Containing Protein 2 (CALCOCO2)/ Nuclear Dot Protein 2 (NDP52) (hereafter called NDP52), Optineurin (OPTN), Neighbor of BRCA1 gene 1 (NBR1) and Tax1 binding protein 1 (TAX1BP1) (Sharma et al. 2018).

p62 is the first described autophagy adaptor as its localization to ubiquitinated protein aggregates was linked to LC3 binding and degradation in autophagosomes during selective autophagy of aggregates (aggrephagy) (Pankiv et al. 2007). Additional to the LIR domain, p62 contains a Phox and Bem1 (PB1) domain, which is responsible for its oligomerization, and a UBA domain that allows binding to K63-linked polyubiquitin chains (Rogov et al. 2014). Furthermore, several E3 ubiquitin ligases interact with p62

in order to ubiquitinate its targets. p62 is also involved in autophagic degradation of other organelles, such as proteins on the MOM in mitophagy or peroxisomes in pexophagy, although the structurally similar NBR1 has major functions here. Additionally, ubiquitin dependent autophagy of invading bacteria, such as *Listeria*, *Shigella* and *Salmonella* (xenophagy) is mediated by p62 binding and subsequent signaling (Rogov et al. 2014). OPTN, NDP52 and TAX1BP1 have important functions in xenophagy of *Salmonella* as well as in activating the inflammatory NF-κB signaling by the recruitment of TRAF family member-associated NF-kappa-B activator (TANK) Binding Kinase 1 (TBK1) (Sharma et al. 2018).

1.4 Lysosomes and the response to lysosomal membrane permeabilization

1.4.1 Lysosomal membrane permeabilization

Lysosomes are cellular organelles that are enclosed by a phospholipid bilayer and were discovered by Christian de Duve in 1955 (Appelmans, Wattiaux, and De Duve 1955). Their acidic lumen containing various hydrolases makes them the most important organelles for recycling of cellular content (Settembre et al. 2013). The lysosomal membrane contains various proteins that are important for its function (Ballabio and Bonifacino 2020). A vacuolar ATPase (v-ATPase) maintains the acidic pH of the lysosomal lumen. LAMPs have protective roles and specialized transport proteins ensure the export of products of lysosomal degradation. The inner part of the membrane is covered by the glycocalyx, a polysaccharide coat that protects from digestion by lysosomal enzymes (Ballabio and Bonifacino 2020). In recent years, it has become clear that lysosomes are not merely degradative organelles but represent sensing and signaling platforms for the nutrient cellular status (for example as described for autophagy in section 1.3.1) (Perera and Zoncu 2016; Ballabio and Bonifacino 2020).

When lysosomes are impaired this has fatal consequences for the cell. LMP leads to the release of acidic lysosomal contents and proteases, such as cathepsins (Boya and Kroemer 2008). Depending on the degree of release, this can result in activation of apoptotic pathways as well as necrosis. Released cathepsins B and D reportedly trigger the mitochondrial cell death pathway by selective Mitochondrial Outer Membrane Permeabilization (MOMP) and subsequent release of pro-apoptotic stimuli (Boya and Kroemer 2008). Among the many internal and external factors that induce LMP are oxidative stress, proteases, photodamage, silica and ureate crystals,

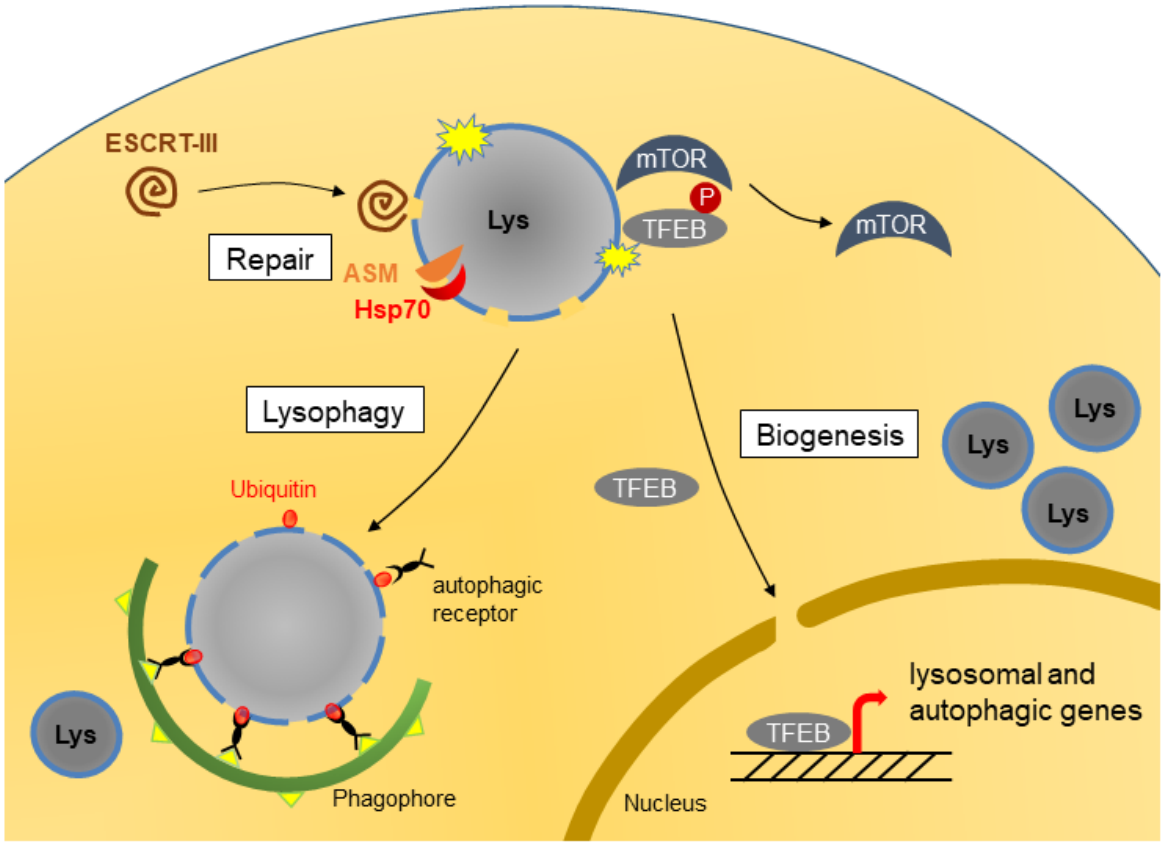

Figure 1.6: Three branches of endolysosomal damage response.

Repair: Early and minor damage of lysosomal membranes is recognized and repaired by ESCRT. Stabilization of the acid sphingomyelinase (ASM) by heat shock protein 70 (Hsp70) balances the lipid composition of damaged membranes. *Biogenesis*: Dissociation of mTOR from ruptured membranes induces transcription of lysosomal and autophagic genes by dephosphorylation and nuclear translocation of TFEB. *Lysophagy*: Lysosomal damage is sensed by galectins and marked by heavy ubiquitination resulting in recruitment of the autophagic machinery and formation of autophagosomal membranes around the organelle to ensure its degradation. Adopted from (Papadopoulos, Kravic, and Meyer 2019).

lysosomotropic drugs and invading bacteria or viruses (Papadopoulos, Kravic, and Meyer 2019).

LMP is also associated with a variety of other diseases. Many genetic risk factors, leading to different neurodegenerative pathologies, were associated with lysosomal damage (Papadopoulos and Meyer 2017). The Apolipoprotein E4 (ApoE4) is the most prevalent risk factor for Alzheimer's disease and its expression was associated with leaky lysosomal membranes. TMEM106B, a lysosomal transmembrane protein and a risk factor for FTD is known to affect the integrity as well as the size of lysosomes. Additionally, endocytosed neurotoxic aggregates, such as α-synuclein, amyloid-β, tau, huntingtin polyglutamine repeats and superoxide dismutase 1 have been reported to

damage lysosomal membranes (Papadopoulos and Meyer 2017). As already described in section 1.1.4, it has evolved that impaired lysosomal integrity is a feature of MSP1 caused by defective p97 (Papadopoulos and Meyer 2017). Disease mutants of p97 cause defects in autophagic clearance of lysosomes in tissue culture models and patient muscle tissue (Papadopoulos et al. 2017). Furthermore, in p97 deficient mouse muscle, defects in lysosomal homeostasis were defined by accumulation of Gal3 positive structures and activation of TFEB. This came along with necrotic myopathy and increased levels of autophagosomes (Arhzaouy et al. 2019). Corresponding to this, disease-mutant p97 causes defects in lysosomal tubular dynamics in *Drosophila*, also leading to accumulation of autophagosomes (Johnson et al. 2015).

1.4.2 Endolysosomal damage response (ELDR)

Eukaryotic cells have evolved sophisticated mechanisms to respond to LMP in order to contain the detrimental consequences of the damage to the cell. The branches of the response have been summarized under the term ELDR and range from signaling that induces *de novo* lysosomal biogenesis, to mechanisms to mediate repair of minor damage or to the clearance of the entire organelle by selective autophagy if the damage is extensive (Papadopoulos, Kravic, and Meyer 2019) (Fig. 1.6).

The biogenesis of new lysosomal proteins is induced by dissociation and thereby inactivation of mTOR from damaged lysosomal membranes (Jia et al. 2018). During basal conditions, mTOR phosphorylates the master lysosomal gene regulator, TFEB, keeping it in the cytosol. Dephosphorylation during lysosomal damage leads to TFEB translocation to the nucleus and subsequent transcription of genes for lysosomal biogenesis and autophagy. TFEB binds to target sequences in the promoters of genes belonging to the Coordinated Lysosomal Expression And Regulation (CLEAR) network. (Settembre et al. 2013) (Fig. 1.6).

Membrane repair is initiated at early steps and low dose treatment after sterile lysosomal damage (not caused by pathogens) and was recently shown to be mediated by the ESCRT machinery (Radulovic et al. 2018; Skowyra et al. 2018). The four consecutive ESCRT complexes 0-III have well described functions in endosomal sorting of proteins to lysosomes in that they trigger the formation of intraluminal vesicles on endosomal membranes (Hurley 2015). Components of these complexes also act in repair of plasma or lysosomal membranes, both induced by Ca^{2+} influx

(Vietri, Radulovic, and Stenmark 2020). During low levels of endolysosomal damage, the release of Ca^{2+} activates the lipid binding activity of the ESCRT III binding protein ALG-2 Interacting Protein (ALIX) in an ubiquitin independent manner. This leads to an instant recruitment of the complex to lysosomal membranes and their repair (Skowyra et al. 2018). Repair of small holes in different membranes is apparently executed by the same ESCRT members. While plasma membrane repair involves shedding of the damaged membrane patch, the exact mechanism of sealing of lysosomal membranes is not known yet (Vietri, Radulovic, and Stenmark 2020). Hence, at low levels of damage, lysosomes are re-acidified (Repnik et al. 2017). Additionally, the Heat Shock Protein 70 (Hsp70) counteracts LMP by stabilization of the Acid Sphingomyelinase (ASM) on lysosomal membranes to balance lipid composition (Kirkegaard et al. 2010) (Fig. 1.6).

Lastly, severe lysosomal membrane damage triggers autophagic clearance, called lysophagy (Hung et al. 2013), which will be described in detail in the next section.

1.4.3 Lysophagy

If damage is extensive, lysosomes are directed towards complete degradation by lysophagy (Fig 1.6). A critical role in this triage are thought to be played by cytosolic lectins, termed galectins (i.e. Galectins (Gal)-1, 3, 8 and 9). Galectins sense extensive damage because it allows influx into the lumen of the lysosomes due to the damage and binding of β-galactosides in the glycocalyx at the inner lysosomal membrane (Maejima et al. 2013) (Fig. 1.6). Due to this property, Gal3 is also used as a convenient marker to visualize endolysosomal damage (Aits et al. 2015; Maejima et al. 2013). It has emerged that galectins possess important recruiting functions, representing the first step towards clearance of damaged lysosomes (Papadopoulos and Meyer 2017). For example, Gal3 influx induces accumulation of Tripartite Motif Family 16 (TRIM16) on lysosomal membranes, leading to subsequent recruitment of the autophagy machinery on chemically damaged lysosomes or after *M.tuberculosis* infection (Chauhan et al. 2016). Similarly, localization of Gal8 to *Salmonella* containing vesicles serves as a signal for NDP52 recruitment and induction of autophagy (Thurston et al. 2012). Moreover, a recent study reports a role for Gal8 and Gal9 in the control of mTOR activity in context with lysosomal damage. Gal8 inhibits mTOR while Gal9 activates AMPK, both leading to efficient activation of the autophagic machinery (Jia et al. 2018).

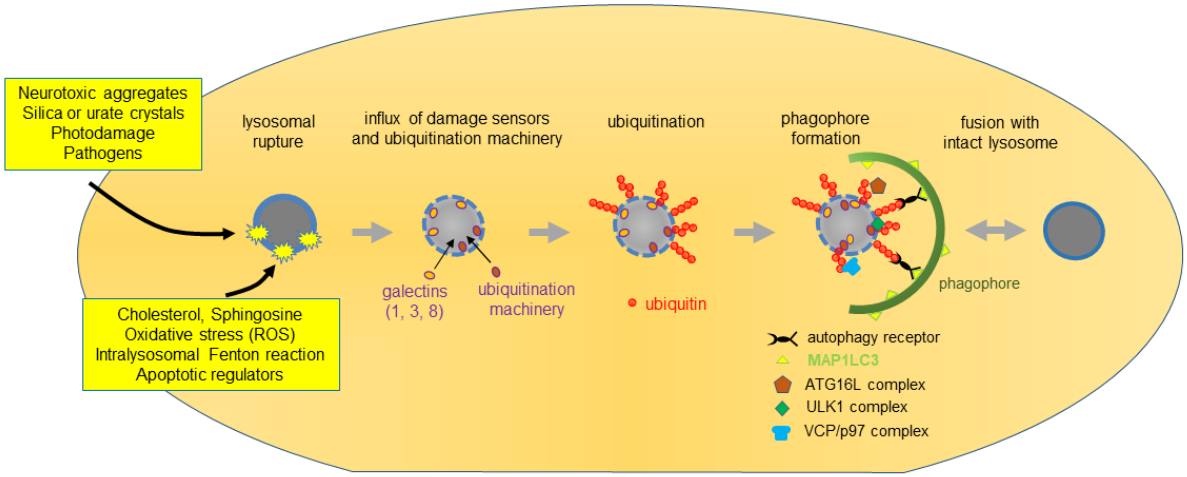

Figure 1.7: Critical steps in lysophagy.
Internal or external stimuli damage lysosomal membranes. This is sensed by cytosolic galectins that bind to exposed β-galactosides on the exposed inner membrane. Extensive ubiquitination with specified linkage types leads to recruitment of a p97 complex, autophagy adaptors and finally the whole autophagic machinery. By this, formation of an autophagosome is ensured and fusion with an intact lysosome completes the autophagic degradation of the damaged organelles. Adopted from (Papadopoulos, Kravic, and Meyer 2019).

The central event in lysophagy is the extensive ubiquitination of lysosomal membrane proteins (Fig. 1.7). Several E3 ligases have been described to contribute to this. The F-box protein FBXO27, which represents a substrate binding component of the S-Phase Kinase-associated Protein 1 (SKP1)/Cullin (CUL)/F-box (SCF) CRL, is myristoylated upon lysosomal damage. This allows translocation to membranes and subsequent binding to β-galactosides on damaged membranes and ubiquitination of the LAMP1 and LAMP2 (Yoshida et al. 2017). The E3 ligase Leucine Rich Repeat And Sterile Alpha Motif Containing 1 (LRSAM1) was reported to be essential for autophagy of *S.thyphimurium* but it is not yet clear whether it ubiquitinates endolysosomal components (Huett et al. 2012b). TRIM16, as mentioned above, is essential for lysophagy by providing a recruiting platform of ubiquitination (Chauhan et al. 2016). However, in contrast to other TRIM proteins, TRIM16 does not possess itself a RING domain and (Bell et al. 2012).

So far, ubiquitin linked via K63 and K48 was found on damaged lysosomes in several studies using different measures to induce the damage (Papadopoulos and Meyer 2017). The different linkage types seem to have specific signaling functions in this process. The conjugation of K63-linked ubiquitin signals towards recruitment of the autophagy receptor p62, as it is common in selective autophagy (Rogov et al. 2014; Papadopoulos et al. 2017). A recent study of the laboratory showed that K48-linked

chains are present on chemically damaged lysosomes at later stages during the response (Papadopoulos et al. 2017). They are recognized by p97, which binds together with its cofactors YOD1, UBXD1 and PLAA (Fig. 1.6). YOD1 is a DUB (described in section 1.1.2.2) and mediates ubiquitin binding of the complex. Furthermore, it might assist in cleaving the K48-chains from target proteins. Removal of these chains is necessary for efficient recruitment of LC3 to damaged lysosomes. Hence, the formation of the autophagosome and the final clearance of damaged lysosomes is dependent on p97 and its designated adaptor proteins (Papadopoulos et al. 2017) (Fig. 1.7). Most probably, p97 has a similar role here as in mitophagy, where it extracts K48-labelled proteins from the membrane in order to facilitate autophagic clearance (Papadopoulos and Meyer 2017). Recent studies demonstrate impaired lysophagy and lysosomal homeostasis as features of MSP1 (Papadopoulos et al. 2017; Arhzaouy et al. 2019). This further underlines p97's role in maintenance of lysosome integrity. It has remained elusive what enzymes of the ubiquitination machinery drive this specified ubiquitination and what are the lysosomal target proteins. (Papadopoulos and Meyer 2017). Identification of involved enzymes will be important in the future to understand the essential signaling steps that follow lysosomal damage.

1.5 The aims of the thesis

The motivation for this study was the finding that the ubiquitin-directed segregase p97 plays crucial roles in the removal of ubiquitin chains from damaged lysosomes and that this was necessary for their subsequent autophagic degradation. This highlighted the importance of ubiquitination in endolysosomal damage response and suggested a sophisticated signaling pathway that is initiated by p97 recruitment to polyubiquitin on the damaged organelles.

The primary goal of this PhD thesis was to shed light on the regulation of ubiquitination that signals towards lysophagy by identifying relevant enzymes of the ubiquitination cascade. To achieve this, we first aimed to establish and to employ a siRNA-mediated screen to identify E2 enzymes in the context of lysophagy.

After identification of UBE2QL1 as the most promising hit, the next goal was to dissect its distinct functional relevance and its position in the ELDR signaling cascade by: (1) verifying an influence of UBE2QL1 on the autophagic clearance of damaged lysosomes, (2) investigating the putative co-operation with p97 and the ELDR components, (3) identifying the chain type specificity of UBE2QL1-mediated ubiquitination on lysosomes and its functional consequences and (4) finding potential target proteins on lysosomal membranes.

We further aimed to evaluate general functions for UBE2QL1 independent of induced lysosomal stress situations in order to gain hints as to its physiological roles and potential involvement in pathologic conditions.

2 Results

2.1 A microscopy based siRNA screen for E2-conjugating enzymes identifies UBE2QL1 to ubiquitinate lysosomes after damage

Ubiquitination of lysosomal membranes upon their damage is a hallmark of the cellular response (Fujita et al. 2013) and a prerequisite to induce efficient autophagic clearance of the organelles (Papadopoulos et al. 2017; Shaid et al. 2013). This in turn ensures cellular survival after lysosomal stress. To date, the enzymes of the ubiquitin machinery that take part in these essential modification steps are poorly investigated. The first aim of this study was to screen for E2-conjugating enzymes that are involved in ubiquitination of lysosomes after damage.

2.1.1 Setup of the screen

Ubiquitination of lysosomes can be demonstrated by co-immuno-fluorescent staining for the lysosomal membrane protein LAMP1 and with antibodies specific for polyubiquitin in general (FK2) or ubiquitin chains linked via lysine 48 (K48-chains). This ubiquitination on lysosomes was shown by us and other laboratories to have specific signaling functions (Fujita et al. 2013; Papadopoulos et al. 2017; Huett et al. 2012a; Radulovic et al. 2018). Using these markers and subsequent confocal laser-scanning microscopy, lysosomes and their colocalization with ubiquitin can be visualized. Automated quantitative image analysis was accomplished using the open-source software CellProfiler, with which it was possible to detect cells and cellular structures in high resolution images, as well as potential overlaps, in an intensity-based manner (Carpenter et al. 2006). As a model for lysosomal damage, we used the lysosomotropic agent LLOMe. LLOMe specifically targets only lysosomal membranes, as it is polymerized and condensed by the lysosomal protease dipeptidyl peptidase I (Cathepsin C) into its membranolytic form (Thiele and Lipsky 1990; Uchimoto et al. 1999; Repnik et al. 2017). As a control treatment we used Ethanol (EtOH) as vehicle alone, as LLOMe was solved in EtOH (depicted as ‘untreated’). We showed in a previous study that K48-chains on lysosomes peaked after 1 h of LLOMe treatment followed by 2 h chase upon washout of the drug (Papadopoulos et al. 2017). To set up the screen, the treatment had to be optimized, as washing steps in a multi-well format should be avoided. We therefore tested if the ubiquitination of lysosomes was comparable after 3 h continuous treatment with LLOMe. HeLa cells were fixed, stained

and analyzed as explained above. Indeed, around 60% of lysosomes colocalized with vesicles positive for FK2 or K48-chains upon damage in this condition (Fig. 2.1A). We therefore decided to use this assay as a readout for the siRNA screen conducted in this study.

To identify E2-conjugating enzymes that are involved in ubiquitination after LLOMe treatment, we made use of reducing their gene expression in cells using Ribonucleic Acid (RNA) Interference (RNAi). Small Interfering RNAs (siRNAs) are designed complementary to messenger RNAs (mRNAs), that are consequently cleaved by specified enzymes to impair gene expression (Hannon 2002). For the screen, a siRNA library targeting 37 human E2-conjugating enzymes individually was pipetted automatically in quadruplicates to 384-well plates for transfection of HeLa cells for 72 h. Subsequently, lysosomal damage was induced by treatment with LLOMe for 3 h. Following staining for the described markers and automated image acquisition with an Opera spinning disk confocal microscope, LAMP1 and ubiquitin signals were detected automatically using the Acapella software and colocalization was determined. Based on the percentage of ubiquitinated lysosomes per cell, robust z-scores were calculated for each sample against the whole plate. We selected this measure of sample-based normalization for reliable hit selection because it is insensitive to expected strong hits, that would be considered as outliers, in comparison to other measures (Birmingham et al. 2009). A robust z-score of ≤ -2 was set as a threshold for significant reduction in lysosomal ubiquitination (Fig. 2.1B).

Next, a stringent analysis pipeline was developed to identify candidates among the 37 E2 enzymes. We decided for a multi-step screening process. In a primary screen, the library of pools of four siRNAs was used and hits that significantly reduced ubiquitination in one of the readouts, FK2 or K48-chains on lysosomes, were selected. They were then re-screened in a secondary screen using the single siRNAs from the pools. At this step, knock-downs of E2 enzymes had to significantly decrease ubiquitination in both stainings to be considered as candidates. As a last step, for functional validation, the positively filtered candidates were investigated for their potential colocalization with lysosomes (Fig. 2.1C).

2.1.2 The screen identifies three candidates

For the primary screen, the siRNA library and siRNAs serving as controls were transfected, stained and analyzed as described above. We used controls that should

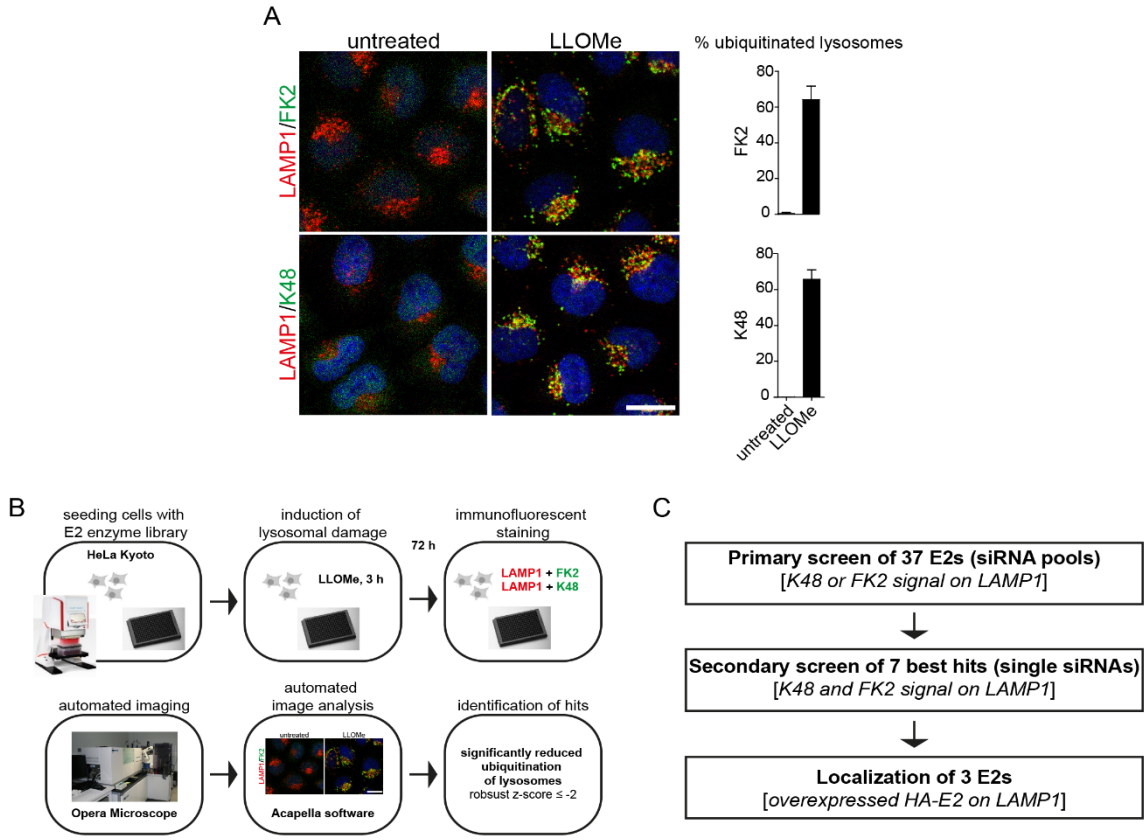

Figure 2.1: A microscopy-based siRNA screen to identify human E2 enzymes involved in ubiquitination in lysosomal damage.

(A) Detection of ubiquitination of lysosomes after LLOMe treatment. HeLa cells were treated with 250 µM LLOMe or vehicle alone (EtOH, untreated), for 3 h and stained with antibodies specific for LAMP1 and pan-polyubiquitin (FK2) or K48-linked ubiquitin chains, respectively. Samples were imaged by confocal laser scanning microscopy and LAMP1 and ubiquitin-positive vesicles were detected automatically using CellProfiler. Graphs show the percentage of lysosomes positive for FK2 or K48-chain signal per cell. Results are from three independent experiments with more than 50 cells per condition. Scale bar, 20 µm. **(B)** Overview of the different steps of the screen **(C)** Schematic overview of the three-step screening process.

not change the ubiquitination status of lysosomes and those that were expected to upregulate lysosomal ubiquitination upon damage to confirm that significant changes could be detected by this method. Transfection with non-targeting siRNA (siCtrl) did not cause any significant change in both stainings (Fig. 2.2A and B). In contrast, depletion of the autophagy genes ATG5 and ATG7 led to increased general ubiquitination of lysosomes, as detected with the FK2 antibody (Fig. 2.2A). This was expected because ubiquitinated organelles are not efficiently degraded and accumulate in cells with impaired autophagy (Maejima et al. 2013). The siRNA pool targeting UBE2J1 scored significantly in both stainings, while UBE2Q2 scored only in the FK2 staining and UBE2D1, UBE2D2, UBE2E1, UBE2L6 and UBE2QL1 exceeded the threshold for K48-chains (Fig.2.2A and B). These seven E2 enzymes were

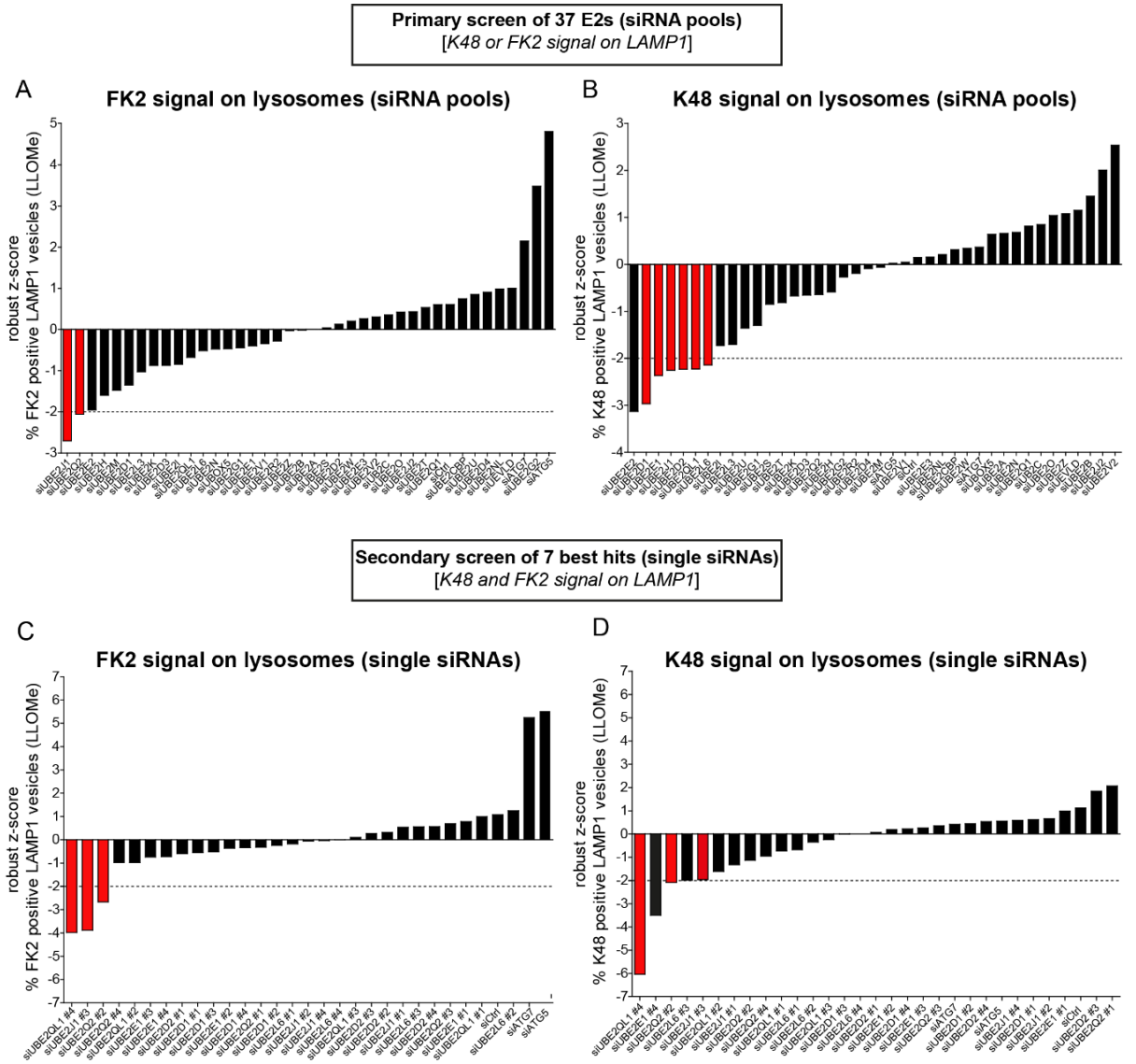

Figure 2.2: The screen reveals three candidates.

(A, B) HeLa cells were transfected with a library of siRNA pools targeting the indicated 37 human E2 enzymes or controls for 72 h in quadruplicates in 384-well plates. Cells were treated and stained as in Fig. 1A and imaged automatically with a scanning disk confocal microscope. Automated image analysis was carried out using the Acapella software. Co-localization between LAMP1 and FK2 (A) or K48-chain (B) signals was determined and robust z-scores for the percentage of ubiquitin-positive lysosomes for each sample against the whole plate were calculated. Exceeding a threshold of a robust z-score of ≤ -2 for either FK2 or K48-chain staining was considered as a significant reduction of lysosomal ubiquitination (highlighted in red). The primary screen revealed seven candidates. **(C, D)** Deconvolution of the primary screen. HeLa cells were transfected with four single siRNAs (#1-4) from the pools of the candidates of the primary screen as in (A, B) and were treated and analyzed as in (A, B). Three knock-downs showed a robust z-score of ≤ -2 in both stainings and these E2 enzymes were considered as candidates in the secondary screen (highlighted in red).

therefore selected as hits from the primary screen and were taken into consideration for the secondary screen. UBE2E2 also scored in the K48-chain staining. However, it was considered as false-positive because experiments from our collaborators already

revealed an inefficient depletion of its expression with this siRNA pool (Behrends laboratory, data not shown). Notably, knock-down of UBE2V2 and UBE2J2 showed significantly increased lysosomal ubiquitination for K48-chains and UBE2G2 for FK2 (Fig. 2.2A and B, robust z-score ≥ 2). This indicated a role in general autophagy, as the ubiquitin-marked organelles seemed to accumulate in these conditions, comparable to the autophagy controls. The present study however focused only on factors directly ubiquitinating lysosomal proteins and thus leading to a decreased signal in this screen. Therefore, these E2-conjugating enzymes were not further characterized here.

For robust candidate selection and to reduce the risk for false positives, the seven identified hits were re-screened using the four individual siRNAs comprising the siRNA pools investigated in the primary screen. Single siRNAs were subjected to the same experimental pipeline and analysis procedure as for the primary screen. Again, siCtrl did not significantly affect lysosomal ubiquitination whereas impairing autophagy by knock-down of ATG5 and ATG7 led to a significant increase in general ubiquitin on lysosomes, as expected (Fig.2.2C and D). E2 enzymes were considered as final candidates of the screening process if a single siRNA scored in both stainings with a robust z-score ≤ -2 in the secondary screen. This was true for UBE2J1, UBE2QL1 and UBE2Q2 (Fig. 2.2C and D), which narrowed down the number of candidates to three.

For further candidate validation, the first step was to transfer the experimental setup to the single-well format. For this purpose, HeLa cells were seeded on coverslips and transfected with the individual siRNAs that scored in the secondary screen targeting the three candidates, co-stained immuno-fluorescently with FK2 and LAMP1 antibodies and imaged manually with a confocal laser scanning microscope. In image analysis with the CellProfiler software, LAMP1 and FK2 positive vesicles were identified and their colocalization was determined. As seen before, FK2 on LAMP1-positive structures dramatically increased after 3 h of LLOMe treatment in control cells (Fig. 2.3A), visualizing the ubiquitination of lysosomal proteins after damage. LAMP1 vesicles were again significantly less ubiquitinated when UBE2J1, UBE2Q2 and UBE2QL1 were depleted from the cells with the single siRNAs from the secondary screen (Fig. 2.3A and B), with UBE2Q2 having the least effect.

We were able to set up a screening approach that revealed three out of 37 E2 enzymes whose siRNA-mediated depletion significantly reduced ubiquitination of lysosomes

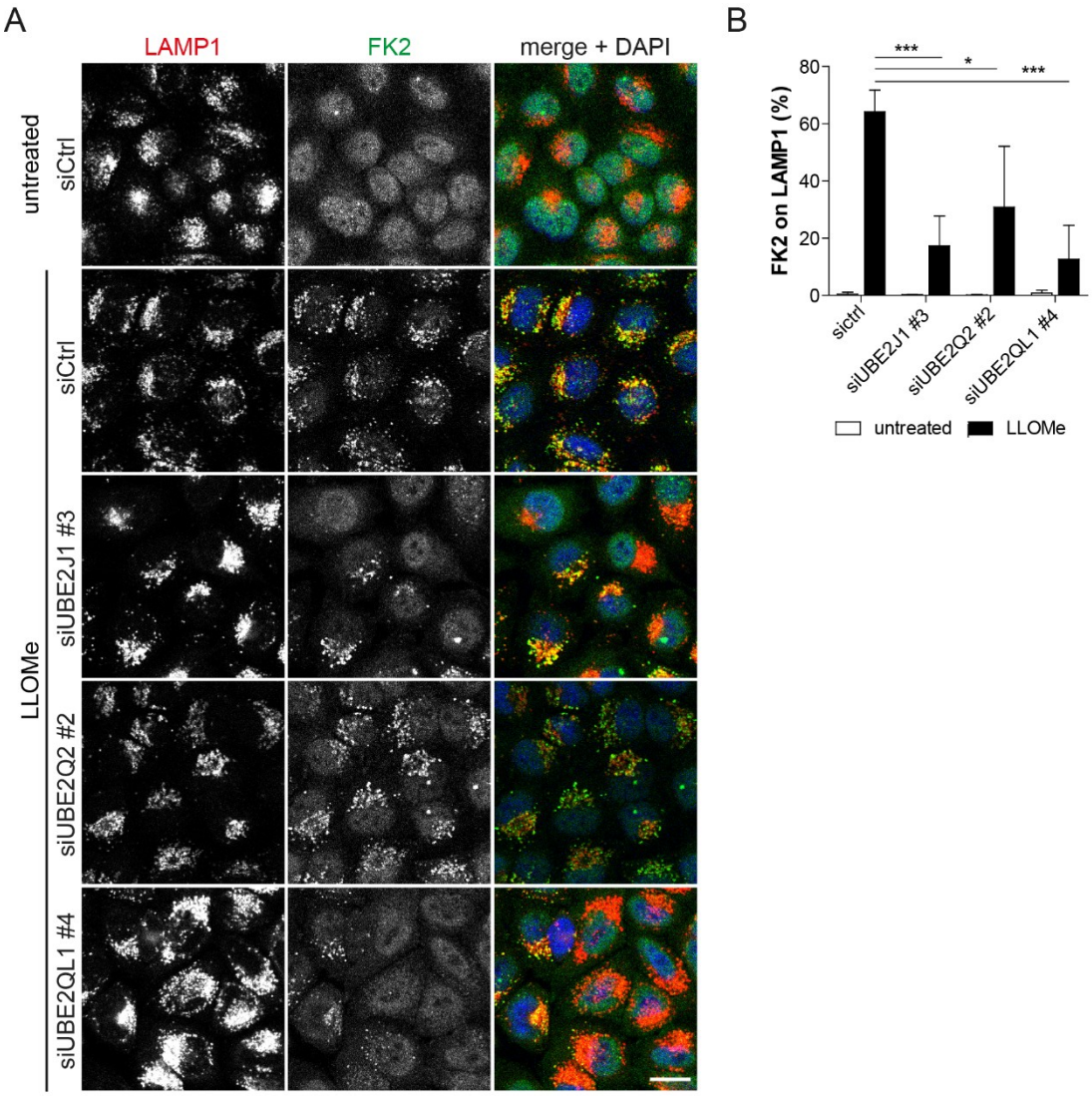

Figure 2.3: Validation of the effect of the candidates on lysosomal ubiquitination after damage.

(A) Lysosomal ubiquitination after induction of damage. HeLa cells were transfected with the indicated single siRNAs from the screen in a single-well format for 72 h and treated with 250 µM LLOMe or EtOH (untreated) for 3 h. LAMP1 and pan-ubiquitin (FK2) were visualized with specific antibodies using a confocal laser scanning microscope. Scale bar, 20 µm. **(B)** Quantification of cells in (A). LAMP1 and FK2 vesicles and their overlap was automatically determined using CellProfiler. Shown is the percentage of lysosomes positive for ubiquitin signal. The graph represents results from three independent experiments with 50 or more cells per condition (mean +SD). *P<0.5; ***P<0.001 (One-way ANOVA with Bonferroni's multiple comparison test).

after LLOMe-treatment. Interestingly, UBE2J1 has been linked to p97 in another cellular signaling pathway before (Burr et al. 2013). It is an ER-transmembrane protein that together with the E3 ligase HRD1 and its adaptor subunit Suppressor/Enhancer of LIN-12-Like (SEL1L) labels substrates, such as Major Histocompatibility Complex Class I Heavy Chains (MHC I HCs), for ER-associated degradation mediated by p97 (Burr et al. 2013). UBE2QL1 and UBE2Q2 are members of the UBE2Q-family. Both

have reported aberrant expressions in diverse cancer cells (Shafiee et al. 2014; Seghatoleslam et al. 2006; Wake et al. 2013) and UBE2Q2 was found to function in prophase during mitosis (Banerjee, Brooks, and Crawford 2007).

2.1.3 Localization of overexpressed UBE2QL1 to lysosomes after damage

Previous work from our laboratory showed that factors involved in ELDR, such as p97 and its co-factors, acutely and robustly translocate to lysosomes when damage is induced (Papadopoulos et al. 2017). It was therefore suggested that E2 enzymes ensuring upstream ubiquitination might also localize to the damaged organelles. Hence, to further validate the function of the candidates identified here, we aimed to investigate their cellular localization in unchallenged and LLOMe-treated cells. For this purpose, cDNA encoding for Human Influenza Hemagglutinin (HA)-tagged versions of the enzymes was transfected in HeLa cells to detect the proteins with an HA-specific antibody and co-staining for LAMP1. For HA-UBE2J1, we could confirm the reported localization to the ER (Lenk et al. 2002), which did not change upon induction of lysosomal damage (Fig. 2.4A). HA-UBE2Q2 was distributed throughout the cytosol and the nucleus and HA-UBE2QL1 was found in the cytosol in untreated cells. While HA-UBE2Q2 localization remained unchanged in LLOMe-treated cells, HA-UBE2QL1 acutely translocated to LAMP1-positive structures when cells were treated with LLOMe (Fig. 2.4A). As a measure for colocalization, Pearson's Correlation Coefficient (P.C.C., from now on called correlation) between HA and LAMP1 signals on LAMP1 structures was automatically determined using the CellProfiler software. It was significantly increased as compared to untreated cells (Fig. 2.4B). The translocation of HA-UBE2QL1 to the organelles was specific for lysosomal damage, since we could show that depolarization of mitochondria by treatment with Carbonyl cyanide 3-chlorophenylhydrazone (CCCP), leading to their ubiquitination, did not affect the cytosolic localization of UBE2QL1 (done by Bojana Kravic) (Koerver et al. 2019).

Thus, of the three identified candidates leading to a decreased ubiquitination, only the overexpressed, HA-tagged version of UBE2QL1 localized to lysosomes upon damage, implicating a potential function in ELDR. UBE2QL1 was therefore chosen for detailed characterization and functional analysis in this pathway.

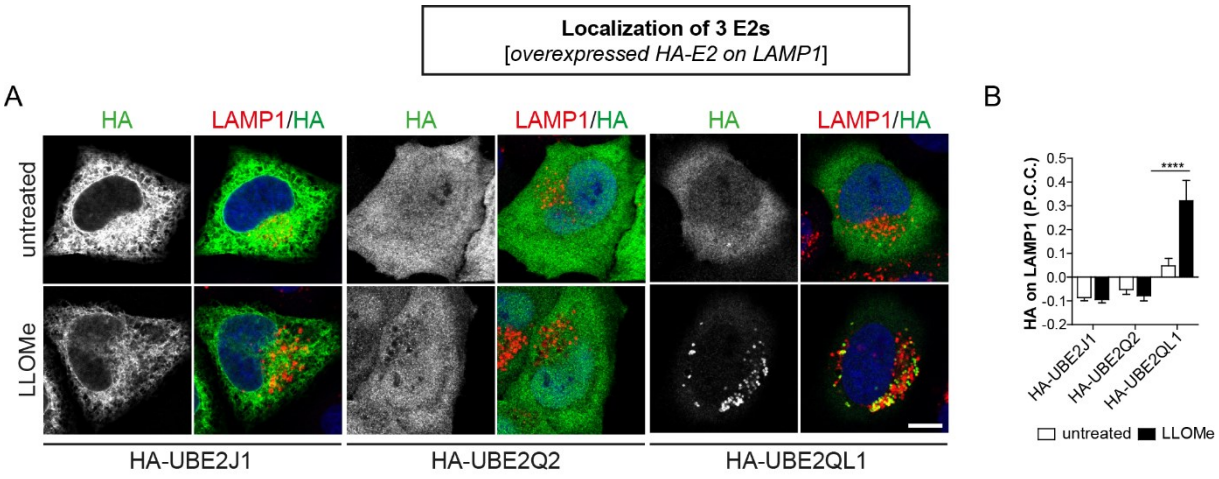

Figure 2.4: Localization of the candidates after LLOMe treatment.
(A) HeLa cells were transfected with cDNA encoding for N-terminally HA-tagged versions of for 3 h. After fixation, samples were stained with antibodies recognizing HA and LAMP1 and imaged by laser scanning confocal microscopy. Scale bar, 10 µm. **(B)** Quantification of cells in (A). Using CellProfiler software, images were automatically analyzed to calculate the Pearson's Correlation Coefficient (P.C.C.) of HA and LAMP1 signals per cell. The Graph represents data from three individual experiments with more than 30 cells per condition (mean +SD). ****P<0.0001 (One-way ANOVA with Bonferroni's multiple comparison test).

2.2 Generation of an UBE2QL1-specific antibody for investigation of the endogenous protein and verification of siRNA effects

UBE2QL1 is so far poorly characterized. It has only recently been annotated and described to share homology with E2-conjugating enzymes and to possess an active site cysteine (Wake et al. 2013). Decreased expression of UBE2QL1 was found in familial forms of Renal Cell Carcinomas (RCC) and it was suggested to function as a potential tumor suppressor gene in RCC cells (Wake et al. 2013). There is no antibody reported to detect the endogenous protein. For further analysis, it was necessary to verify knock-down efficiencies of the used siRNAs and to confirm the localization of overexpressed UBE2QL1 for the endogenous protein. Therefore, we raised an antibody against UBE2QL1 in rabbit.

2.2.1 Establishing the detection of endogenous UBE2QL1 in cell lysates

The UBE2QL1 mRNA consists of only two exons and a large intron (not depicted here) and 3' untranslated region (UTR). The siRNAs from the screen that affected lysosomal ubiquitination, siUBE2QL1 #2 and #4 both target the 3'UTR (Fig. 2.5A). We designed an additional siRNA (siUBE2QL1 #5) that binds the Coding Sequence (CDS) (Fig. 2.5A). The UBE2QL1 protein exhibits the typical and UBC domain at the N-terminus

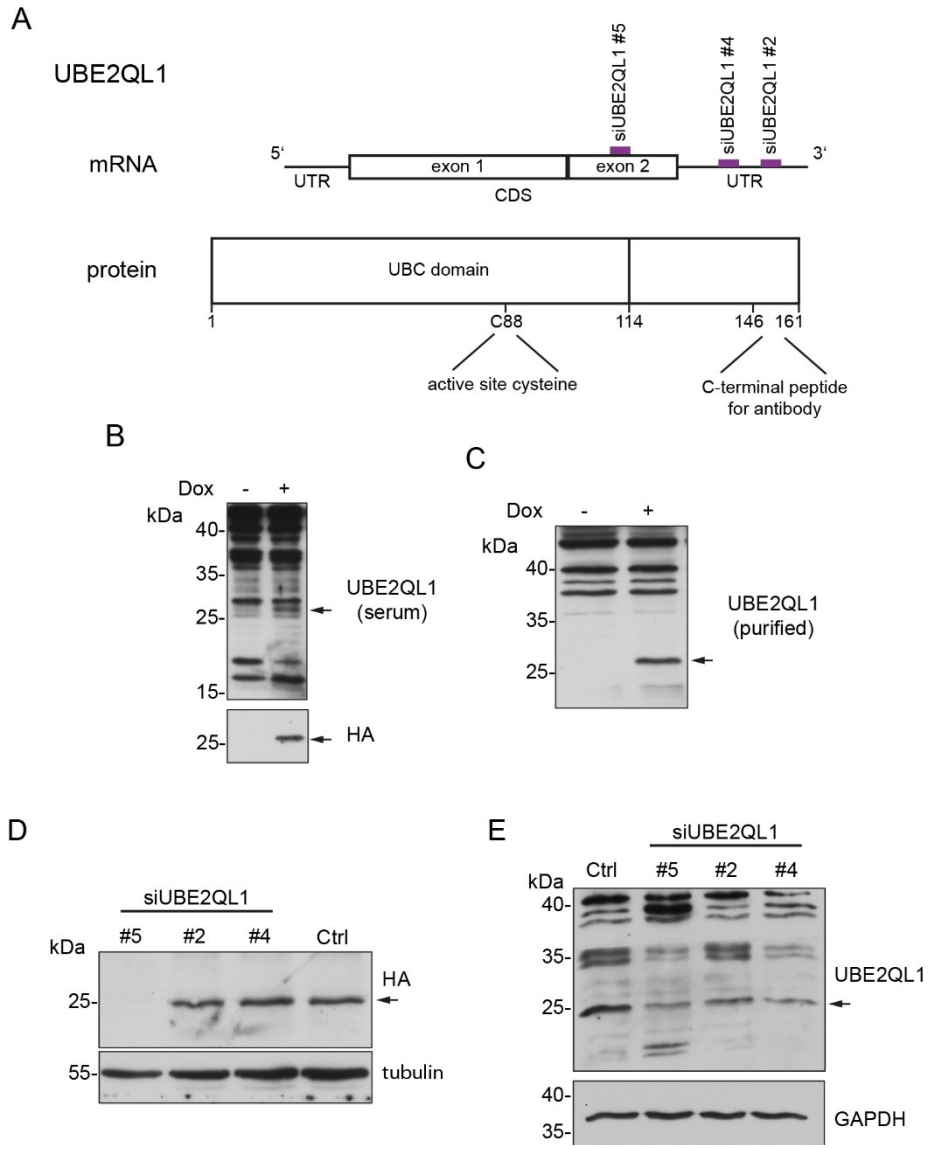

Figure 2.5: A UBE2QL1 antibody confirms expression in HeLa cells and siRNA efficiency.

(A) Scheme of UBE2QL1 mRNA and protein. Positions of siRNAs complementary to the mRNA coding sequence (CDS) or untranslated region (UTR) are depicted. The ubiquitin-conjugtion (UBC) domain of the UBE2QL1 protein, the active site cysteine at position 88 and region of the peptide used for immunization for generation of the antibody are indicated. **(B)** The antibody against UBE2QL1 recognizes the overexpressed protein in cell lysates. The expression of UBE2QL1-HA in stable HeLa FRT cells was induced with 1 µg/ml doxycyline for 24 h and cells were lysed in extraction buffer and analyzed by Western blot using an HA antibody or the rabbit serum immunized with the UBE2QL1 peptide. The band corresponding to UBE2QL1-HA is indicated. **(C)** Stable HeLa FRT cells were treated and lysed as in (A) and were probed with the antibody purified from the serum after Western blotting. Arrows indicate the band specific for the HA-tagged UBE2QL1. **(D)** Stable HeLa FRT cells were transfected with indicated siRNAs against UBE2QL1 for 72 h. In the final 24 h, expression of UBE2QL1-HA was induced with 1 µg/ml doxycyline. Cells were lysed in extraction buffer and analyzed by Western blotting using an antibody specific for HA. Tubulin was probed as a loading control. The position of UBE2QL1-HA is indicated. **(E)** HeLa cells were transfected with the siRNAs from (D) and were harvested after 72 h and homogenized with a dounce homogenizer. Samples were analyzed by Western blot using the UBE2QL1 antibody and GAPDH as a loading control. The band corresponding to endogenous UBE2QL1 is indicated.

and a short C-terminus. An antibody against a C-terminal peptide of UBE2QL1 was raised in rabbit and its specificity was to be determined (Fig. 2.5A). For this, using the Flp/In^{TM} system, HeLa cells with a Flp recombination target site (HeLa FRT) that expressed UBE2QL1-HA under control of a tetracycline repressor (induced with doxycycline) were generated. We first used the full rabbit serum to detect UBE2QL1 by Western blot to compare this with the affinity-purified antibody. Additionally to several unspecific signals, a band was detected at the position where the HA-antibody recognized the overexpressed UBE2QL1-HA at 25 kDa when cell lysates were analyzed by Western blot with the full serum (Fig. 2.5B). However, it was not clearly distinguishable which band corresponded to endogenous UBE2QL1 with an expected size of around 18 kDa (Fig. 2.5B). Affinity-purification improved the staining pattern by strongly reducing the unspecific bands. Although the overexpressed protein was again seen as a clear band, endogenous UBE2QL1 failed to be detected by this approach (Fig. 2.5C).

For verification of the specificity of the siRNAs, stable HeLa cells were transfected with two siRNAs from the library (siUBE2QL1 #2 and #4, with #4 having the best effect in the screen) and the additionally designed siUBE2QL1 #5 (Fig. 2.5A). After induction of expression of UBE2QL1-HA in siRNA-transfected cells, they were lysed and analyzed by Western blotting and stained for the HA tag. As expected, the transfection with siUBE2QL1 #5 led to a reduction in expression of UBE2QL1-HA. In contrast, siUBE2QL1 #2 and #4 did not affect the expression, as they only target the Untranslated Region (UTR), which is not present in the UBE2QL1-HA mRNA (Fig. 2.5D). To prove the depletion efficiencies of siUBE2QL1 #2 and #4 for the endogenous protein, we tried different lysis conditions to optimize the detection of endogenous UBE2QL1 by Western blotting. Mechanical homogenization of cells was identified as the most efficient method to detect a band at the expected size of 18 kDa. This band was strongly reduced by all three siRNAs (Fig. 2.5E, done by Bojana Kravic). By this, we confirmed that siUBE2QL1 #4 was more efficient in depleting the protein than siUBE2QL1 #2, which corresponded to the effects in the screen. siUBE2QL1 #5 showed however an even stronger reduction of the protein.

2.2.2 Rescue of effects of UBE2QL1 siRNA by transient overexpression of the WT and catalytically inactive protein

To exclude that the effects of the siRNAs targeting UBE2QL1 were off-target, a rescue experiment for the readout of ubiquitination of lysosomes after LLOMe treatment in UBE2QL1 depleted cells was established. For this purpose, cells were transfected first with control or UBE2QL1 targeting siRNAs. After 24 h, cDNA encoding Green Fluorescent Protein (GFP) (as control transfection) or UBE2QL1 as WT or catalytically inactive form (C88S) with a C-terminal HA tag was transfected for another 48 h. It was noted that this version of the protein was more efficiently expressed in HeLa cells than the N-terminal tagged protein used before (see Fig. 2.4). SiUBE2QL1 #4 was used here since it targets only the endogenous and not the overexpressed form of the protein (see Fig. 2.5). After induction of lysosomal damage using LLOMe, ubiquitination of lysosomes was monitored in all conditions by staining with FK2 and LAMP1 antibodies and confocal microscopy. The reduction of lysosomal ubiquitination as an effect of siUBE2QL1 #4, in contrast to control depleted cells, which was observed before (Fig. 2.3) could be reproduced under the conditions of GFP transfection (Fig. 2.6A). UBE2QL1 WT and C88S were visualized by staining for the HA tag and localized both to LAMP1 positive structures in control depleted cells when the damage was induced. Importantly, when UBE2QL1 WT was expressed in UBE2QL1 depleted cells, lysosomes were again labeled with ubiquitin in LLOMe-treated conditions (Fig. 2.6A). This was also automatically quantified by measuring the percentage of lysosomes labeled with ubiquitin and setting the control depletion to a value of 100 (Fig. 2.6B). In contrast, the expression of UBE2QL1 C88S did not rescue the effect of the siRNA and lysosomes were still inefficiently ubiquitinated (Fig. 2.6A and B). It was moreover observed, that the recruitment of the mutant protein was less efficient in UBE2QL1 depleted cells (Fig. 2.6A).

The knock-down efficiency and overexpression of UBE2QL1 was confirmed by western blotting for the endogenous protein (done by Bojana Kravic) (Fig. 2.6C).

2.2.3 Establishing the immuno-fluorescent staining for endogenous UBE2QL1

To investigate the cellular localization of endogenous UBE2QL1, we tested the antibody in immuno-fluorescent staining in HeLa cells after treatment with LLOMe and co-stained it for LAMP1 or Gal3 for analysis by laser scanning confocal microscopy. LMP leads to the influx of cytosolic galectins and staining for Gal3 and detection of

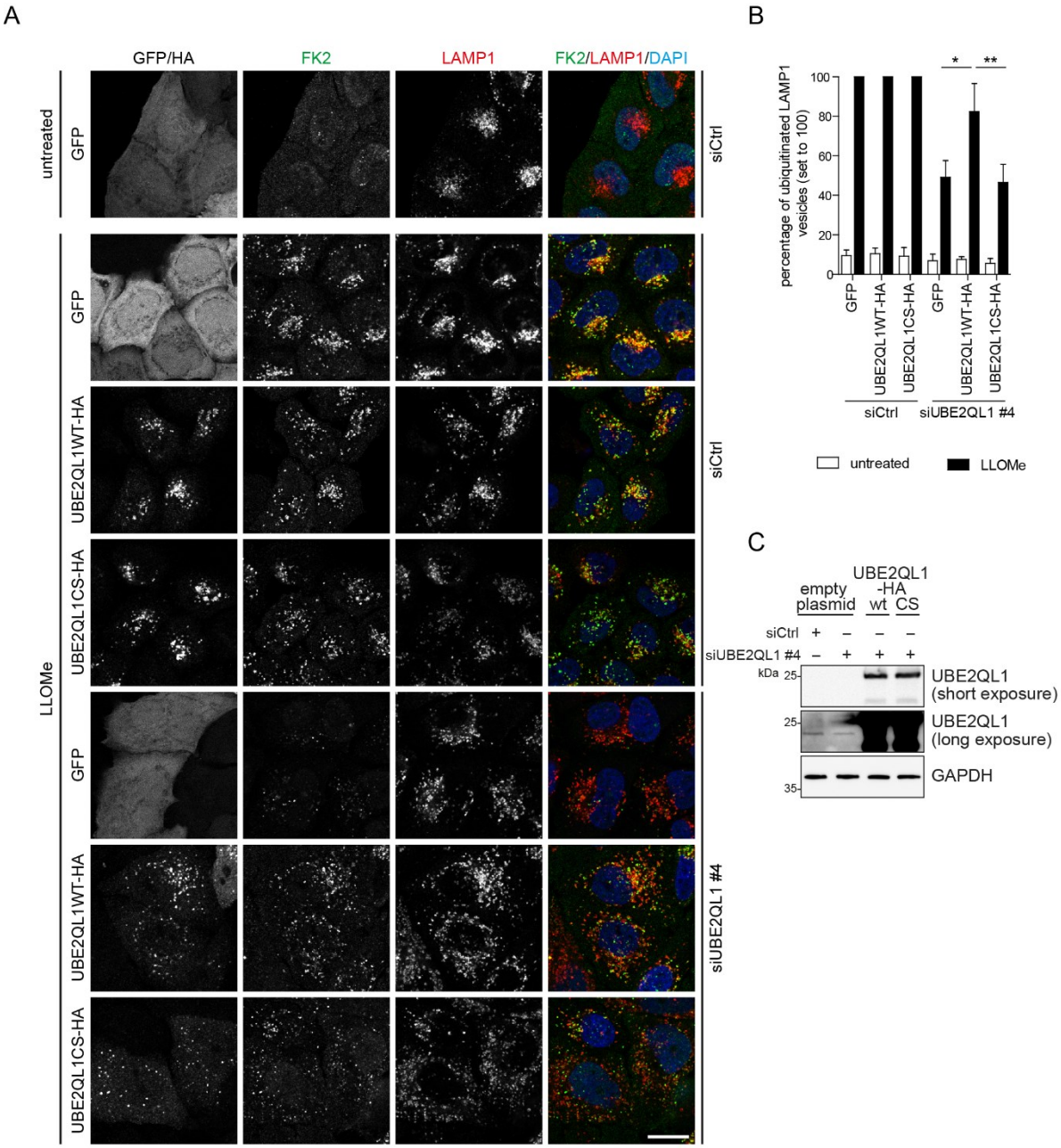

Figure 2.6: Rescue of effects of UBE2QL1 depletion on lysosomal ubiquitination.

(A) Rescue of effects of UBE2QL1 depletion on lysosomal ubiquitination after damage. HeLa cells were transfected with siCtrl or siUBE2QL1 #4 for a total of 72 h. 24 h after beginning of siRNA treatments, cells were transfected with expression plasmids for UBE2QL1 wild-type (WT) or the catalytic inactive mutant C88S (CS) tagged with HA, or GFP alone as control as indicated. Lysosomal damage was induced by 250 µM LLOMe or EtOH alone (untreated) for 3 h. Cells were fixed and processed for immunofluorescence confocal laser microscopy with antibodies specific for the HA tag, polyubiquitin (FK2) and LAMP1. Scale bar, 20 µm. **(B)** Automated quantification of (A). FK2 and LAMP1 vesicles were identified using the Cell Profiler software and the percentage of LAMP1 vesicles that were positive for ubiquitin was determined. The LLOMe-treated siCtrl control was set to 100 % for each type of overexpressed protein. The graph represents data from three independent experiments with ≥ 25 cells per condition (mean ± SD). *P<0.05; **P<0.01 (One-way-ANOVA with Dunnett's multiple comparison test). **(C)** Western blot analysis with UBE2QL1 antibody of indicated samples related to the rescue experiment in (A). Note that the band of endogenous UBE2QL1 is only visible after long exposure. GAPDH was probed as a loading control.

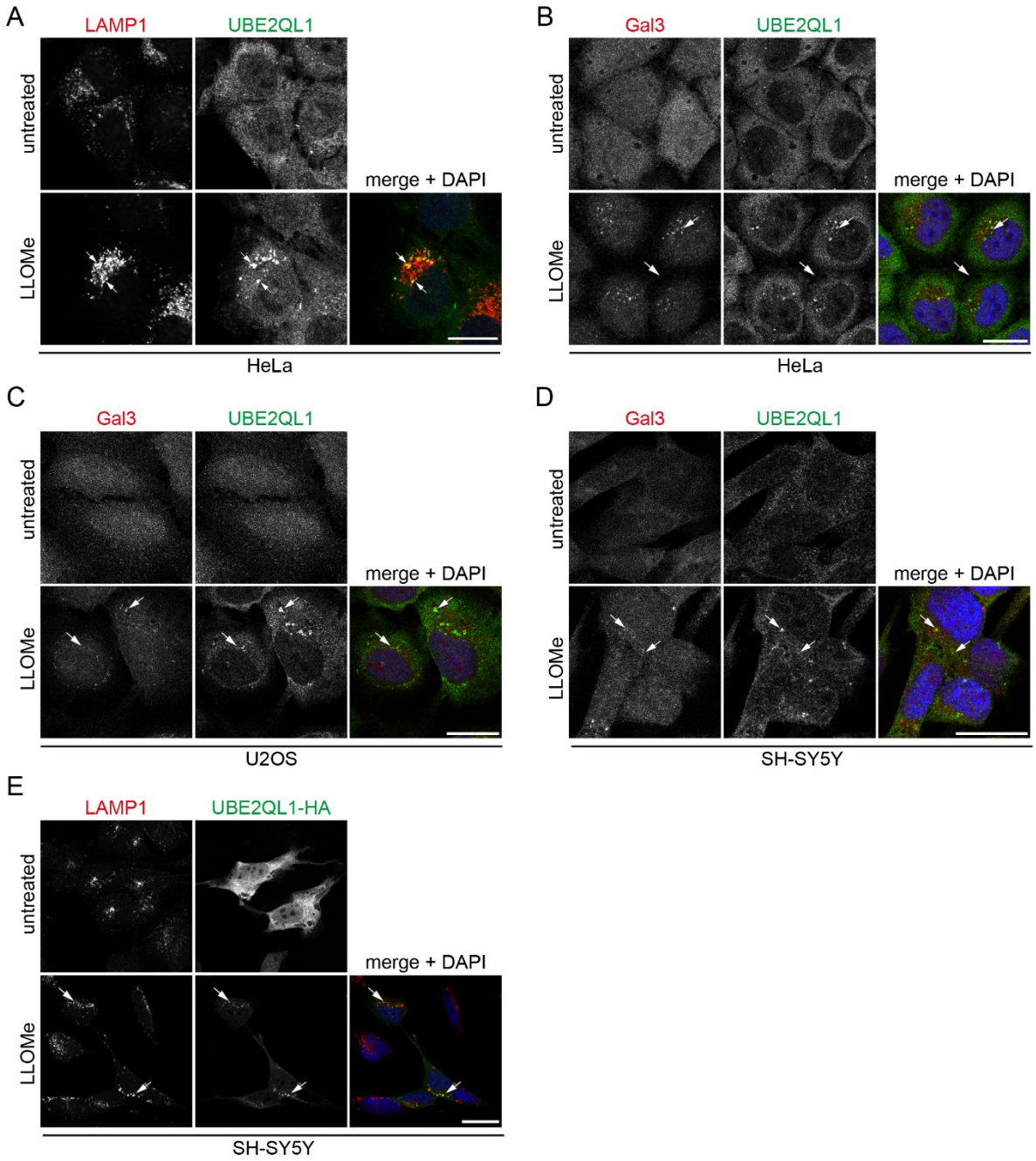

Figure 2.7: Immuno-fluorescence microscopy using the UBE2QL1 antibody in different cell types.

(A) The antibody gives a signal on lysosomes in LLOMe-treated cells. HeLa cells were treated with 250 µM LLOMe or EtOH (untreated) for 3 h and were fixed and stained with antibodies against LAMP1 and UBE2QL1 (purified). Samples were imaged with a confocal laser scanning microscope. Arrows indicate UBE2QL1 on LAMP1 vesicles. Scale bar, 20 µm **(B)** HeLa cells were treated as in (A) and UBE2QL1 was co-stained for Gal3 to visualize co-localization with damaged lysosomes with a confocal laser scanning microscope. Arrows indicate co-localizing vesicles. Scale bar, 20 µm. **(C)** U2OS cells were treated with 500 µM LLOMe for 1 h and stained and imaged as in (B). Scale bar, 20 µm. **(D)** SH-SY5Y cells were treated, stained and imaged as in (A). Scale bar, 20 µm. **(E)** SH-SY5Y cells were transfected with UBE2QL1-HA for 24 h and treated with 1 mM LLOMe for 3 h. UBE2QL1-HA on lysosomes was visualized with antibodies specific for LAMP1 and HA and imaged as in (A). Scale bar, 20 µm.

puncta has been established as a reliable method to visualize and quantify damaged lysosomes by microscopy in cells and organisms (Aits et al. 2015). In untreated cells, the signal of UBE2QL1 was diffuse and cytosolic, with some puncta that were not positive for LAMP1 or Gal3. However, in LLOMe-treated conditions, a clear vesicular signal was detected with the antibody, that colocalized with LAMP1 and Gal3 (Fig. 2.7A and B). This confirms a similar localization of the endogenous and overexpressed protein and thereby underlines the previous results. Importantly, a significant reduction of the specific signal on LAMP1-positive structures was demonstrated when HeLa cells were transfected with the three siRNAs against UBE2QL1 (done by Giulia Rota) (Koerver et al. 2019), confirming the specificity of the antibody and of the siRNAs. To investigate whether UBE2QL1 showed a similar behavior in other cell lines, conditions of LLOMe treatment to detect damaged lysosomes were adjusted in U2OS and SH-SY5Y cells (Fig. 2.7C and D). Importantly, endogenous UBE2QL1 translocated to Gal3-positive vesicles also in U2OS and SH-SY5Y cells when lysosomes were permeabilized (Fig. 2.7C and D). Additionally, the translocation of overexpressed HA-UBE2QL1 to LAMP1 upon lysosomal damage (see Fig. 2.4) was verified also in SH-SY5Y cells (Fig. 2.7E).

We next aimed to improve the staining conditions for the UBE2QL1 antibody. For this, cells were pre-extracted before Parafomaldehyde (PFA)-fixation to reduce the background signal. Pre-extraction with Piperazine-N,N′-bis(2-Ethanesulfonic Acid) (PIPES) solution led to a decreased cytosolic background in HeLa cells treated with LLOMe, while the specific signal on LAMP1-vesicles was maintained (Fig. 2.8A). These optimized conditions were applied for detailed analysis of endogenous UBE2QL1 localization during damage and subsequent clearance of lysosomes. To illustrate this, HeLa cells were treated with LLOMe for 1 h and washed and chased in fresh medium for up to 10 h. Work from our laboratory showed that damaged organelles are cleared at these late time-points (Papadopoulos et al. 2017). The localization correlation of UBE2QL1 and LAMP1 signals strongly increased in comparison to untreated cells at the 2 h time-point, while it gradually decreased again from 4-10 h (Fig. 2.8B and C).

Here we established an antibody to confirm the expression of endogenous UBE2QL1 in HeLa cells and to verify the depletion efficiencies of three siRNAs, which was essential for further characterization of UBE2QL1. Additionally, the data support the

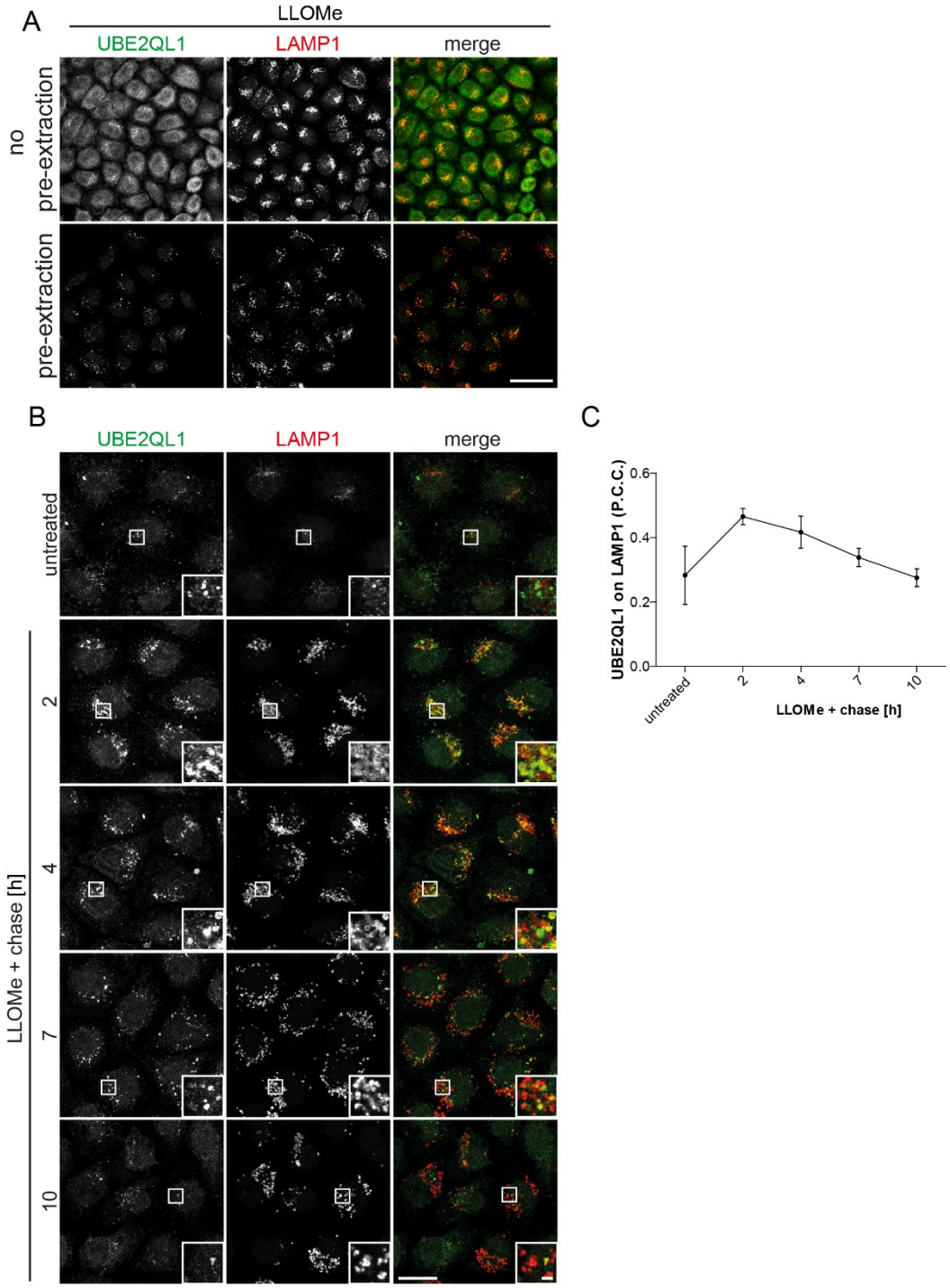

Figure 2.8: Localization of endogenous UBE2QL1 at different time-points after damage.

(A) Pre-extraction reduces background of UBE2QL1 staining. HeLa cells were treated with 250 µM LLOMe for 3 h and fixed with or without pre-extraction. Samples were then stained with antibodies specific for UBE2QL1 and LAMP1 and imaged with a confocal laser scanning microscope. Scale bar, 50 µm. **(B)** UBE2QL1 dissociates from lysosomes when damage is cleared. HeLa cells were treated with 250 µM LLOMe for 1 h. After washout of LLOMe, cells were chased in fresh medium, pre-extracted and fixed at indicated the time-points. Samples were stained and imaged as in (A). Scale bar, 20 µm and 2 µm for inlays. **(C)** Quantification of samples in (A). Using CellProfiler Software, the Pearson's correlation coefficient (P.C.C.) of signals of UBE2QL1 and LAMP1 was measured per cell. The graph represents data from three independent experiments with 20 or more cells per condition (mean +SD).

notion that translocation of endogenous UBE2QL1 is specific for permeabilized lysosomes.

2.3 Regulation of lysophagy by UBE2QL1-mediated ubiquitination

In the previous experiments, it was revealed that overexpressed as well as endogenous UBE2QL1 translocates to lysosomes upon damage (see Fig. 2.4 and 2.8). Previous work from our laboratory dissected the timing of recruitment of the different components involved in the response to lysosomal damage in detail. It was shown that, while K63-linked ubiquitin chains (K63-chains) and the autophagy markers p62 and LC3 arise at 1 h after LLOMe treatment, K48-chains and p97 peaked only after 2 h of chase (Papadopoulos et al. 2017). This points out the functional relationships during the response, as the autophagy adapter p62 is known to be recruited to K63-linked polyubiquitinated substrates (Rogov et al. 2014; Seibenhener et al. 2004), whereas we could show that p97 targets and removes the K48-chains on lysosomes (Papadopoulos et al. 2017). To examine the role of UBE2QL1 during ELDR in more detail, we investigated the described components of the pathway in relation with UBE2QL1 in different assays.

2.3.1 UBE2QL1 emerges on lysosomes together with K48-linked ubiquitin chains

To determine the exact timing of UBE2QL1 recruitment to lysosomes, HeLa cells were transfected with plasmids encoding for UBE2QL1 C-terminally tagged with HA. Cells were treated with LLOMe for 30, 60, 120 or 180 min, mimicking the time-points used in the previous study (Papadopoulos et al. 2017). In the present setup, LAMP1 was always co-stained with HA and additionally either with antibodies specific for K48-chains, K63-chains or p62 and samples were prepared for imaging with a confocal laser scanning microscope. Localization correlations between the signals of LAMP1 and the markers or HA were calculated automatically using the CellProfiler software (Fig. 2.9). Of note, the kinetics of the occurrence of K48-chains, K63-chains and p62 with LAMP1 were comparable to our published data (Papadopoulos et al. 2017). K63-chains and p62 showed some puncta as early as after 30 min treatment and the correlation with LAMP1 signals peaked at 60 min. The correlation of K48-chains and LAMP1 increased from 30 min on but reached a maximum only at 120-180 min (Fig. 2.9A and B). Interestingly, UBE2QL1-HA on lysosomes showed the same temporal appearance as K48-chains. At 30 and 60 min we observed more K63-chains and p62-

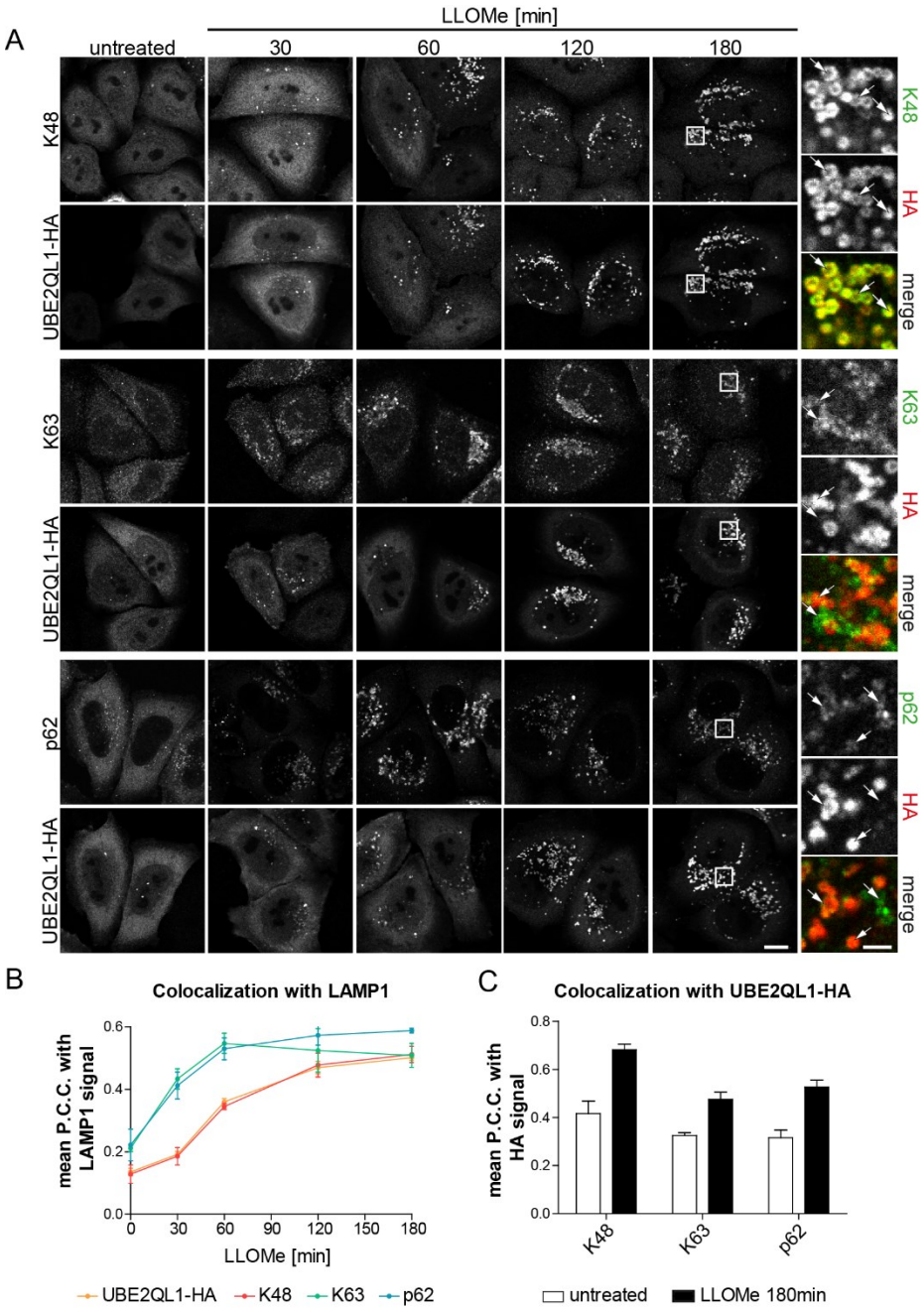

Figure 2.9: Colocalization of UBE2QL1-HA with components of ELDR.

(A) HeLa cells were transiently transfected with UBE2QL1-HA for 24 h and treated with 250 µM LLOMe for indicated times before fixation. HA was co-stained with antibodies for LAMP1 (not shown) and either K48-chains, K63-chains or the autophagy receptor p62. Arrows indicate colocalizing or non-colocalizing vesicles. Scale bar, 10 µm and 2 µm for inlays. **(B, C)** Quantifications of images in (A). Automated quantifications of P.C.C.'s per cell using CellProfiler Software for HA, K48-chains, K63-chains or p62 signals with LAMP1 (B) and HA signals with K48-chains, K63-chains or p62 (C). Graphs represent results from three independent experiments with more than 30 cells per condition (mean +SD).

positive structures on lysosomes than UBE2QL1-HA or K48-chains (Fig. 2.9A). As a next step, we investigated the colocalization between UBE2QL1-HA and the three markers. It was depicted that after 180 min of treatment, all UBE2QL1-HA vesicles

were labelled with K48-chains. In contrast, some, but not all K63-chains and p62-positive structures were decorated with UBE2QL1-HA (Fig. 2.9A). This finding was confirmed by automated quantification of the correlation between HA and K48-chain signals that increased strongly after 180 min treatment as compared to untreated cells, while the increase was milder for the correlation of UBE2QL1-HA with K63-chains or p62, respectively (Fig. 2.9C).

These data show in two lines of evidence that UBE2QL1 emerges on the subpopulation of lysosomes labelled with K48-chains after induction of damage in a spatiotemporal way. First, the kinetics of appearance of K48-chains and UBE2QL1-HA on LAMP1 vesicles highly coincided. Second, the overlap of UBE2QL1-HA with K48-chains after lysosomal damage was much higher than with K63-chains or p62.

2.3.2 UBE2QL1 mediates the formation of K48-chains and K63-chains on lysosomes after damage

Most E2-conjugating enzymes are only fully activated by interaction with an E3 ligase. Still, they can determine the ubiquitin chain type that is formed on the substrate (Stewart et al. 2016; Ye and Rape 2009). Data from the screen only considered K48-chains and total ubiquitination, so that no conclusion could be drawn about effects on K63-chains. Considering the previous result that showed UBE2QL1 colocalizing stronger with K48-chains than with K63-chains, a specificity for this ubiquitin chain type was suggested. To explore this, UBE2QL1 was depleted from cells using one siRNA from the screen and the ubiquitin chain types were visualized by staining with specific antibodies after lysosomal damage induced by LLOMe and co-stained for LAMP1. Again, images were obtained by confocal laser scanning microscopy and LAMP1 and ubiquitin vesicles, as well as their colocalization, were determined using the CellProfiler software (Fig. 2.10). In line with earlier experiments, 60% of the lysosomes were labelled with K48-chains after 3 h of treatment with LLOMe in control cells, which was similar for K63-chains (Fig. 2.10). Consistent with the data from the screen, depletion of UBE2QL1 led to a significant decrease in K48-chain lysosomal ubiquitination. Namely, less than 20% of the LAMP1-positive vesicles were marked with K48-chains (Fig. 2.10A and B). Importantly, a reduction of the signal of K63-chains was also observed and K63-chains on lysosomes were decreased to around 30% (Fig. 2.10A and C). These results were confirmed with a second UBE2QL1 siRNA (#5) by Giulia Rota (Koerver et al. 2019).

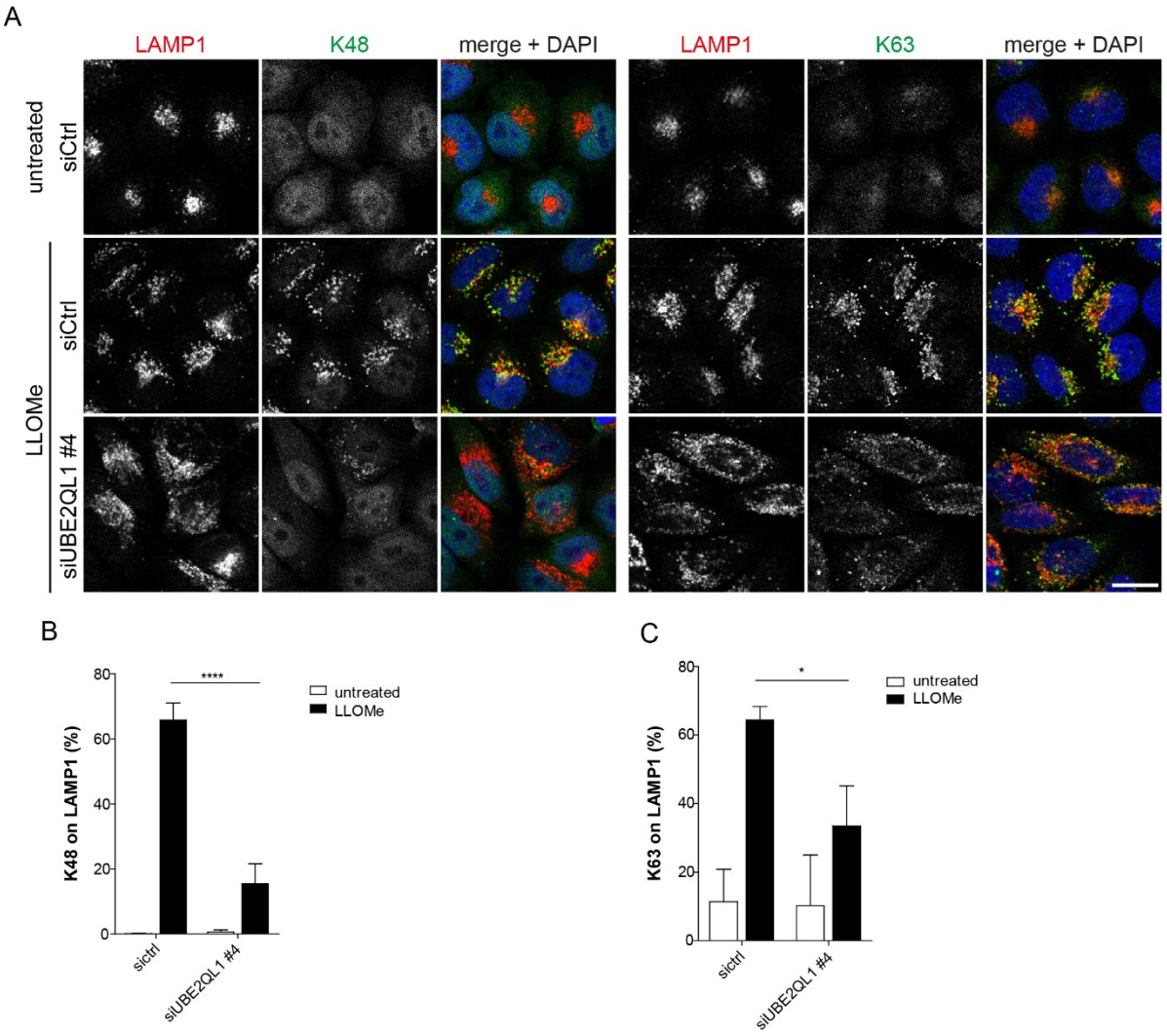

Figure 2.10: UBE2QL1 depletion reduces ubiquitination linked via K48 and K63 on lysosomes after LLOMe treatment.

(A) HeLa cells were depleted for UBE2QL1 for 60 h. To induce lysosomal damage, cells were treated with LLOMe or EtOH (untreated) for 3 h. After fixation, cells were stained with antibodies specific for LAMP1 and K48-chains or K63-chains and imaged by confocal laser scanning microscopy to visualize lysosomal ubiquitination. Scale bar, 20 µm. **(B, C)** Quantification of cells in (A). Using CellProfiler Software, LAMP1 and K48-chain or K63-chain positive vesicles were identified and their co-localization was determined automatically. Shown is the percentage of ubiquitinated lysosomes. Graphs represent data from three independent experiments with 50 or more cells per condition (mean +SD). *P<0.05; ****P<0.0001 (One-way ANOVA with Bonferroni's multiple comparison test).

Consistent with data from the screen and the colocalization of UBE2QL1 and K48-chains on lysosomes, we confirmed here the effect of depletion of the E2 enzyme on K48-chains of lysosomes after damage. In addition, decoration of lysosomes with K63-chains was also impaired when UBE2QL1 was depleted.

2.3.3 UBE2QL1 affects recruitment of p97

p97 is known to preferentially target K48-chains on substrates for their dissociation from membranes or complexes (Bodnar and Rapoport 2017; Blythe et al. 2017). We have shown recently, that p97 is specifically recruited to the population of lysosomes labelled with K48-chains during ELDR and, together with its cofactors, removes them in order to allow autophagic clearance (Papadopoulos et al. 2017). Depletion of UBE2QL1 prevented formation of K48-chains on lysosomes after LLOMe treatment (see Fig. 2.10). As a next step, it was therefore explored if p97 recruitment was impaired when UBE2QL1 is depleted from cells.

As a first attempt, we used an antibody specific for p97 for immuno-fluorescent co-staining with LAMP1 in HeLa cells transfected with siRNA targeting UBE2QL1 and subsequently used confocal microscopy for visualization. In accordance with previous data (Papadopoulos et al. 2017) we could reproduce the robust recruitment of endogenous p97 to structures positive for K48-chains in HeLa cells after treatment with LLOMe, while it was distributed in the cytosol and nucleus in untreated cells (Fig. 2.11A). UBE2QL1 depletion led to a reduction in K48-chains after lysosomal damage. Importantly, p97 puncta were also markedly decreased (Fig. 2.11A). To further explore these findings, stable HeLa FRT cells expressing p97-GFP under the control of the tetracycline repressor were generated. After induction of expression of p97-GFP with doxycycline, cells were treated with LLOMe and were stained for K48-chains and LAMP1 for confocal microscopy to determine colocalization. While p97-GFP was distributed in the cytosol in unchallenged cells, lysosomal damage induced its acute translocation to vesicles that were positive for LAMP1 and K48-chains. Reduction of protein levels of UBE2QL1 with two different siRNAs led to an impaired recruitment of p97-GFP (Fig. 2.11B). Measuring correlations between signals of LAMP1 and K48-chains with the CellProfiler software confirmed the previous results of significant reduction of K48-chains on lysosomes for both siRNAs (Fig. 2.11C). Additionally, the correlation between p97-GFP and LAMP1 signals was also significantly reduced in knock-downs of UBE2QL1 as compared to the control (Fig. 2.11D). Importantly, a connection between K48-chains and p97-GFP signals on lysosomes could be drawn: on the few lysosomes with remaining K48-chains in UBE2QL1 depleted cells, p97-GFP was also present, while all lysosomes negative for K48-chains also lacked p97-GFP (Fig. 2.11B).

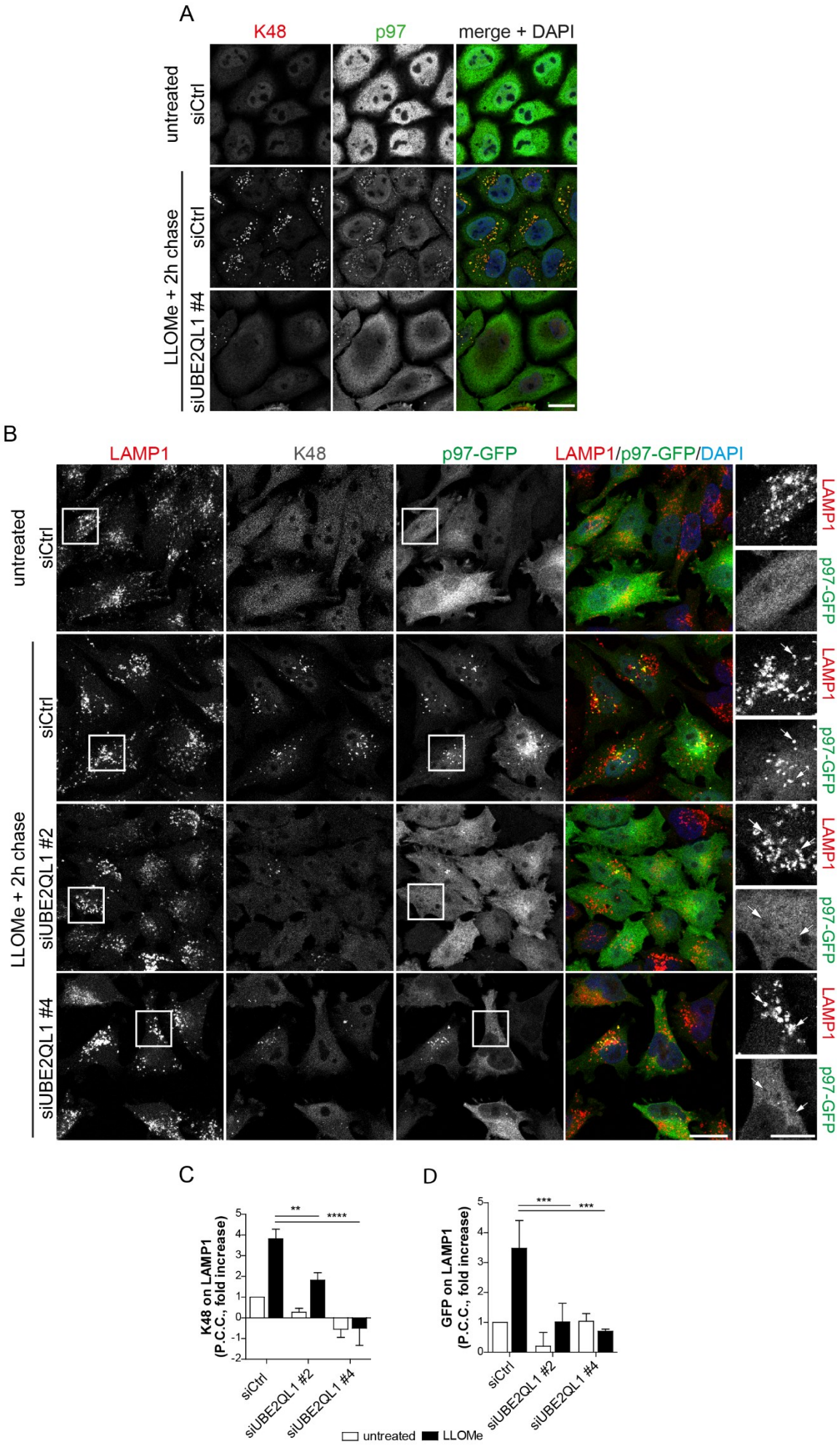
A
K48
p97
merge + DAPI
untreated
siCtrl
LLOMe + 2h chase
siCtrl
siUBE2QL1 #4
B
LAMP1
K48
p97-GFP
LAMP1/p97-GFP/DAPI
untreated
siCtrl
LLOMe + 2h chase
siCtrl
siUBE2QL1 #2
siUBE2QL1 #4
LAMP1
p97-GFP
C
K48 on LAMP1 (P.C.C., fold increase)
**
****
siCtrl
siUBE2QL1 #2
siUBE2QL1 #4
D
GFP on LAMP1 (P.C.C., fold increase)
***
***
siCtrl
siUBE2QL1 #2
siUBE2QL1 #4
untreated
LLOMe

Figure 2.11: UBE2QL1 is essential for the recruitment of p97 to lysosomes upon damage.

(A) Localization of endogenous p97. HeLa cells were transfected with indicated siRNAs targeting UBE2QL1 for 60 h and lysosomal damage was induced with 250 µM LLOMe for 1 h. Cells were chased in fresh medium for additional 2 h before fixation. Endogenous p97 and K48-chains were detected using specific antibodies and imaging on a confocal laser scanning microscope. Scale bar, 20 µm. **(B)** Localization of p97-GFP. Stable HeLa FRT p97-GFP cells were transfected with two different siRNAs against UBE2QL1 for 48 h. In the final 24 h, expression of p97-GFP was induced with 1 µg/ml doxycycline. Cells were treated as in (A) and stained for K48-chains and LAMP1 using specific antibodies to visualize co-localization with p97-GFP with a confocal laser-scanning microscope. Arrows indicate LAMP1 with or without p97-GFP. Scale bar, 20 µm and 10 µm for inlays. **(C, D)** Quantification of images in (B). The P.C.C. of signals of LAMP1 with K48-chains (C) or p97-GFP (D) per cell was automatically measured using CellProfiler Software. Shown are fold increases normalized to untreated siCtrl (mean +SD). Graph represents results from four individual experiments with 30 or more cells per condition. **P<0.01; ***P<0.001; ****P<0.0001 (One-way ANOVA with Bonferroni's multiple comparison test).

Thus, we could show here that UBE2QL1 depletion impaired recruitment of endogenous and overexpressed p97 to lysosomes upon damage.

2.3.4 Depletion of UBE2QL1 impairs the assembly of the autophagic machinery on damaged lysosomes

Ubiquitination on damaged lysosomal membranes has important functions. p97 translocation to lysosomes, that is mediated by K48-chains, has implications on autophagosome maturation (Papadopoulos et al. 2017). Polyubiquitination linked via K63 is necessary for the recruitment of autophagy receptors in selective autophagy in general (Shaid et al. 2013) and was also found on the damaged organelles (Papadopoulos et al. 2017; Fujita et al. 2013). We already showed here that UBE2QL1 is essential for polyubiquitination linked via K48 on lysosomes after damage (see Fig.2.10 and 2.11). Because knock-down of UBE2QL1 also led to reduction in K63-chains on lysosomes, it was speculated that the recruitment of the autophagy receptor p62 and consequently autophagic membranes could also be affected.

To explore this, HeLa cells depleted for UBE2QL1 were exposed to lysosomal damage by LLOMe treatment, stained for LAMP1 and p62 and imaged by confocal microscopy. As reported (Maejima et al. 2013; Papadopoulos et al. 2017) and shown in the results above (see Fig. 2.9), p62 strongly localizes to lysosomes after 1 h of treatment with LLOMe in control cells. Of note, depletion of UBE2QL1 led to less efficient p62-recruitment (Fig. 2.12A). The correlation between LAMP1 and p62 signals was automatically measured for all conditions and showed a significant reduction in cells

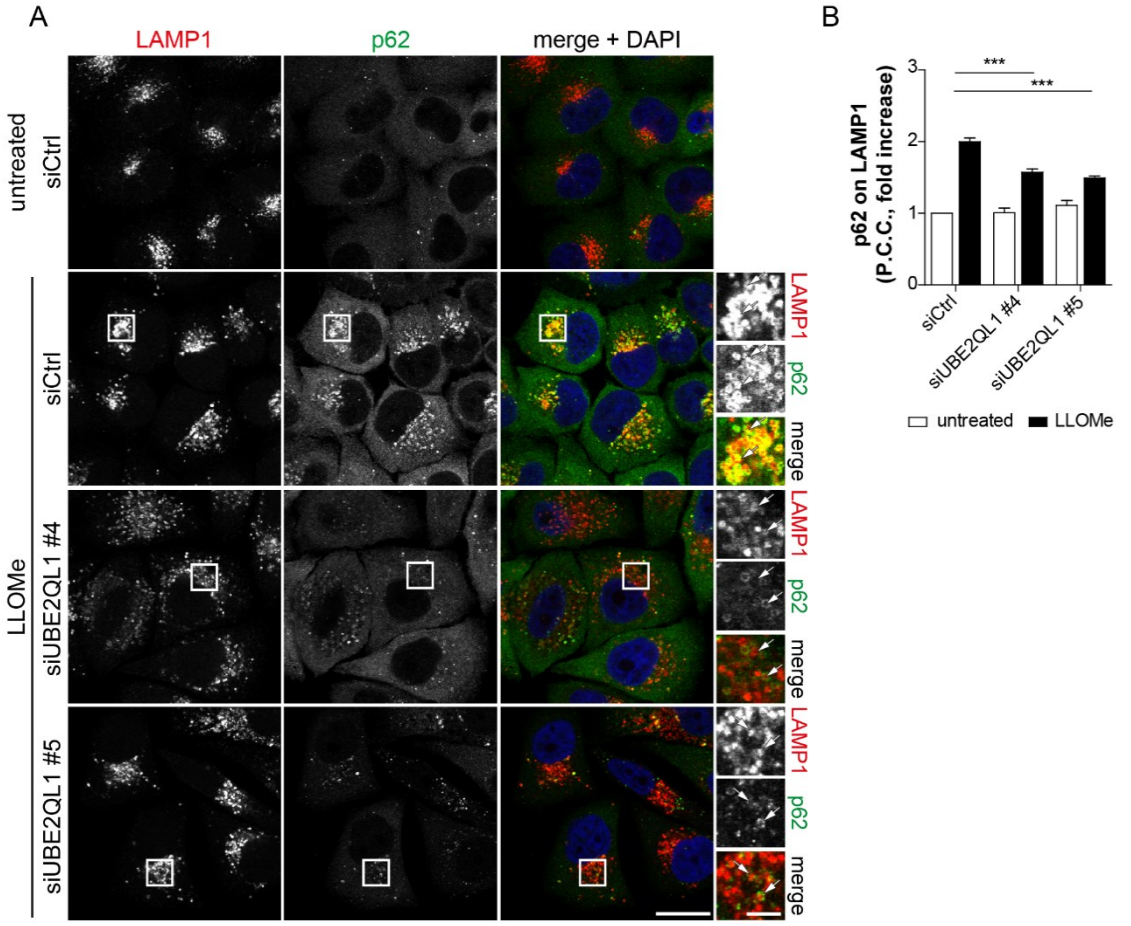

Figure 2.12: Depletion of UBE2QL1 impairs p62 assembly on lysosomes during ELDR.

(A) HeLa cells were transfected with different siRNAs targeting UBE2QL1 and were fixed after treatment with 250 µM LLOMe for 1 h. For visualization of the autophagy marker p62 on lysosomes, p62 and LAMP1 antibodies were used and samples were imaged by confocal laser scanning microscopy. Arrows indicate LAMP1 vesicles with or without p62. Scale bar, 20 µm and 5 µm for enlargement. **(B)** Quantification of cells in (A). The correlation (P.C.C.) of p62 and LAMP1 signals per cell was automatically calculated with CellProfiler Software. The graph shows is the fold increase normalized to untreated control and represents data from three independent experiments with 30 or more cells per condition (mean +SD). ***P<0.001 (One-way ANOVA with Bonferroni's multiple comparison test).

treated with LLOMe that were transfected with two different UBE2QL1 siRNAs instead of control siRNA (Fig. 2.12B).

p62 binds to ubiquitinated substrates via its UBA domain (Vadlamudi et al. 1996) and marks them for autophagic degradation by simultaneously binding, via its LIR-motif, to LC3 and GABARABs that are found on autophagosomal membranes (Pankiv et al. 2007). We speculated that the reduced recruitment of p62 could also affect the sequestration of autophagosomal membranes to damaged organelles in UBE2QL1 depleted cells. To visualize this, HeLa cells transfected with UBE2QL1 or control siRNAs were treated with LLOMe and stained for Gal3 and LC3 to specifically

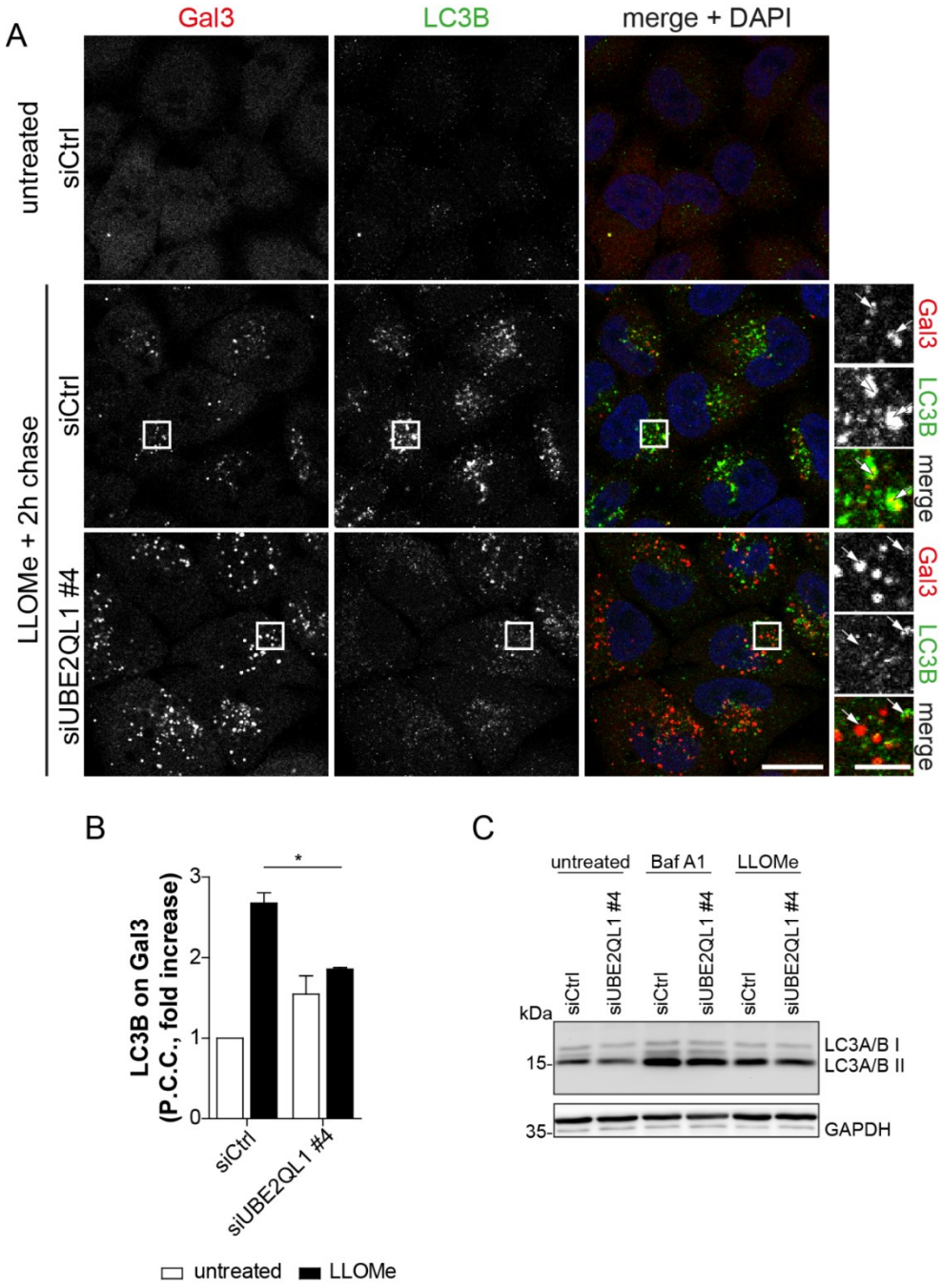

Figure 2.13: UBE2QL1 is needed for the formation of autophagic membranes on damaged lysosomes.

(A) HeLa cells were depleted for UBE2QL1 for 60 h and fixed after 1 h of treatment with 250 µM LLOMe and 2 h chase in fresh medium. To detect LC3B on Gal3-positive lysosomes, cells were stained with specific antibodies and imaged by confocal laser-scanning microscopy. Arrows indicate Gal3 vesicles with or without LC3B. Scale bar, 20 µm and 5 µm for inlays. (B) Quantification of samples in (A). Co-localization of LC3B and Gal3 was measured automatically with the P.C.C. using CellProfiler Software. The graph shows the fold increase normalized to untreated siCtrl and represents data from three independent experiments with 50 or more cells per condition (mean +SD). *P<0.05 (One-way ANOVA with Bonferroni's multiple comparison test). **(C)** HeLa cells were transfected with UBE2QL1 or control siRNA for 72 h, treated with 200 nM Bafilomycin A1 for 5 h or 250 µM LLOMe for 3 h as indicated, lysed in LC3 lysis buffer and probed with an antibody specific for LC3A/B in Western blot analysis. GAPDH was probed as loading control.

investigate autophagosome formation on the damaged organelles by confocal microscopy. Gal3 puncta were labelled with LC3 in control depleted cells after LLOMe treatment, whereas this was reduced in UBE2QL1 knock-down cells (Fig. 2.13A). We confirmed this by measuring the correlation between the two signals with the CellProfiler software, which displayed a significant decrease (Fig. 2.13B). To ensure that these findings were specific for LC3 recruitment during lysophagy and not due to a general activation of autophagy, we investigated the lipidation status of LC3 in UBE2QL1 depleted cells by Western blot analysis (Fig. 2.13C). LC3 is conjugated to phosphatidylethanolamine (PE) when it is associated with autophagosomal membranes (Yoshii and Mizushima 2017). Measuring the ratio of non-lipidated (LC3I) and lipidated (LC3II) forms of the protein in Western blot is an established method to monitor autophagy (Yoshii and Mizushima 2017). Firstly, the ratio of LC3I and the faster migrating LC3II were unchanged in untreated cells when comparing control and UBE2QL1 depletion, excluding a basal activation of autophagy (Fig. 2.13C). Secondly, the formation of LC3II was not generally impaired in UBE2QL1 depleted cells when cells were treated with LLOMe, as the ratio of LC3II to LC3I increased in the same manner for control and UBE2QL1 siRNA transfected cells (Fig. 2.13C). Lastly, an impairment in autophagic flux could as well be excluded, as the LC3II band was comparable for both samples when general autophagy was blocked by treatment with Bafilomycin A1 (Fig. 2.13C).

Thus, we showed that UBE2QL1 depletion also compromised the accumulation of p62 and LC3 on damaged lysosomes, indicating inefficient autophagosome formation.

2.3.5 The autophagy receptor TAX1BP1 localizes to damaged lysosomes in a UBE2QL1-independent manner

Results from this study suggest that UBE2QL1 is important for recruiting the autophagy receptor p62 to damaged lysosomes (see Fig. 2.12), forming an integral part of the response. Using a proximity labeling approach, we have found another autophagy receptor, TAX1BP1, in the vicinity of UBE2QL1 after LLOMe treatment (Koerver et al. 2019). TAX1BP1 is well characterized in xenophagy and was shown to mediate autophagy during viral infections as well as during defense against invading *Salmonella* (Sharma et al. 2018).

Using HeLa cells that were treated with LLOMe to induce lysosomal damage we firstly stained with an antibody recognizing endogenous TAX1BP1. Indeed, a strong increase

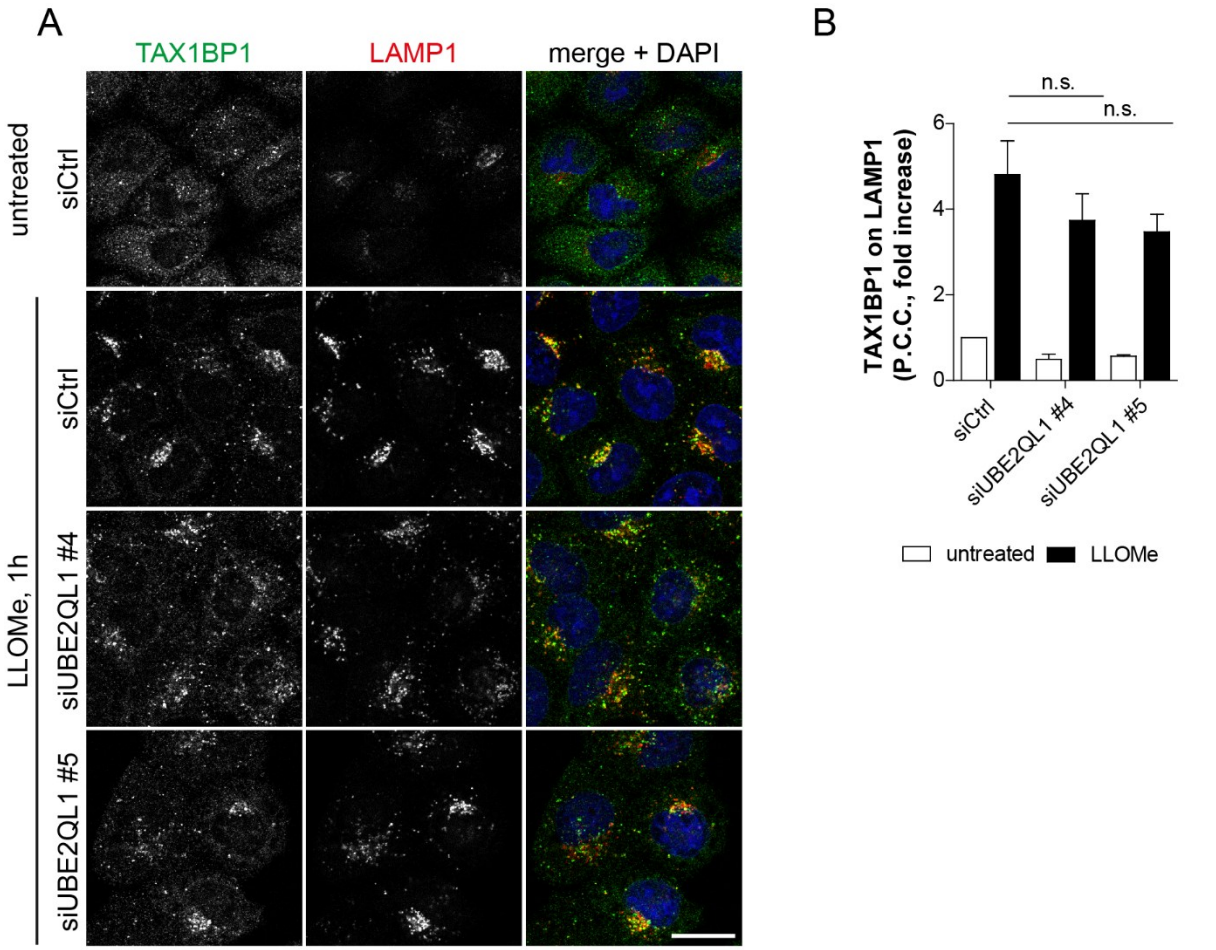

Figure 2.14: TAX1BP1 is recruited to lysosomes after LLOMe treatment in a UBE2QL1-independet manner.

(A) HeLa cells were transfected with control or the indicated siRNAs targeting UBE2QL1 for 60 h and treated with LLOMe for 1 h. After methanol fixation, TAX1BP1 and LAMP1 were stained with specific antibodies and images were obtained by confocal microscopy. Arrows indicate co-localizing vesicles. Scale bar, 20 µm. **(B**) P.C.C. of signals of TAX1BP1 and LAMP1 was measured automatically using CellProfiler Software. The graph shows data from three independent experiments with 50 or more cells per condition (mean +SD). Not significant (n.s.) (One-way ANOVA with Bonferroni's multiple comparison test).

of signal on lysosomes could be observed in contrast to the untreated condition in control depleted cells (Fig. 2.14A). Furthermore, UBE2QL1 was depleted from these cells using two different siRNAs and the recruitment of TAX1BP1 was monitored. No significant difference in localization of TAX1BP1 to lysosomes was observed, which was also quantified automatically by measuring the correlation between TAX1BP1 and LAMP1 signals using the CellProfiler software (Fig. 2.14A and B).

It was shown here that another autophagy receptor, TAX1BP1 is recruited to lysosomes after LLOMe-induced damage. However, UBE2QL1, in contrast to p62 recruitment, is not responsible for this step during lysophagy.

2.3.6 UBE2QL1 is essential for efficient clearance of damaged lysosomes and cell survival after LLOMe treatment

The results of this study suggested that UBE2QL1 is important for critical steps of lysophagy, such as ubiquitination and recruitment of p97 and proteins of the autophagic machinery. We therefore asked whether damaged lysosomes were efficiently cleared in UBE2QL1 knock-down conditions. To analyze this, as a next step we made use of the Gal3-puncta clearance assay. Our group and others have shown that after formation of Gal3-puncta upon LLOMe-treatment, labelled organelles are cleared from cells within 12 h of chase after damage, which is impaired when essential components of the autophagic machinery or ELDR are compromised (Maejima et al. 2013; Papadopoulos et al. 2017).

Hence, UBE2QL1 and control-depleted HeLa cells were treated with LLOMe for 1 h to induce lysosomal damage and then chased in fresh medium for 2 or 12 h. The appearance and subsequent clearance of Gal3-positive lysosomes was monitored by immuno-fluorescent staining with a specific Gal3 antibody, confocal imaging and automated quantification of Gal3-puncta using the CellProfiler software (Fig. 2.15). After 2 h of chase, almost 100% of the cells in control depletion exhibited three or more Gal3-puncta, which were mostly cleared within 12 h (Fig. 2.15A and B). Influx of Gal3 into lysosomes after 2 h chase was not impaired when UBE2QL1 was depleted from cells. However, around 25-70% of Gal3-positive lysosomes (dependent on the siRNA) persisted at the 12 h time-point, which was significant for one of the siRNAs (Fig. 2.15A and B). Additionally, around 40% of cells transfected with siUBE2QL1 #5 showed Gal3-puncta already in the untreated condition (Fig. 2.15B) and Gal3 signals for both siRNAs after 2 h chase were more intense as compared to the control siRNA (Fig. 2.15A).

HeLa cells can tolerate treatments with LLOMe up to 4 mM without induction of apoptosis although lysosomal membranes are completely permeabilized (Repnik et al. 2017). Work from our laboratory has shown that p97, being required for the autophagic clearance of damaged lysosomes, also has a role in cell survival during LLOMe treatment (Papadopoulos et al. 2017). Because we found here the requirement of UBE2QL1 for lysophagy, we asked whether its depletion could also sensitize cells for LLOMe. To explore this, HeLa cells transfected with siRNAs targeting UBE2QL1 were exposed to increasing concentrations of LLOMe for 12 h and cell viability was measured with the MTS assay. While control cells tolerated LLOMe concentrations up

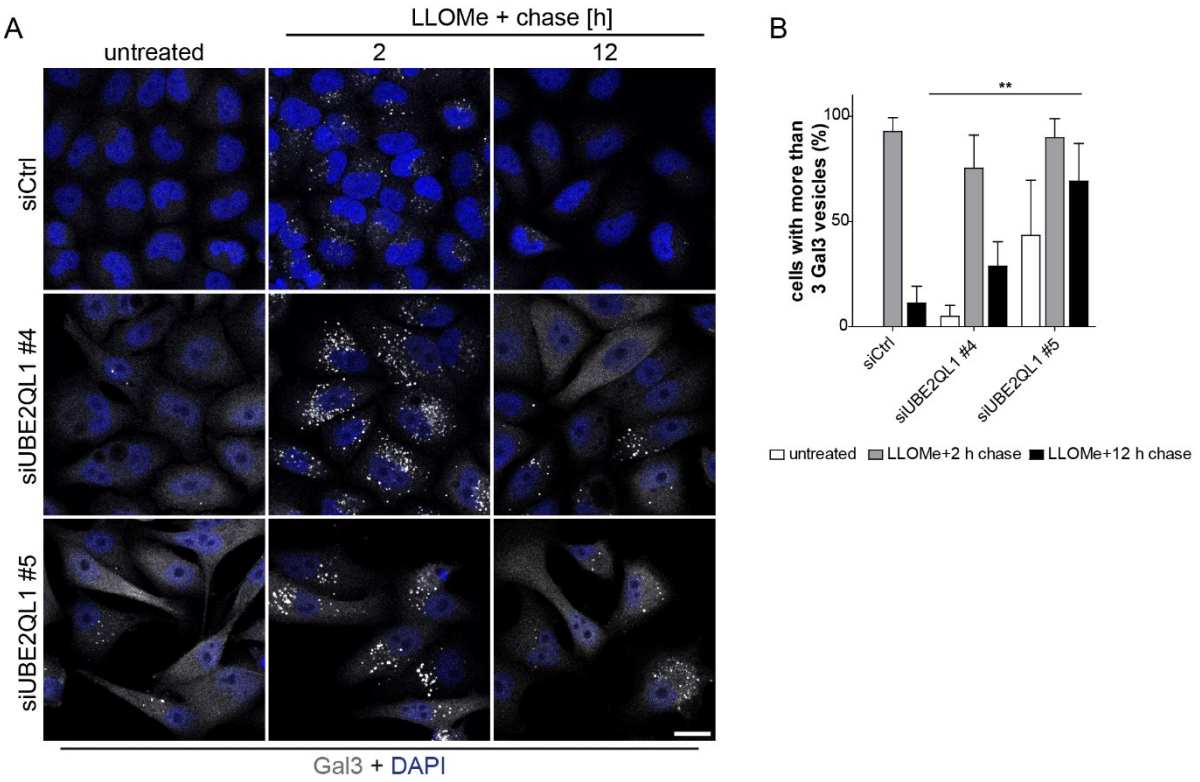

Figure 2.15: UBE2QL1 is required for efficient clearance of damaged lysosomes after LLOMe treatment.

(A) For the Gal3-puncta assay, HeLa cells were depleted for UBE2QL1 with different siRNAs for 72 h in total. Treatment with 250 µM LLOMe was followed by washout and chase for the indicated time-points. Gal3 puncta were visualized using a specific antibody. Scale bar, 10 µm. **(B)** Quantification of (A). Using CellProfiler Software, Gal3-positive vesicles were automatically detected and cells with more than three Gal3-puncta were counted (shown as percentage of cells). The graph represents results from three individual experiments with 60 or more cells per condition (mean +SD). **P<0.01 (One-way ANOVA with Bonferroni's multiple comparison test).

to 500 µM, UBE2QL1 depletion led to a significant decrease in survival to around 70% at 250 and 500 µM LLOMe (Fig. 2.16A). Interestingly, even untreated cells showed less viability when UBE2QL1 expression was targeted by siRNAs as compared to the control (Fig. 2.16B). In concordance with this, several attempts to generate HeLa UBE2QL1 knock-out cells using the CRISPR-Cas9 method, have failed (data not shown), pointing towards the essentiality of the protein.

Overall, these data raise the possibility that UBE2QL1 has an important role in lysophagy, as it affected clearance of damages organelles and cell survival after lysosomal stress.

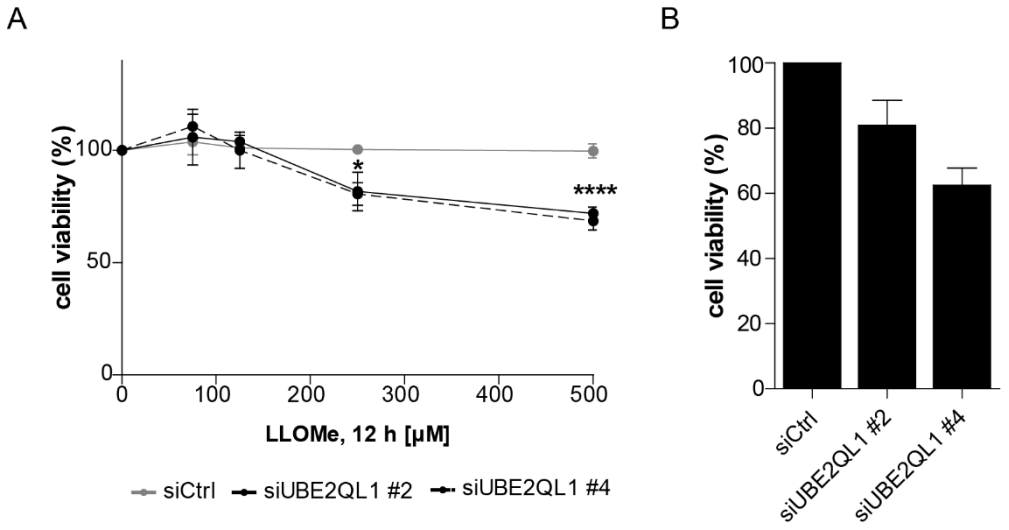

Figure 2.16: Depletion of UBE2QL1 sensitizes cells for death upon lysosomal stress. **(A)** HeLa cells were transfected with siRNAs targeting UBE2QL1 for 48 h. In the final 12 h, cells were treated with indicated concentrations of LLOMe. Cell viability was measured with the MTS assay. The graph shows the percentage of cells surviving, as normalized to the untreated controls of each siRNA. **(B)** HeLa cells depleted as in (A) were left untreated exposed to the MTS assay. Shown is the percentage of survival, normalized to siCtrl. Both graphs represent data from one experiment with three technical replicates (mean +SD). *P<0.05; ****P<0.0001 (One-way ANOVA with Bonferroni's multiple comparison test).

2.3.7 Recruitment of UBE2QL1 to lysosomes after damage is not mediated by Galectins

Galectins are a group of mostly cytosolic proteins with the ability to bind to β-galactosides.Gal-1, 3, 8 and 9 were shown to accumulate in ruptured endolysosomal compartments due to subsequently exposed luminal glycans after damage (Papadopoulos and Meyer 2017) and Gal3 is frequently used as a damage marker for such organelles (Aits et al. 2015). Gal3 and Gal8 play important roles in recruitment of subsequent signaling factors. Gal3 accumulation after chemically induced damage or *M.tubercolosis* infection is essential for TRIM16 recruitment, which in turn interacts with regulators of the autophagic machinery (Chauhan et al. 2016). Gal8 was shown to target *Salmonella* containing endosomal compartments for efficient autophagic clearance by recruiting the autophagy receptor NDP52 (Thurston et al. 2012). Results from this study indicate that UBE2QL1 has a role in recruiting several factors, including members of the autophagy machinery and ELDR components. It is however not clear what factors mediate the strong localization of UBE2QL1 itself to lysosomes after damage. Importantly, we found UBE2QL1 localizing in the proximity of Galectins during lysophagy (Koerver et al. 2019). It was therefore tested whether Galectins were responsible for this.

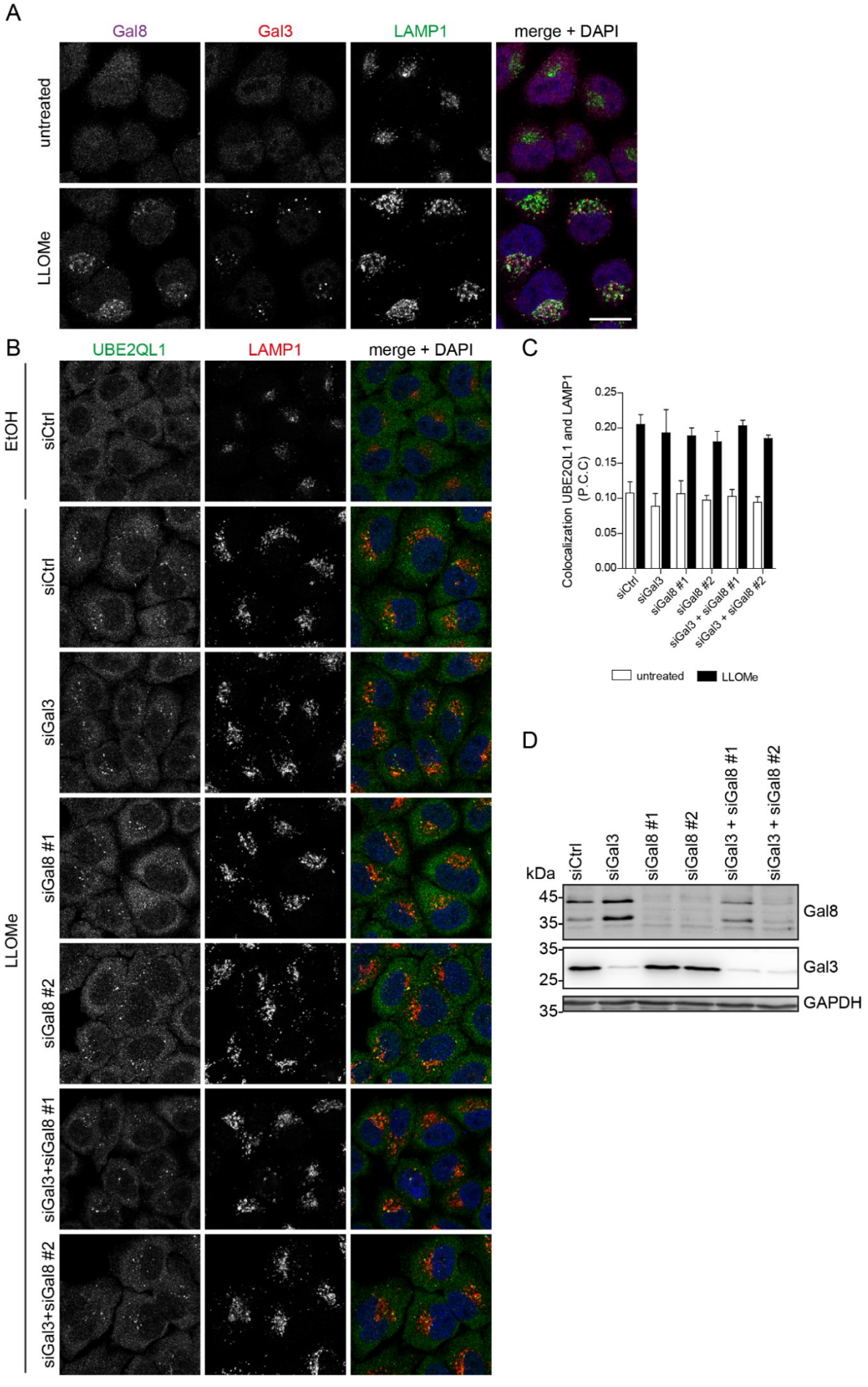
A
Gal8
Gal3
LAMP1
merge + DAPI
untreated
LLOMe
B
UBE2QL1
LAMP1
merge + DAPI
EtOH
siCtrl
LLOMe
siCtrl
siGal3
siGal8 #1
siGal8 #2
siGal3+siGal8 #1
siGal3+siGal8 #2
C
Colocalization UBE2QL1 and LAMP1 (P.C.C)
0.25
0.20
0.15
0.10
0.05
0.00
siCtrl
siGal3
siGal8 #1
siGal8 #2
siGal3 + siGal8 #1
siGal3 + siGal8 #2
untreated
LLOMe
D
kDa
siCtrl
siGal3
siGal8 #1
siGal8 #2
siGal3 + siGal8 #1
siGal3 + siGal8 #2
45
35
Gal8
35
25
Gal3
35
GAPDH

Figure 2.17: UBE2QL1 recruitment to lysosomes after damage is independent on Gal3 and Gal8.

(A) HeLa cells were treated with 250 µM LLOMe or EtOH (untreated) for 3 h, fixed, stained with antibodies specific for Gal3 and Gal8 and imaged with a confocal laser scanning microscope. Scale bar, 20 µM **(B)** HeLa cells were transfected with siRNAs targeting Gal3 or Gal8 individually, or both together for 48 h and either LLOMe (250 µM) or control-treated (untreated) for 3 h. Cells were fixed and immuno-stained for LAMP1 along with an antibody specific for UBE2QL1 as indicated and imaged by confocal laser scanning microscopy. Scale bar, 20 µm. **(C)** Automated quantification of (A). Shown are the Pearson's correlation coefficients (P.C.C.) representing colocalization of endogenous UBE2QL1 and LAMP1. Graphs represent data from three independent experiments with ≥ 35 cells per condition (mean ± SD). N.S. (One-way-ANOVA with Bonferroni's multiple comparison test). **(D)** Western blot analysis of depletion efficiency of Gal3 and Gal8 siRNAs. Cells were transfected with indicated siRNAs and lysates were probed with antibodies specific to Gal3 and Gal8 as indicated. GAPDH was probed as loading control.

As a first step we investigated if Gal8 localizes to lysosomes also after damage induced by LLOMe treatment, as this was shown only for Glycyl-L-Phenylalanine 2-Naphthylamide (GPN) treatment so far (Jia et al. 2018). For this, HeLa cells were treated with LLOMe and stained with antibodies recognizing endogenous Gal3 and Gal8 together with LAMP1 (Fig. 2.17A). Indeed, not only Gal3 puncta arose on lysosomes after LLOMe-induced damage, but also Gal8 localized to lysosomes. (Fig. 2.17A). To investigate a potential role of Galectins in recruitment of UBE2QL1, their protein levels were depleted in HeLa cells using siRNAs. After 48 h of depletion, cells were treated with LLOMe and immuno-stained with the antibody against endogenous UBE2QL1. No difference in localization of UBE2QL1 to LAMP1 positive structures could be observed in knock-downs of Gal3 or Gal8 alone or double knock-down of both proteins (Fig. 2.17B). This was quantified by automatically counting UBE2QL1 and LAMP1 colocalizing vesicles (Fig. 2.17C). Knock-down efficiencies of Gal3 and Gal8 were monitored in a Western blot (Fig. 2.17D).

We thus showed that two important recruitment factors on damaged lysosomes, Gal3 and Gal8, are not responsible for targeting UBE2QL1 to these organelles.

2.4 A role for UBE2QL1 in lysosome homeostasis

Increased Gal3-puncta and impaired viability at basal conditions seen in earlier experiments (see Fig. 2.15 and 2.16) indicate a potential role for UBE2QL1 in lysosomal homeostasis. The main regulator of lysosomal homeostasis is the transcription factor TFEB that controls genes for lysosomal biogenesis, autophagy and lysosomal exocytosis (Napolitano and Ballabio 2016). Under basal conditions, TFEB is phosphorylated and inhibited by mTOR on lysosomes. mTOR inactivation, for

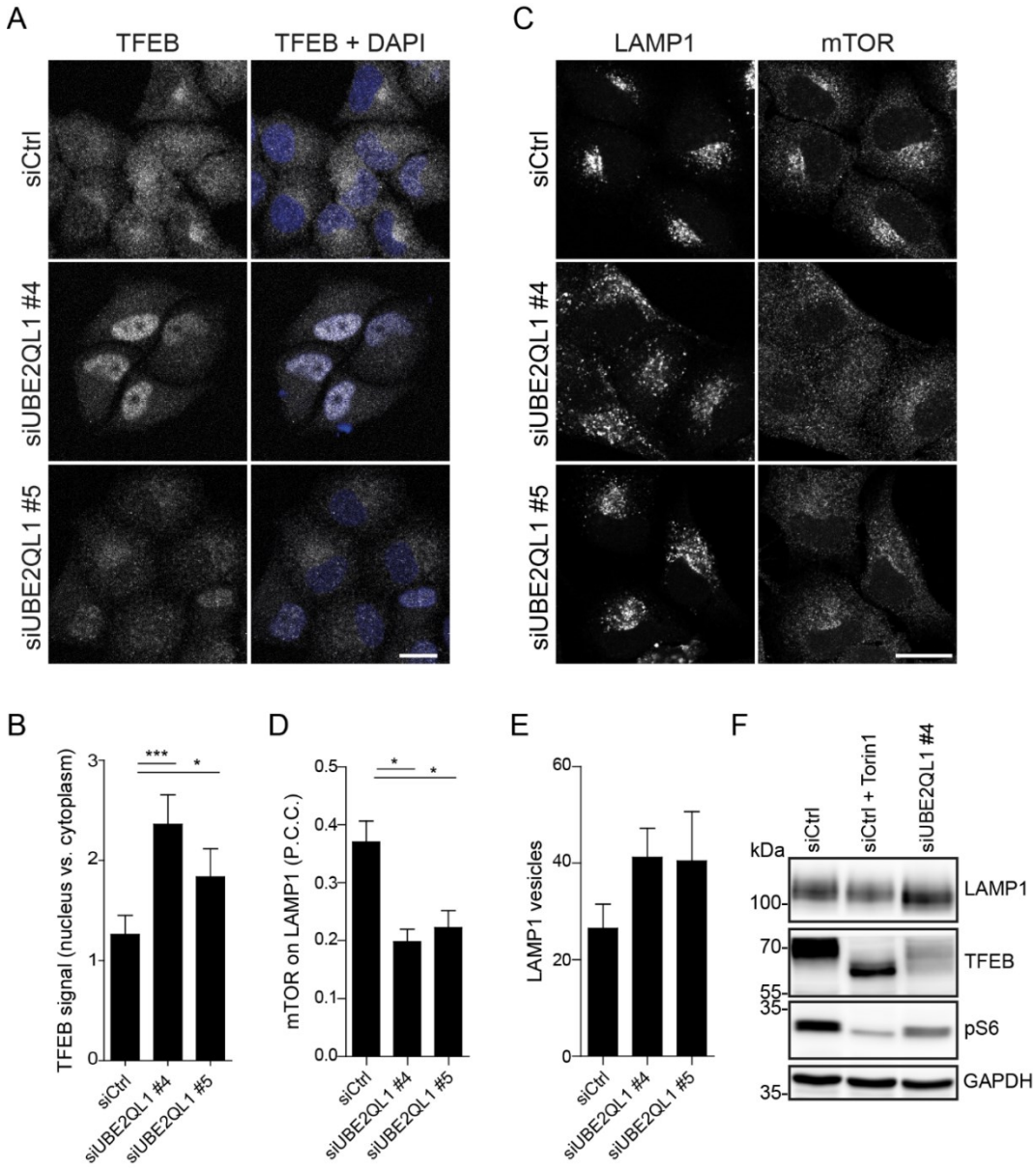

Figure 2.18: Lysosomal homeostasis is affected in UBE2QL1-depleted cells.

(A) TFEB shows a nuclear localization in UBE2QL1-depleted cells. After 60 h of transfection of HeLa cells with different siRNAs targeting UBE2QL1, cells were fixed, stained with a TFEB-specific antibody and imaged automatically with a confocal laser scanning microscope. Scale bar, 20 µm. **(B)** Quantification of (A). The ratio of TFEB signal intensity between the nucleus and cytoplasm was automatically determined using CellProfiler Software. The graph shows data from four independent experiments with ? or more cells per condition (mean +SD). *P<0.05; ***P<0.001 (One-way ANOVA with Bonferroni's multiple comparison test). **(C)** mTOR is dissociated from lysosomes. Cells as in (A) were stained for LAMP1 and mTOR to visualize mTOR localization. Samples were imaged with a confocal laser scanning microscope. Scale bar, 20 µm. **(D, E)** Quantification of cells in (C). Automated image quantification with CellProfiler Software measured the P.C.C. of LAMP1 and mTOR signals (D) or counted the number of LAMP1 vesicles per cell (E). Shown are graphs representing results from three independent experiments with 70 or more cells per condition (mean +SD). *P<0.05 (One-way ANOVA with Bonferroni's multiple comparison test). **(F)** HeLa cells as in (A) and treated with 1 µM of the mTOR inhibitor Torin1 for 2 h were lysed with RIPA buffer and analyzed by Western blotting. Antibodies specific for LAMP1, the mTOR substrates TFEB and phosphorylated ribosomal protein S6 (p-S6) or GAPDH, as a loading control, were probed.

example by starvation or lysosomal stress, leads to TFEB dephosphorylation and consequent activation and translocation to the nucleus (Settembre et al. 2012). It has been reported that impairment of lysosomal integrity facilitated mTOR dissociation from the organelles and its following inactivation (Zhitomirsky et al. 2018). With the purpose to investigate the status of lysosomal integrity in UBE2QL1 depleted cells, the cellular localization of TFEB was monitored in untreated cells by immuno-fluorescent staining with a specific antibody and subsequent confocal imaging. TFEB was distributed in the cytosol of control-depleted cells, while a cytosolic and nuclear localization was observed in cells transfected with siRNA against UBE2QL1 (Fig. 2.18A). To measure this, the nucleus and cytoplasm of imaged cells were determined automatically and TFEB signal intensity was determined in both. From this, the ratio between nuclear and cytosolic TFEB intensities was determined. It was significantly increased in cells with impaired UBE2QL1 expression (Fig. 2.18B). When staining these cells for LAMP1 and mTOR, the lysosomal localization was confirmed in control depleted cells. Consistent with the previous result, mTOR was strongly and significantly dissociated from LAMP1-positive vesicles in UBE2QL1-depleted cells, demonstrated by automatically measuring the correlation between the two signals (Fig. 2.18C and D). To evaluate a potential change in lysosomes in UBE2QL1 knock-down cells, LAMP1 vesicles were automatically counted. Indeed, cells depleted for UBE2QL1 showed more lysosomes per cell (Fig. 2.18E). Additionally, total protein levels of LAMP1 in these cells were increased in lysates analyzed by Western blotting (Fig. 2.18F). Further investigation of mTOR signaling in the Western blot confirmed reduction of phosphorylation of its substrates TFEB and the ribosomal protein S6. This was monitored by a shift in the TFEB band and lower levels of Phosphorylated S6 (pS6) in UBE2QL1 depleted cells. As a control for this, mTOR was chemically inhibited by treatment of the cells with Torin1, confirming the effects on the substrates (Fig. 2.18F). These results demonstrate that UBE2QL1 might have an impact on basal lysosomal homeostasis apart from its function after induction of damage.

3 Discussion

Ubiquitination of membrane proteins is an essential component of lysophagy and it signals towards recruitment of autophagy effectors to ensure the clearance of the damaged organelles (Maejima et al. 2013; Fujita et al. 2013). Specific enzymes that drive ubiquitination have, however, not been identified yet (Papadopoulos and Meyer 2017). In this study, with the help of an imaging-based screen for E2-conjugating enzymes, we have identified UBE2QL1 as the first ubiquitinating enzyme in the context of autophagic clearance of lysosomes. With this, we were able to specifically block ubiquitination, at least partly, for the first time in this pathway. This confirmed that ubiquitination is essential during lysophagy. The subsequent findings of this study shed light on the range of downstream effectors that are dependent on UBE2QL1-induced ubiquitination. UBE2QL1 was essential for the accumulation of the autophagic machinery on damaged lysosomes and consequently for their autophagic clearance. Importantly, we showed that p97 is recruited to lysosomal membranes by UBE2QL1-mediated ubiquitin chains. Furthermore, UBE2QL1 depletion and p97 mutation cause a similar phenotype with respect to regulation of lysosome integrity on basal levels in cells and in vivo, suggesting a similar or even mutual role in pathologies. These results will contribute to future investigations on additional ubiquitinating enzymes, the precise substrates on the lysosomal membranes, regulation of UBE2QL1 recruitment and the role of ELDR in pathologies caused by p97 mutations.

3.1 Systematic screening reveals UBE2QL1 as a regulatory E2 enzyme in lysophagy

The primary goal of this thesis was to find regulators of lysophagy. Since ubiquitination is a prerequisite for the following steps of lysophagy to occur, we decided to investigate general polyubiquitination and K48-linked chains on LAMP1 (Fig. 2.1A), rather than to focus at later events, such as autophagic clearance or cell death. Detection of changes in levels of ubiquitinated lysosomes is established and straightforward to measure. To realize this, we established a systematic siRNA screening method for E2-conjugating enzymes. In contrast to screening for E3 ligases, this constitutes a feasible and less complex strategy. Although high-throughput screens for E3 ligases are possible, the number (more than 700 (Huang and Dixit 2016)) makes is time-consuming. In particular, we expected highly important results from it, as E2 enzymes are pivotal

players at the heart of the ubiquitinating cascade and provide ubiquitin chain type specificities (Stewart et al. 2016; Ye and Rape 2009; van Wijk and Timmers 2010).

Regarding the way of gene silencing used in a screen, one has to consider the Clustered Regularly Interspaced Short Palindromic Repeats (CRISPR)/CRISPR Associated Protein (Cas) technique, which is widely used in cell biology and animal models. Also, genetic screens are often performed with this approach (Evers et al. 2016). The clear disadvantages of RNAi based downregulation of gene expression, such as off-target effects and variability of knock-down efficiencies, are overcome by CRISPR approaches (Evers et al. 2016). For us, however, a siRNA-mediated screen was more feasible, as we had access to a siRNA library, targeting almost all human E2 enzymes. Also, as we found later, knocking out UBE2QL1 was by CRISPR/Cas9 was not possible, as all our experimental attempts failed (data not shown) and it is most probably an essential gene. Such genes are typically excluded from CRISPR screens, which constitutes an advantage of RNAi.

Since a primary screen involved pools of four siRNAs against each E2 enzyme, the strategy was to deconvolve this in the second screen and to re-screen the hits using the single siRNAs (Fig. 2.1C). This is a commonly used screening method when using siRNA libraries (Goktug, Chai, and Chen 2013). Our stringent screening procedure allowed us to narrow down the number from seven hits to three in the re-screen (Fig. 2.1C). During RNAi screening procedures, false discovery rates are mainly influenced by off-target effects, low transfection rates and methods of hit selection (Goktug, Chai, and Chen 2013). While we were not able to verify the transfection efficiencies of all samples during our screen, we improved hit selection by using the robust z-score (instead of z-score), that is less sensitive for outliers and constitutes the statistical method of choice for RNAi screens (Birmingham et al. 2009).

Of the three final hits (UBE2J1, UBE2QL1, UBE2Q2), UBE2QL1 was the most promising, because it showed a robust translocation to damaged lysosomes in validation experiments (Fig. 2.4). We excluded off-target effects of the siRNAs targeting UBE2QL1 by a sophisticated rescue experiment (Fig. 2.6), as recommended by the research community (Echeverri et al. 2006). Thus, with stringent screening, hit selection and control of off-target effects, we were able to select a reliable hit.

3.1.1 Possible functional relevance of the three identified hits

UBE2QL1 was only recently described to possess E2-enzyme structure and functions and has only been investigated in one study so far (Wake et al. 2013). Wake *et al.* found it to be downregulated in renal cell carcinoma cells (RCC) (Wake et al. 2013). Re-expression of UBE2QL1 rescued tumor-specific phenotypes in those cells, rendering it a potential tumor suppressor. Of note, UBE2QL1 interacts with FBXW7, an F-box protein for substrate recognition in the SCF-ubiquitin ligase complex (Wake et al. 2013) (see section 3.3). Furthermore, expression of UBE2QL1 in these cancer cells reduced levels of mTOR (Wake et al. 2013), indicating a role in autophagy (see section 3.2).

The measurement of specific translocation to damaged lysosomes that identified UBE2QL1 as the most promising hit does however not exclude potential roles for the other candidates, UBE2J1 and UBE2Q2. Their interaction with substrates could be indirect and hence not detectable with the experimental setup chosen. The cooperation between the E2 enzyme and the E3 ligase could be transient, so that only the ubiquitin-loaded E3 ligases translocate to designated lysosomes. In fact, it will be interesting to investigate potential roles in lysophagy of the other two E2 enzyme candidates for several reasons.

UBE2J1 is a transmembrane protein of the ER and works together with the E3 ligase HRD1 in ubiquitination of misfolded MHC I HCs. Ubiquitination targets them for ERAD, which is accomplished by p97 extracting them from the ER membrane (Burr et al. 2013). Although UBE2J1 is stably located at the ER membrane this does not exclude potential ubiquitination on lysosomes, as the ER can form contact sites with the endolysosomal system (Eden 2016). Indeed, UBE2J1, together with the E3 ligase RNF26, regulates lysosomal positioning to the perinuclear region in a ubiquitin-dependent manner (Cremer et al. 2021).

UBE2Q2 has a role in mitotic regulation and is dysregulated in some cancers (Banerjee, Brooks, and Crawford 2007). It was has not been associated with lysosomes or autophagy, yet. But, together with UBE2Q1, it belongs to the same E2 enzyme family as UBE2QL1 (Stewart et al. 2016).

3.2 UBE2QL1 mainly drives K48-linked ubiquitination on damaged lysosomes

E2 enzymes take over crucial roles in the cascade of ubiquitinating enzymes, as they actively determine length and topology of the ubiquitin chains (Stewart et al. 2016; Ye and Rape 2009; van Wijk and Timmers 2010). Therefore, the discovery and characterization of UBE2QL1 as the first E2 enzyme with essential functions in lysophagy majorly contributes to the understanding of the signaling cascades during lysosomal damage.

Several pieces of evidence speak for UBE2QL1 to decorate damaged lysosomal membranes with K48-linked ubiquitin chains. We confirmed the decrease of K48-ubqiuitination on damaged lysosomes in UBE2QL1-depleted cells in a single-well validation experiment and further observed that K63-ubiquitination was also affected, although to a lesser extent (Fig. 2.10). In line with this, we detected that UBE2QL1 emerges on lysosomes together with K48-chains at later stages after induction of damage (60 min), while K63-chains were found on LAMP1 vesicles already after 30 min, together with p62 (Fig. 2.9). This further supports the notion that UBE2QL1 mainly drives K48-chains on lysosomes. Probably, the small amount of UBE2QL1 that localizes to lysosomes already after 30 min (Fig. 2.9) accounts for driving a part of the observed K63-chains. Other enzymes might be involved here to drive K63-ubiquitination.

From our data we cannot exclude that other ubiquitin chain types are formed on damaged lysosomes and provide signaling functions during lysophagy. Firstly, antibodies for other chain types are not well suited for immunofluorescent staining. Secondly, also branched chains could play a role here and antibodies do not discriminate. K11/K48 chains are for example recognized by p97 for protein extraction from the ER or the MOM (Yau and Rape 2016) and should be considered as a potential effector in lysophagy as well.

3.2.1 What enzymes cooperate with UBE2QL1 in ubiquitination?

The specificity for chain types that are generated by the ubiquitination cascade is determined by the last enzyme holding the ubiquitin molecule (Stewart et al. 2016). Hence, in case of HECT and RBR ligases, the E3 ligases provide specificity. In contrast, when cooperating with RING ligases, E2 enzymes take over that task. They can have priming or chain elongating functions or both (Stewart et al. 2016). From our

results we can neither determine with what type of E3 ligase UBE2QL1 interacts, nor if it provides the observed specificity itself.

Future questions will be how the chain type specificity of UBE2QL1 is achieved. For this, it will be important to find the cooperating E3 ligases. From the literature, we can learn important things regarding ubiquitinating enzymes involved in lysosomal damage response that have to be taken into account. Ubiquitination of lysosomal membranes during damage induced by LLOMe and *M.tuberculosis* was shown to be coordinated by TRIM16 that cooperates with Gal3 in recognition of damage and recruits essential autophagy proteins (Chauhan et al. 2016). However, unlike other TRIM-type E3 ligases, TRIM16 does not possess a conventional RING domain (Bell et al. 2012). Although it is supposed to possess E3 ligase functions carried out by its B-domains (Bell et al. 2012), a direct ubiquitinating function is not shown here (Chauhan et al. 2016). In contrast, the multimeric RING E3-ligase SCF^{FBXO27} has been reported to directly build K48-linked ubiquitin chains on several lysosomal glycoproteins, preferentially LAMP2, upon LLOMe treatment (Yoshida et al. 2017). LAMP2 ubiquitination was important for autophagy effectors to accumulate and drive efficient clearance of the organelles (Yoshida et al. 2017). There are three similarities between the reported functions of SCF^{FBXO27} and our findings on UBE2QL1. Firstly, we also found LAMP2 together with UBE2QL1 in LLOMe-treated cells. We mapped proteins in the vicinity of UBE2QL1 in collaboration with Lukas Brecht from Christian Behrends' laboratory in Munich, using proximity biotinylation by expression of UBE2QL1 with a C-terminal fusion of C (APEX2) (Koerver et al. 2019). We found LAMP1, LAMP2 and other lysosomal membrane proteins significantly elevated in proximity to UBE2QL1 (Koerver et al. 2019), suggesting them as targets for ubiquitination (see section 3.4). Secondly, we found UBE2QL1 to mediate primarily K48-linked ubiquitin chains (Fig. 2.9 and 2.10) (see section 3.2). And lastly, impaired lysosomal ubiquitination caused by UBE2QL1 depletion in HeLa cells also abrogated the recruitment of the autophagic machinery (Fig. 2.12 and 2.13). Besides this line of similarities, we can exclude a cooperation of SCF^{FBXO27} with UBE2QL1 as the study was conducted in PANC-1 cells (Yoshida et al. 2017) and FBXO27 is not expressed in HeLa cells (Papadopoulos and Meyer 2017). Hence, one conclusion could be that UBE2QL1 takes over similar tasks as SCF^{FBXO27} in a tissue-specific manner together with another E3 ligase. Indeed, UBE2QL1 has been associated with another F-box protein, FBXW7 (Wake et al. 2013). Overexpression of UBE2QL1 enhanced degradation of FBXW7 substrates CyclinE1

(CCNE1) and mTOR in HeLa cells (Wake et al. 2013), suggesting a cooperative role of them. A FBXW7 binding domain was detected in the structure of UBE2QL1 in this study (Wake et al. 2013). This rather leads to the conclusion that UBE2QL1 itself is a substrate of SCF^{FBXW7}, as the F-box protein is responsible for binding the substrate of the E3 ligase, not the interacting E2 enzyme (Metzger et al. 2014).

Overall, hints from the literature did not lead to identification of E3 ligases that cooperate with UBE2QL1 during lysophagy in our setup. Even the APEX screen did not reveal significant elevation of E3 ligases in the proximity to UBE2QL1 (Koerver et al. 2019). This is possibly due to weak and transient interactions. Probably, several E3 ligases and E2 enzymes build a regulatory network in ubiquitination of lysosomal membrane substrates, as it is the case during mitophagy: two important E3 ligases, Parkin and Mitochondrial Ubiquitin Ligase Activator of NF-κB (MULAN), both cooperate with several E2 enzymes with different consequences (Fiesel et al. 2014; Ambivero et al. 2014). Networks of ubiquitinating enzymes could also work in parallel for different substrates and provide tissue specificities. This emphasizes the plethora of potential enzymes and combinations, and their identification will include more research in the future.

3.2.2 Where does UBE2QL1 initiate ubiquitination?

An additional question to chain type specificity and interacting ubiquitinating enzymes is where UBE2QL1-driven ubiquitination exactly occurs. Together with our collaboration partners, we gained two experimental hints that UBE2QL1 decorates its substrates at the luminal part of the lysosomal membrane. Firstly, UBE2QL1 was in close proximity to Gal3 (and Gal1) in the APEX screen (Koerver et al. 2019). Galectins sense and bind to β-galactosides on the luminal part of lysosomal proteins when porous membranes allow them to enter (Maejima et al. 2013). Secondly, Tineke Veenendaal from the Klumperman laboratory performed immuno-electron microscopy of LLOMe-treated cells. Importantly, UBE2QL1 localized to the lumen of lysosomes together with K48-chains, YOD1 and, as expected, Gal3 (Koerver et al. 2019). Indeed, Yoshida *et al.* observed that LAMP2 and other membrane proteins were ubiquitinated at the luminal side by SCF^{FBXO27} (Yoshida et al. 2017). This further supports the notion that essential decoration of proteins with ubiquitin during ELDR is initiated in the lysosomal lumen rather than at the cytosolic site. Experimentally, this could be clarified by analyzing the ubiquitination landscape after LLOMe treatment in HeLa cells by

tryptic digestion and usage of a diGly antibody with subsequent Mass spectrometry (MS) analysis, as done by Yoshida and colleagues (Yoshida et al. 2017), for example. Hence, there is compelling evidence that UBE2QL1 and subsequent ubiquitination, as well as components of the ELDR complex start acting inside the lysosomal lumen. Since the autophagic machinery (as shown in EM for p62) accumulates on the cytosolic site (Koerver et al. 2019), it is an intriguing question, how the ubiquitination signal moves to the outside. One possibility is that the ubiquitin chain grows through the pores of the permeabilized membrane. A second scenario would be that the ubiquitinated substrates “flip” through these pores to expose their luminal site and the ubiquitin signal to the cytosol (Papadopoulos, Kravic, and Meyer 2019). Since LMP begins to restore as early as 30 min after beginning of LLOMe treatment and is repaired after 4 h (Repnik et al. 2017), the timing is critical here and it will be interesting to approach this question in the future.

3.3 UBE2QL1 is a key regulator of ELDR and lysophagy

The decoration of lysosomal membranes with ubiquitin is a prerequisite for lysophagy. This study shows in a line of several pieces of experimental evidence that UBE2QL1-mediated ubiquitination serves as a signal for autophagic clearance of damaged lysosomes (Fig.3.1). We have demonstrated that UBE2QL1 is necessary for the autophagy adaptor p62 to accumulate on lysosomes in LLOMe-treated cells (Fig. 2.12). Not surprisingly, also the recruitment of LC3 (Fig. 2.13) was decreased upon depletion of UBE2QL1, as LC3 it binds to autophagy adapters like p62 to initiate the formation of the autophagosome (Sharma et al. 2018). These results demonstrate that UBE2QL1 regulates the assembly of the autophagic machinery and consequently the clearance of damaged organelles from cells. Indeed, our results demonstrate that Gal3-positive vesicles persisted when UBE2QL1 was depleted, in contrast to control cells, where lysosomes marked with Gal3 were cleared 12 hours after washout of LLOMe (Fig. 2.15). In line with this, we revealed here that UBE2QL1 was needed for HeLa cells to survive long treatments with LLOMe, as UBE2QL1-depleted cells show decreased survival already at 250 µM LLOMe (Fig. 2.16). Although LLOMe is not supposed to cause cathepsin release, HeLa cells tolerate only certain concentrations of LLOMe (4 mM) before they undergo apoptosis (Repnik et al. 2017). This again emphasizes that UBE2QL1-mediated recruitment of lysophagy effectors is essential for the cell to combat lysosomal damage.

Moreover, p97 recruitment was affected in UBE2QL1-depleted cells (Fig. 2.11) (see section 3.4). Consistent with this finding, UBE2QL1 was responsible mainly for the formation of K48-linked ubiquitin and only for a smaller amount of K63-linked chains (discussed in section 3.3). Data from our group had shown before that p97 recognized and removed K48-linked chains on damaged lysosomes and that this was necessary for LC3 to accumulate. However, p97 was not needed for p62 recruitment, which is in line with p62 recruitment occurring before p97 (Papadopoulos et al. 2017). We showed in this study that UBE2QL1 appears on damaged lysosomes together with K48 chains, timely separated from the earlier occurrence of K63-chains and p62 (Fig. 2.9). This contrasts with the finding that UBE2QL1 is needed for p62 recruitment. It is conceivable that barely detectable amounts of UBE2QL1 already localize to damaged lysosomes at early stages after damage, catalyzing K63-chains, and this is necessary for p62 binding. K63-linked ubiquitination of substrates is the main recruiting signal for autophagy receptors (Shaid et al. 2013). This notion leads to the idea that the formation of UBE2QL1-independent K63-ubiquitin-chains is driven by a different subset of enzymes and has distinct signaling outcomes.

Interestingly, we have found another autophagy receptor, TAX1BP1, in close proximity to UBE2QL1 under damage conditions in the APEX screen (Koerver et al. 2019). We confirmed TAX1BP1 localization to LLOMe-damaged lysosomes in our immunofluorescence setup (Fig. 2.14). However, TAX1BP1 recruitment did not depend on UBE2QL1 (Fig.2.14). TAX1BP1 has been described to regulate autophagy responses during xenophagy as well as mitophagy (Sharma et al. 2018; Vainshtein and Grumati 2020), but has not been associated with lysophagy yet. This points towards a second, parallel strand of ubiquitination and autophagy regulation during lysophagy.

Results from other studies that investigated the regulation of autophagy after lysosomal damage also support the notion that clearance of lysosomes is mediated by several pathways that could act in a parallel, overlapping or tissue-specific manner. Jia and colleagues found that Gal8 inhibited mTOR activity when lysosomal membranes are damaged (Jia et al. 2018). Concomitantly, AMPK is activated by Gal9 via TAK1 and together this was called the GALTOR apparatus which activates the autophagic machinery upon chemically induced lysosomal damage (Jia et al. 2018). This group further found that Gal9 was essential for general ubiquitination of lysosomal membranes after damage and specific Transforming growth factor beta-Activated

Kinase 1 (TAK1) ubiquitination with K62 chains (Jia et al. 2020). p97 was found here in proteomic analysis in proximity to Gal9, while no other component of the ELDR complex or UBE2QL1 was detected (Jia et al. 2020). Hence, it will be interesting to investigate how Gal9-driven K63-ubiquitination on damaged lysosomes is intertwined with UBE2QL1-mediated ubiquitination and subsequent signaling.

3.4 UBE2QL1-mediated ubiquitination recruits p97 to damaged lysosomes

By characterizing UBE2QL1 and its ubiquitinating function during ELDR in this study, we gained insight to the crucial role of p97 and K48 ubiquitin chains, and thereby contributed important findings to the research field. More precisely, with the methods developed here, we could show for the first time that localization of p97 to lysosomes is indeed dependent on recognition of K48-labelled proteins on the lysosomal membrane. We called this part of lysophagy the p97-UBE2QL1-K48 axis and demonstrated the interactions and dependencies in three lines of experimental evidence.

First, we found that UBE2QL1 is responsible for the formation of K48-chains after lysosomal damage (see section 3.2). Second, the strong recruitment of p97 to damaged lysosomes was decreased in UBE2QL1-depleted cells (Fig. 2.11). Of note, in UBE2QL1 depletion experiments, some cells showed K48-ubiquitination on a few LAMP1-positive structures, possibly due to incomplete UBE2QL1 depletion. p97 was also detectable on these lysosomes (Fig. 2.11). This underscores the notion that p97 recognizes K48-linked ubiquitin chains on lysosomes. Third, the findings of the proximity labelling assay suggest an interplay between UBE2QL1, p97 and its cofactors during ELDR, as we have detected not only p97 (with very high significance) but also PLAA that cooperates with p97 on damaged lysosomes and NPL4, FAF1 and Ataxin-3 (Koerver et al. 2019). These are known co-factors of p97 that were not yet implicated with lysosomal damage.

Hence, the results from this study suggest that UBE2QL1 is required to recruit p97 to damaged lysosomes. It has been shown before that ubiquitination with K48-linked chains at damaged lysosomal membranes and their removal, probably by p97, are essential for the autophagic machinery to ensure lysophagy (Papadopoulos et al. 2017; Papadopoulos and Meyer 2017). However, the exact targets and functions of

p97 are unclear (Papadopoulos and Meyer 2017) and will be discussed in the next section.

3.4.1 Potential targets and functions of the p97-UBE2QL1-K48 axis

Although we established that p97 is attracted to lysosomal membranes by K48 chains, the specific proteins targeted here with ubiquitin are still to be identified. LAMP2 (and to a lesser extent LAMP1) was described as a target of the E3 ligase SCF^{FBXO27} in LLOMe-treated PANC-1 cells (Yoshida et al. 2017). Yoshida *et al.* could show that this ubiquitination is important for the autophagic clearance of damaged lysosomes (Yoshida et al. 2017). We have also shown that UBE2QL1-mediated ubiquitination drives lysophagy and moreover found LAMP1 and LAMP2 (and other lysosomal membrane proteins: Niemann-Pick C1 (NPC1), NPC1-Like protein (NPC1L), Clathrin Interactor 1 (CLINT1), Spartin) in the proximity biotinylation screen (Koerver et al. 2019). Since it is unlikely that SCF^{FBXO27} and UBE2QL1 interact in our setup (see section 3.2.1), the findings of the study suggest that LAMP2 (and possibly also the other detected membrane proteins in vicinity of UBE2QL1) are prone to ubiquitination after lysosomal damage and hence are very likely targets of UBE2QL1. This has to be confirmed in the future by further interaction studies, such as co-immunoprecipitation experiments, and investigation of the ubiquitination status of the potential targets.

In addition to the question on specific ubiquitination targets is the question of the purpose of their extraction. We have shown in an earlier study that removal of K48-chains from damaged lysosomal membranes by p97 is a prerequisite for LC3 binding to those organelles, while p62 accumulation was not dependent on the function of p97 (Papadopoulos et al. 2017). We show here that UBE2QL1-directed ubiquitination is necessary for p62 to localize to lysosomes after LLOMe treatment (Fig. 2.12). One possible scenario is that the small amount of K63-ubiquitin mediated by UBE2QL1 (see section 3.2) recruits p62. The larger amount of K48-ubiquitin in turn recruits p97 to extract the targets from the membrane that interfere with p62 oligomerization. This would finally lead to LC3 binding and initiation of autophagy (Fig. 3.1). A second possibility is that extraction of K48-labelled proteins leads to morphological changes in lysosomes that favors LC3 binding, similar as observed in mitophagy. p97 has several roles in mitochondrial pathways, such as protein import and translation surveillance, as well as apoptosis and mitophagy (Escobar-Henriques and Anton 2020). During mitophagy, p97 removes, among others, ubiquitin-labelled mitofusins Mfn1 and Mfn2

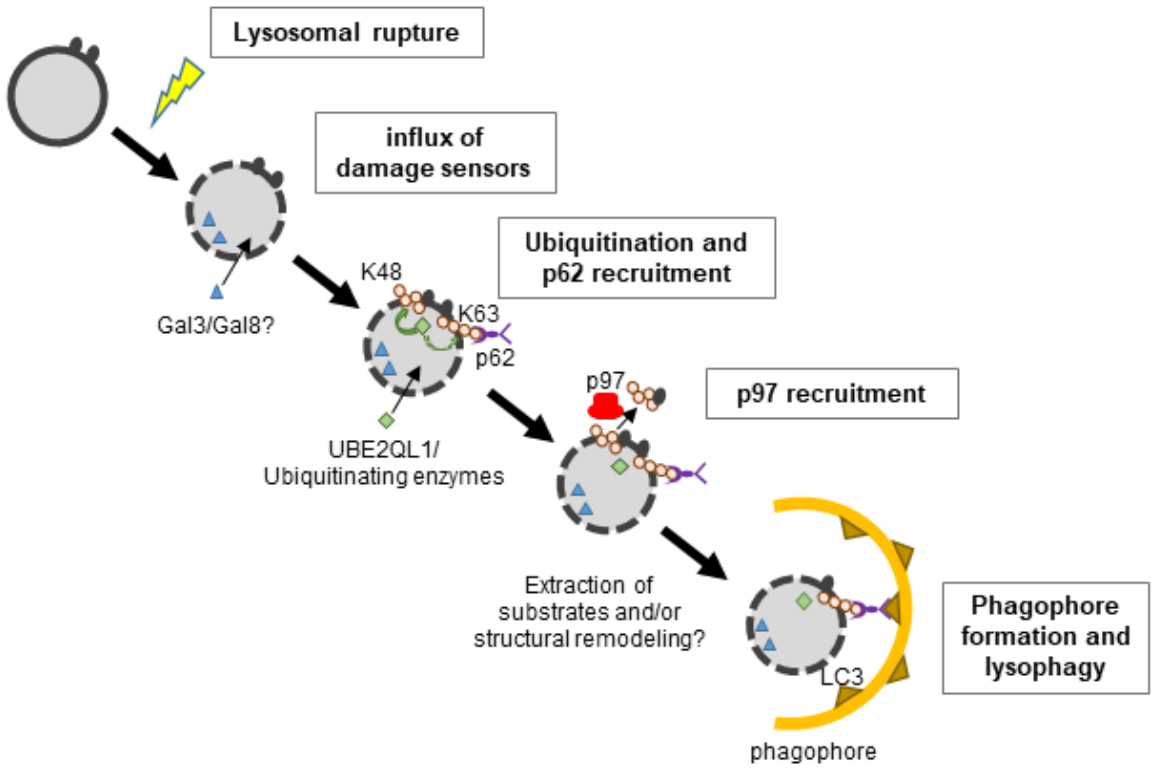

Figure 3.1: Model for the role of UBE2QL1 in lysophagy.
Upon treatment with LLOMe, lysosomal membranes are ruptured, leading to influx of damage sensors such as Gal3. UBE2QL1 (and the cooperating enzymes of the ubiquitination machinery) localizes inside lysosomes and ubiquitinates designated substrate proteins with primarily K48 but also K63-chains. This leads to recruitment of p62 and p97. p97-mediated extraction of substrates is necessary for LC3 to bind to p62 and initiation of phagophore formation around the damaged organelle. This is necessary to combat hindrance of p62 oligomerization or recognition by LC3 and might involve structural remodeling of the lysosomal shape. Finally, damaged lysosomes are cleared by autophagic digestion.

from the mitochondrial membrane for their degradation by the proteasome. This prevents fusion of mitochondria and paves the way for the autophagy machinery to accumulate here (Escobar-Henriques and Anton 2020). A similar mechanism could be exerted by the UBE2QL1-p97-K48 axis during lysophagy. The potential extraction of putative ubiquitination targets (for example integral membrane proteins such as LAMP1, LAMP2, NPC1, NPC1L, Signal Transducing Adapter Molecule (STAM), Hepatocte Growth factor-regulated tyrosine kinase Substrate (HGS) and Lysosomal Integral Membrane Protein 2 (LIMP2) (Koerver et al. 2019)) could lead to morphological changes. This might be is a prerequisite for the autophagy receptors to bind and initiate lysophagy (Fig.3.1). Indeed, there is evidence that lysosomes are not solely in a rigid vesicular structure as they are depicted in textbooks. Recent studies have focused on the dynamics on lysosomal networks, primarily in *Drosophila* muscles

(Johnson et al. 2015; Murakawa et al. 2020). Interestingly, Johnson and colleagues found a tubular lysosomal network and lysosomes that undergo extension, retraction, fusion and fission by live imaging *in vivo* (Johnson et al. 2015). *Drosophila* VCP was required to maintain this network and human p97 was able to rescue effects upon loss of *Drosophila* VCP (Johnson et al. 2015). It will be interesting to investigate if lysosomal dynamics are changed upon response to damage by the UBE2QL1-p97-K48 axis in muscle models.

3.5 How is UBE2QL1 recruited to lysosomes?

UBE2QL1 is a prerequisite for ubiquitination of damaged lysosomes and the accumulation of autophagy effectors in this process. For a complete understanding of the pathway, it will be vital to identify the recruitment mechanism for UBE2QL1.

3.5.1 Detailed analysis of UBE2QL1 lysosomal localization

In this study, we have shown that overexpressed as well as endogenous UBE2QL1 localizes to lysosomes after LLOMe-induced damage (Fig. 2.4, 2.7 and 2.8). We confirmed that the translocation is specific for lysosomal damage, since UBE2QL1 did not accumulate on depolarized mitochondria after CCCP treatment (done by Bojana Kravic) (Koerver et al. 2019). Additionally, we have seen in a rescue experiment that the catalytically inactive form of UBE2QL1 (C88S) is less efficiently recruited to lysosomes when the endogenous UBE2QL1 was depleted (Fig 2.6A). This means that the signal for translocation requires the ubiquitination activity. These findings are in line with former studies of our laboratory, in which we have observed a strong translocation of the essential players of lysophagy (p97 and its designated co-factors) to the respective sites on lysosomes (Papadopoulos et al. 2017).

We have analyzed UBE2QL1's localization in detail in three lines of experimental setups.

First, we decoded the timing of occurrence of ubiquitin (K48- and K63-linked) and the autophagy marker p62 in correlation with LAMP1 and UBE2QL1 (Fig. 2.9). We found that UBE2QL1 appears at the same time as K48-linked ubiquitin on damaged lysosomes, namely after accumulation of p62 and K63-linked chains (Fig. 2.9A and B) (discussed in section 3.3).

Second, in cooperation the Klumperman laboratory has confirmed the localization of UBE2QL1, together with K48 chains, YOD1 and Gal3, to damaged lysosomes after

LLOMe treatment using immuno-electron microscopy (Koerver et al. 2019). This corresponded to the similar timing of recruitment of UBE2QL1 and K48-linked ubiquitin (Fig. 2.9).

Third, in the APEX screen (described in section 3.2) we found lysosomal proteins as well as galectins (Gal1 and Gal3), autophagy receptors (TAX1BP1 and p62) and p97 and its cofactor PLAA significantly elevated in proximity to UBE2QL1 in LLOMe-treated cells (Koerver et al. 2019). This constitutes additional evidence confirming the lysosomal localization of UBE2QL1 upon LLOMe treatment and underlines its function in autophagy. Also, the colocalization with galectins was again emphasized here, making them potential recruiting signals for UBE2QL1, which will be discussed in the next section.

3.5.2 Regulation of UBE2QL1 recruitment

When speculating about potential recruitment factors for UBE2QL1 to damaged lysosomes, the APEX screen that our collaboration partner (Christian Behrends) performed gives some interesting hints (Koerver et al. 2019). Among others, galectins 1 and 3 were found in close proximity to UBE2QL1 in LLOMe-treated cells (Koerver et al. 2019).

Galectins bind to the glycocalyx at the inner lysosomal membrane when holes caused by different means of damage allow them to enter (Maejima et al. 2013). Several studies describe galectins (Gal-1, 3, 8 and 9) with essential recruiting functions for autophagy effectors in ELDR (Chauhan et al. 2016; Thurston et al. 2012; Jia et al. 2018). In the course of decoding UBE2QL1 recruitment to lysosomes, we hence investigated Gal3 and Gal8. While the influx of Gal3 to lysosomes damaged by LLOMe treatment is well-described (Maejima et al. 2013; Aits et al. 2015), Gal8 had not been associated with this specific damage yet. We showed here for the first time that Gal8 strongly localizes to LAMP1-positive structures upon LLOMe treatment (Fig. 2.17A). However, we could exclude a recruiting mechanism for UBE2QL1 relying on Gal3 and Gal8 by a cellular depletion experiment (Fig. 2.17B). The localization of UBE2QL1 to lysosomes upon LLOMe treatment was unchanged when levels of Gal3 or Gal8 (either alone or both at the same time) were downregulated using siRNA in HeLa cells (Fig 2.17B). Jia and colleagues found that Gal8 and Gal9 control mTOR and AMPK during lysosomal damage (Jia et al. 2018) (see in section 3.3). Since we saw Gal8 also on lysosomes after LLOMe treatment, we suggest a role for it in this type of damage. As

we have evidence for UBE2QL1 being essential for the accumulation of LC3 and p62 on lysosomes, it will be interesting to investigate a potential interplay of Gal8 and UBE2QL1 in the activation of autophagy in this context.

Other hits from the APEX screen are for example the ESCRT proteins STAM and HGS (Koerver et al. 2019). The best known role for ESCRT complexes -0, -I, –II and –III is the formation of Multivesicular Bodies (MVB) during sorting of ubiquitinated cargo from endosomes to lysosomes but they also play important roles in membrane repair (Hurley 2015). Recent studies have revealed a repairing function for ESCRT proteins also on lysosomal membranes damaged by LLOMe (Radulovic et al. 2018; Skowyra et al. 2018). However, STAM and HGS form the ESCRT-0 complex, which is known to act in Intraluminal Vesicles (ILV) biogenesis to from MVB but not in membrane repair (Bohannon and Hanson 2020). Moreover, the repairing function of ESCRTs on lysosomes is considered an early event at low dose damage, separated from lysophagy itself (Papadopoulos, Kravic, and Meyer 2019). As most of the remaining hits of the APEX screen are membrane-anchored proteins with distinct functions for the stability of the lysosomal membrane (LAMP1, LAMP2, NPC1, NPC1L, CLINT1, Spartin, LIMP2), we would rather classify them as potential ubiquitination targets (see section 3.4.1) than as recruiting factors. Moreover, it might be that UBE2QL1 is only indirectly recruited through an interacting E3 ligase.

A possible mechanism of UBE2QL1 recruitment might be by posttranslational modification of the protein itself. Modification with ubiquitin or UBLs is for example a common mechanism of E2 enzyme activation (van Wijk and Timmers 2010; Stewart et al. 2016). At least for UBE2R2, it has been described that phosphorylation by Casein Kinase II (CK2) at its acidic tail probably additionally facilitates its localization (Sadowski et al. 2007; Coccetti et al. 2008). It will be interesting to investigate potential ubiquitination and phosphorylation sites in UBE2QL1 that could serve as such regulatory signals.

3.6 A role for UBE2QL1 in lysosomal homeostasis and degenerative diseases

The results of this study provide several pieces of evidence that UBE2QL1 has an additional role in maintenance of basal lysosome homeostasis, in this case detached from lysophagy induced under stress conditions. Firstly, we observed an increase in Gal3 puncta in UBE2QL1-depleted cells even without induction of lysosomal damage

(Fig. 2.15), indicating towards LMP and disturbed lysosomal integrity. Secondly, UBE2QL1 depletion led to impaired survival of cells even without any further stress induction (Fig. 2.16). Third, on the molecular level, deficiency of UBE2QL1 led to mTOR dissociation from lysosomes and TFEB dephosphorylation and translocation to the nucleus (Fig. 2.18). Under basal conditions, mTOR resides on lysosomes and phosphorylates TFEB (Settembre et al. 2013). When lysosomes are not intact, mTOR is dissociated and inactivated (Roczniak-Ferguson et al. 2012). This in turn leads to dephosphorylation of TFEB and transcription of genes for lysosomal biogenesis, autophagy and other lysosome-associated processes (Settembre et al. 2013). Indeed, we also noticed an increased number of lysosomes in UBE2QL1-depleted but otherwise unchallenged cells, displaying a potential consequence of TFEB dephosphorylation and transcription of genes for lysosomal biogenesis (Fig. 2.18). Altogether, this suggests that UBE2QL1 might be essential for the maintenance of lysosomal integrity and avoidance of LMP in the normal cellular environment (Fig.3.2). In line with this, our collaboration partners Bin Liu and Marja Jäättelä from Copenhagen have observed similar functions for UBC-25, the *C. elegans* orthologue of UBE2QL1 (Koerver et al. 2019). Gal3-positive structures were found in *ubc-25* mutant worms (Koerver et al. 2019). This indicates that the here observed role of UBE2QL1 in basal lysosomal homeostasis is conserved among human and worms. The effect was even more increased in double mutants of Scavenger receptor (SD36 family) related (*scav-3)* and *ubc-25* (Koerver et al. 2019). SCAV-3 is the homolog of the human LIMP2, a lysosomal transmembrane protein, and is involved in lysosomal membrane integrity (Li et al. 2016). In line with this, LIMP2 was also found in proximity to UBE2QL1 in LLOMe-treated cells (Koerver et al. 2019).

It remains to be clarified, whether this role of UBE2QL1 in unchallenged cells is attributed to its ubiquitinating features or if other processes are involved here. Based on our data and data from other groups, we propose LAMP1 and LAMP2 as potential ubiquitination targets of UBE2QL1 during lysophagy (see 1.4.1). However, these proteins have no influence on the lysosomal integrity under basal conditions (Li et al. 2016). A possible scenario is that UBE2QL1 has distinct functions under normal and stress situations. Although we observed a clear role for lysosomal integrity without induced stress, UBE2QL1 does not primarily localize to lysosomes in untreated cells (Fig. 2.4). Possibly, it constantly ubiquitinates and thereby stabilizes proteins that ensure lysosomal integrity, such as LIMP2, at low levels (Fig. 3.2). Hence, no specific

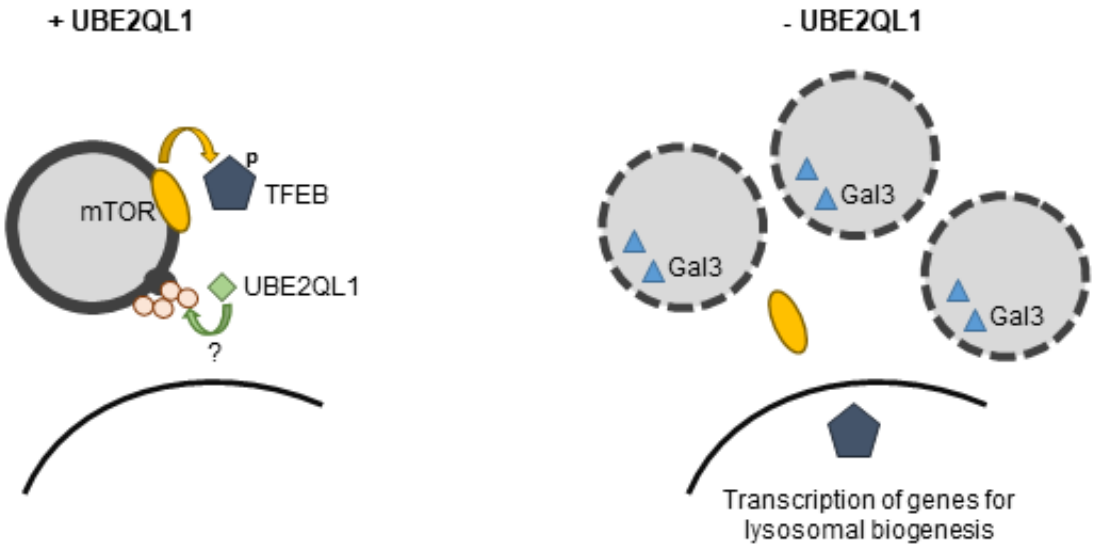

Figure 3.2: Model for the function of UBE2QL1 in basal lysosomal homeostasis.
Under normal cellular conditions, mTOR resides on lysosomal membranes and phosphorylates TFEB. This holds TFEB in the cytosol. When UBE2QL1 is missing, lysosomes are harmed (seen by Gal3 influx) and mTOR is dissociated from membranes and thereby inactivated. The resulting de-phosphorylation of TFEB leads to its translocation to the nucleus and transcription of target genes, for example for lysosomal biogenesis. This is probably the cause for the higher number of lysosomes in UBE2QL1-depleted cells. Possibly, UBE2QL1 constantly ubiquitinates lysosomal membrane proteins at low levels (without detectable translocation), contributing to the integrity of the membrane.

translocation can be measured, at least in our setup. Increased LMP after UBE2QL1 depletion would then lead to mTOR dissociation and TFEB activation and transcription of genes for lysosomal biogenesis, in agreement with the increased number of lysosomes that we found in UBE2QL1-depleted cells (Fig. 2.18 and 3.2). Speaking for a role detached from classical lysophagy is that depletion of ATG5 and ATG7 did not cause Gal3 puncta (Koerver et al. 2019).

There are hints that other that enzymes acting in the response to lysosomal damage are also involved in lysosomal biogenesis under normal cellular conditions. KO of TRIM16 also caused TFEB nuclear localization (Chauhan et al. 2016). Also, p97 was linked to lysosomal biogenesis and compromised lysosome integrity was identified as a hallmark in p97 KO mouse skeletal muscle (Arhzaouy et al. 2019). The p97 KO phenotype in skeletal muscle shows similarities to UBE2QL1 depletion: Arhzaouy and colleagues found Gal3 puncta and persistent TFEB activation, which is probably the cause for the observed myofiber necrosis (Arhzaouy et al. 2019). This indicates that the p97-UBE2QL1(-K48) axis needs to be active in order to cope with basal damage

of the lysosomal system and that disturbances have severe consequences for cells and tissues.

MSP1 is caused by different p97 mutations and affects several types of tissues, including muscles. Notably, all phenotypes are described as degenerative (Meyer and Weihl 2014). Of note, also UBC-25 in *C. elegans* is reported to be essential for neuro-muscular functions and its depletion causes protein aggregation, a hallmark of degenerative diseases (Schulze et al. 2003). This is an additional hint for a potential relevance of UBE2QL1 in pathologies. This is most likely linked to its described interaction with p97 during lysophagy and their function in lysosome homeostasis.

4 Material and Methods

4.1 Lists of antibodies used in this study

Table 4.1: Primary antibodies

Antigen	Species	Dilution IF	Dilution WB	Source
Galectin-3	mouse	1:250	-	Santa Cruz Biotechnology (sc-32790)
Galectin-3	rabbit	1:250	-	Santa Cruz Biotechnology (sc-20157)
Galectin-8	goat	1:200	1:200	R&D Systems (AF1305)
GAPDH	mouse	-	1:10,000	Sigma-Aldrich (G8795)
HA	rabbit	1:500	-	Sigma-Aldrich (H6908)
HA	goat	1:500	-	Abcam (ab9134)
HA	mouse	1:500	1:2000	Covance (MMS-101R)
K48 ubiquitin	rabbit	1:800	-	Millipore (clone Apu2)
K63 ubiquitin	rabbit	1:500	-	Millipore (clone Apu3)
LAMP1	mouse	1:350	-	Santa Cruz Biotechnology (sc-20011)
LAMP1	rabbit	1:500	1:1000	Cell Signaling Technology (C54H11)
LC3A/B	rabbit	1:500	1:2000	Sigma-Aldrich (L8918)
LC3B	mouse	1:500	-	Cosmo Bio (LC3-1703)
mTOR	rabbit	1:500	-	Cell Signaling Technology (7C10)
p62	rabbit	1:500	-	Sigma-Aldrich (P0067)
VCP	mouse	1:500	-	Santa Cruz Biotechnology (sc-57492)
Phospho-S6 ribosomal protein (Ser236/236)	rabbit	-	1:2000	Cell Signaling Technolgy (2211)

Polyubiquitin	mouse	1:1000	-	Millipore (clone FK2)
TAX1BP1	rabbit	1:500	-	Sigma-Aldrich (HPA024432)
TFEB	rabbit	1:100	1:1000	Cell Signaling Technology (42405)
UBE2QL1	rabbit	1:500	1:1000	Raised against C-terminal peptide: CTHEKYGWVTPPVSDG by Eurogentec

Table 4.2: Secondary antibodies

Antigen	Species	Dilution IF	Dilution WB	Source
HRP anti-mouse	goat	-	1:10,000	BioRad
HRP anti-rabbit	goat	-	1:10,000	BioRad
Alexa Fluor 488 anti-mouse	goat	1:500	-	Invitrogen
Alexa Fluor 488 anti-rabbit	goat	1:500	-	Invitrogen
Alexa Fluor 488 anti-rabbit	donkey	1:500	-	Invitrogen
Alexa Fluor 561 anti-mouse	goat	1:500	-	Invitrogen
Alexa Fluor 561 anti-mouse	donkey	1:500	-	Invitrogen
Alexa Fluor 561 anti-rabbit	goat	1:500	-	Invitrogen
Alexa Fluor 633 anti-goat	donkey	1:500	-	Invitrogen
Alexa Fluor 633 anti-mouse	goat	1:500	-	Invitrogen

4.2 List of buffers and solutions used in this study

Extraction buffer
150 mM KCl
5 mM MgCl2
25 mM Tris-HCl
1% Triton X-100
5% Glycerol
2 mM ß-Mercaptoethanol
pH 7.4

Protease inhibitor 100x
1 protease inhibitor tablet
(Roche, Complete EDTA-free) in 500
µL PBS

Phosphatase inhibitor 10x
1 phosphatase inhibitor tablet
(Roche, PosSTOP) in 1 ml PBS

6x SDS loading buffer
0.35 M Tris, pH 6.8
30% glycerol (87%)
10% SDS
600 mM DTT
0.02% bromphenol blue

SDS running buffer
190 mM glycine
25 mM Tris pH 8.8
0.1% SDS

Wet blot transfer buffer
192 mM glycine
25 mM Tris pH 8.8
0.04% SDS
20% Methanol

LB medium
10g peptone (Fluka)
10 g NaCl
5 g yeast extract (Applichem)
ad 1 l Mili-Q H2O
pH 7.0
autoclave

LB agar
20 g agar (Applichem)
ad 1 l LB medium
autoclave

10x PBS pH 7.4
100 mM Na2HPO4
21.7 NaH2PO4
1.54 M NaCl
pH 7.4

PBS-T
0.05 % Tween 20
in PBS pH 7.5

10x TBS pH 7.6
1.5 M NaCl
100 mM Tris
pH 7.6

TBS-T
0.1% Tween 20
in TBS pH 7.6

PIPES solution
80 mM PIPES
5 mM EGTA
1 mM MgCl2
pH 7.0
0.01% saponin before use

PFA solution
4% paraformaldehyde
in PBS pH 7.4
store at -20°C

IF blocking solution
3% BSA (Albumin fraction V,
Applichem)
0.1% Triton X-100
0.1% Saponin
in PBS pH 7.4

RIPA buffer
25 mM Tris-HCl (pH 7.5)
150 mM NaCl
1% Nonident P-40
1% Na-deoxycholate
0.1% SDS

LC3 lysis buffer
10 mM HEPES (pH 7.9)
10 mM KCl
0.1 mM EDTA
300 mM NaCl
1% Nonident P-40

4.3 Molecular cloning

4.3.1 Site directed mutagenesis

To introduce single amino acid exchanges into the sequence of expression plasmids, site directed mutagenesis was done using the QuickChangesite®-directed mutagenesis kit (Stratagene). DNA primers were designed complementary to the target sequence with a single base difference flanked by at least 10 nucleotides (see in table 4.5).

Table 4.3: Reaction mixture for mutagenesis PCR

Component	Final concentration
dNTPs	10 µM each
PfuUltra II reaction buffer	1x
Forward primer	0.3 µM
Reverse primer	0.3 µM
Template DNA	50 ng
PfuUltra II DNA polymerase	1.25 U

The polymerase chain reaction (PCR) with the PfuUltra II DNA polymerase (Agilent) was run in a Mastercycler nexus SX1e Thermal Cycler (Eppendorf). The reaction mixture is described in table 4.3.

Table 4.4: General cycling program for mutagenesis PCR

Cycle step	Temperature	Time	cycles
Initial denaturation	95°C	30 s	1
Denaturation	95°C	30 s	16
Annealing	60°C	60 s	16
Extension	70 °C	6 min 30 s	16
Final extension	70 °C	15 min	1

In order to digest the template DNA, the PCR product was digested with 5U *DpnI* (NEB) for 1 h at 37°C. After purification with the PCR Clean-up kit (Machery-Nagel), the DNA was transformed into DH5α cells by heat shock at 42°C for 45 min. Bacteria were grown on Lysogeny Both (LB) agar plates containing 50 µg/ml ampicillin or 25 µg/ml kanamycin for selection and positive clones were expanded in liquid cultures with

selection antibiotics over night at 37°C, shaking at 250 rpm. The DNA was purified with the NucleoSpin® plasmid kit (Machery-Nagel).

Table 4.5: DNA primers

Name	sequence	Data base #
UBE2J1_stop fwd	CCGACTTTGAGTTATAACCAACTTTCTTGG	1805
UBE2J1_stop rev	CCAAGAAAGTTGGTTATAACTCAAAGTCGG	1806
UBE2Q2_stop fwd	CCCAAAGGAAGATGGCTAACCCAACTTTCTTGG	1813
UBE2Q2_stop rev	CCAAGAAAGTTGGGTTAGCCATCTTCCTTTGGG	1814
UBE2J1_missense fwd	GCCAGTACATCGTACGGACTCCAGAATTCC	1803
UBE2J1_missense rev	GGAATTCTGGAGTCCGTACGATGTACTGGC	1804
UBE2QL1_removestop fwd	GGGGACAATTTGTACAAAAAAGCAGGCTTCATGAAGGAGCTGCAGGACATCGC	1815
UBE2QL1_removestop rev	GGGGACCACTTTGTACAAGAAAGCTGGGTCCTATCAGCCGTCGGACACGG	1816
Gal3_HindII fwd	GTACATAAGCTTTGGCAGACAATTTTTCGC	1797
Gal3_EcoRI rev	ACTGCGGAATTCTTATATCATGGTATATGAAGC	1798
UBE2QL1_C88S fwd	GACGGCGGCGCCATCGCCATGGAGCTGCTCAC	1817
UBE2QL1_C88S rev	GTGAGCAGCTCCATGGCGATGGCGCCGCCGTC	1818

4.3.2 Generation of expression plasmids

Table 4.6: DNA expression plasmids

Name	Species	Source	Database #
pmCherry-Gal3	human	Molecular cloning	1485
pDNR223-UBE2J1 (w/o stop)	human	ORFeome, gift from Christian Behrends	1499
pDNR223-UBE2J1 (w stop)	human	Site directed mutagenesis	1504
pDNR223-UBE2Q2 *isoform 1* (w/o stop)	human	ORFeome, gift from Christian Behrends	1501
pDNR223-UBE2Q2 (w stop)	human	Site-directed mutagenesis	1506
pDNR221-UBE2QL1 (w stop codon)	human	Gateway cloning	1502
pDNR221-UBE2QL1 (w/o stop codon)	human	Site directed mutagenesis	1503
pcDNA5FRT/TO-Strep/HA-UBE2J1	human	Gateway cloning	1507
pcDNA5FRT/TO-Strep/HA-UBE2Q2	human	Gateway cloning	1509
pcDNA5FRT/TO-Strep/HA-UBE2QL1	human	Gateway cloning	1510
pcDNA5FRT/TO-UBE2QL1-Strep/HA	human	Gateway cloning	1515
pcDNA5FRT/TO-UBE2QL1 C88S-Strep/HA	human	Site directed mutagenesis	1516
pcDNA5FRT/TO-p97-GFP	human	AG Meyer database	514

For generation of plasmids encoding UBE2QL1, a DNA image clone was ordered (IDT) that contained the whole coding sequence of UBE2QL1 (NM_00114516) flanked by attB sites (underlined) for cloning with the Gateway® Technology with Clonase™ II (Invitrogen) (with attB1 and attB2 underlined and start and stop codons of UBE2QL1 CDS in bold):

GGGGACAAGTTTGTACAAAAAAGCAGGCTTCTCGAGC**ATG**AAGGAGCTGCAGG
ACATCGCGCGCCTTAGCGACCGCTTCATCTCCGTGGAGCTGGTGGACGAGAGC
CTGTTCGACTGGAACGTGAAGCTGCACCAGGTGGACAAGGACTCGGTGCTGTG
GCAGGACATGAAGGAGACCAACACCGAGTTCATCCTGCTCAACCTCACCTTCCC
CGACAACTTCCCCTTCTCGCCGCCCTTCATGCGGGTGCTCAGCCCGCGCCTGG
AGAACGGCTACGTGCTGGACGGCGGCGCCATCTGCATGGAGCTGCTCACGCC
GCGCGGCTGGTCCAGCGCCTACACCGTGGAGGCCGTCATGCGCCAGTTCGCA
GCCAGCCTGGTCAAGGGCCAGGGACGGATCTGTAGAAAAGCTGGCAAATCAAA
AAAGTCCTTCAGTCGCAAGGAAGCTGAAGCTACCTTTAAGAGTTTGGTGAAGAC
GCATGAAAAATATGGTTGGGTCACCCCGCCCGTGTCCGACGGC**TGA**GGAATTC
ACCCAGCTTTCTTGTACAAAGTGGTCCCC

To generate an entry clone, UBE2QL1 insert was shuttled into pENTR221 vector with the BP reaction according to the manufacturer's instructions, resulting in pDNR221-UBE2QL1. For destination vectors containing UBE2J1 and UBE2Q2, pDNR223-UBE2J1 and pDNR223-UBE2Q2 were subjected to site directed mutagenesis with the indicated primers (table 4.5) in order to insert stop codons for N-terminal tagging. To remove a missense mutation in pDNR223-UBE2J1 (L214V), site directed mutagenesis (described in 4.3.1) was applied to reverse it. The E2 enzymes were then shuttled into pcDNA5FRT/TO-Strep/HA (N-terminal) destination vector with the LR reaction according to the manufacturer's instructions. For C-terminal tagging of UBE2QL1, pDNR221-UBE2QL1 was subjected to site directed mutagenesis (described in 4.3.1) in order to remove the stop codon. pDNR221-UBE2QL1 without stop codon was then subjected to LR reactions with pcDNA5FRT/TO-Strep/HA and pcDNA5FRT/TO-GFP (both C-terminal).

For expression of Gal3 in mammalian cells, Gal3 *isoform 1* was amplified from U2OS cDNA (kindly provided by the Knauer laboratory) with primers introducing restriction sites for *HindIII* and *EcoRI* (described in table 4.5, designed by Philipp Kirchner) by PCR with the Phusion High Fidelity Polymerase (NEB) (see table 4.7 for reaction mixture and table 4.8 for cycling program).

Table 4.7: Reaction mixture for amplification of Gal3 from cDNA

Component	Final concentration
dNTPs	5 µM each
5 x Phusion HF Buffer	1x
Forward primer	0.3 µM
Reverse primer	0.3 µM
Template cDNA	100 ng
Phusion HF DNA polymerase	5 U

Table 4.8: Cycling program for PCR for amplification of Gal3

Cycle step	Temperature	Time	cycles
Initial denaturation	98°C	2 min	1
Denaturation	98°C	30 s	30
Annealing	58°C	30 s	30
Extension	72°C	60 s	30
Final extension	72°C	10 min	1

After purification of the PCR product, restriction digest with 10 U *HindIII* and *EcoRI* (NEB) of the designated insert and pmCherry-C1 empty vector for 30 min at 37°C was followed by ligation with T4 DNA ligase (NEB) in a 1:3 ratio of plasmid and insert for 90 min at 16°C.

4.4 Cell culture and cell based assays

4.4.1 General cell culture

HeLa Kyoto and U2OS cells were cultured in medium consisting of Dulbecco's modified Eagle's medium (DMEM, PAN Biotech) supplemented with 10% Fetal Bovine Serum (FBS, PAN Biotech) and 1% Penicillin/Streptomycin (Pen/Strep, PAN Biotech) in a humidified incubator at 37°C and 5% CO_2. SH-SY5Y cells were grown in DMEM/F-12 (1:1) medium (PAN Biotech) with 10% FBS and 1% Pen/Strep under the same conditions.

4.4.2 Transfection of plasmids for transient expression

HeLa cells were transfected at approximately 50% confluence using Lipofecatmine 2000 (ThermoFisher Scientific) for 24 h before analysis. For experiments in 6-well plates, 0.5 µg plasmid DNA and 1.5 µl Lipofectamine 2000 were mixed in Opti-Minimal Essential Medium (Opti-MEM) (PAN Biotech) and applied to the cells according to the manufacturer's instructions. SH-SY5Y cells were transfected using JetPRIME (Polyplus) at approximately 50% confluence 24 h before analysis. For a 6-well plate, 1 µg plasmid DNA and 2 µl JetPRIME were used according to the manufacturer's instructions. For all conditions, culturing medium was replaced 4 h after transfection.

4.4.3 Generation of stable cell lines

For generation of stable cell lines using the Flp/In™ system (Invitrogen), parental HeLa cells with a single genomic Flp recombination target site (HeLa FRT) cells stably

expressing a tetracycline repressor were a kind gift of Gerhard Müller-Newen). They were cultured in DMEM supplemented with 10% tetracycline-free FBS, 1% Pen/Strep, 15 µg/ml blasticidin (ThermoFisher Scientific) and 200 µg/ml zeocin (ThermoFisher Scientific). For transfection, the medium was changed to full medium only containing 15 µg/ml blasticidin without zeocin. Cells were co-transfected with the pOG44 Flp-recombinase plasmid (Invitrogen) and plasmids encoding UBE2QL1-HA (pcDNA5FRT/TO-UBE2QL1-Strep/HA) or p97-GFP (pcDNA5FRT/TO-p97-GFP) in a 9:1 ratio using Lipofectamine 2000, as described before. Selection of positive clones was carried out with selection antibiotics (15 µg/ml blasticidin (ThermoFisher Scientific) and 250 µg/ml hygromycin (PAN Biotech)) for approximately 2 weeks. When positive clones were expanded and confirmed by Western blot analysis, they were cultured without selection antibiotics for further experiments. Expression of proteins was induced with 1 µg/ml Doxycyline (Sigma Aldrich) for 24 h.

HeLa cells stably expressing mCherry-Gal3 were generated by Chrisovalantis Papadopoulos (Koerver et al. 2019) and cultured in DMEM supplemented with 10% FBS in the presence of pen/strep with 500 µg/ml Geneticin (G418) (VWR).

4.4.4 RNA interference (RNAi)

For depletion of proteins in HeLa cells, RNAi was induced by transfection of siRNAs with Lipofectamine RNAiMAX (ThermoFisher Scientific). Cells were reversely transfected at the time of seeding and analyzed after 48, 60 or 72 h, as indicated. For experiments in a 6-well plate, 10 nM small interfering RNAs (siRNAs) were mixed with 3.2 µl RNAiMAX according to the manufacturer’s instructions.

Table 4.9: RNA interferance

Name	Sequence	Reference	Database #
siCtrl		Dharmacon (D-001810-10-05)	1194
siUBE2J1 #3	GAUGUCCUGUUGCCUUUAA	Dharmacon (J-007266-07)	1833
siUBE2Q2 #2		Dharmacon (J-008326-10)	1840
siUBE2QL1 #2	CCACUUAGAUAUCGACUCA	Dharmacon (J-024273-10)	1844
siUBE2QL1 #4	GACUAAAGAUUGUCAACGA	Dharmacon (J-024273-12)	1846
siUBE2QL1 #5	AAGCUGAAGCUACCUUUAATT	Microsynth, designed for this study	1847
siTAX1BP1 (pool)	GAUCAACAGUCAAUUGUGU/ GCAGUUAUGUUUGGCUGAA/ GGAUAUUACCUUCCAAAUG/ UCUGUUACGUUACCCAUAA	Dharmacon (L-016892-00-0005)	1855
sip62	GCAUUGAAGUUGAUAUCGATT	Microsynth (Pankiv et al. 2007)	1035
sip97 S3	AAGUAGGGUAUGAUGACAUUGTT	Microsynth	740
siGal8 #1	CCCACGCCUGAAUAUUAAAGCAUUU	Microsynth (Thurston et al. 2012)	1858

siGal8 #2	GGACAAAUUCCAGGUGGCUGUAAAU	Microsynth (Thurston et al. 2012)	1859
siGal3 (pool)	GGAGAGUCAUUGUUUGCAA GUACAAUCAUCGGGUUAAA GGCCACUGAUUGUGCCUUA CGGUGAAGCCCAAUGCAAA	Dharmacon (L-010606-00)	1853

4.4.5 Pharmacological treatments of cells

To induce lysosomal damage, cells were treated with 250 µM LLOMe (Sigma Aldrich) for the indicated times. For chase experiments, cells were washed once with Phosphate Buffered Saline (PBS) (PAN Biotech) and fresh culturing medium was added for the desired time-points. Cells were treated with 200 nM Bafilomycin A1 (Biomol) to inhibit acidification of lysosomes for 5 h or 1 µM Torin1 (Torcis Bioscience) for inhibition of mTOR for 2 h.

4.4.6 Cell viability assay

HeLa cells were seeded at a density of 3,500 cells per well in 96-well plates in triplicates and were reversely transfected with siRNAs as described before for 48 h. In the last 12 h, lysosomal damage was induced by treatment with increasing concentrations of LLOMe. Cell viability was measured using the 96® AQueous One Solution Cell Proliferation Assay (Promega) according the manufacturer's instructions. Emission at 490 nm was measured at a SpectraMay plus plate reader (Molecular Devices). The mean of the triplicates was calculated and values were normalized to 100% survival in untreated controls.

4.5 Immunofluorescence staining and microscopy

4.5.1 Processing of microscopy samples

HeLa cells were seeded on glass coverslips (12mm, 0.17 ± 0.005 mm, Roth) in 24-well plates in a density of 17,000 or 36,000 cells per well for 60-72 h or 48 h, respectively. HeLa FRT cells were seeded at a density of 22,000 or 40,000 for 60-72 h or 48 h, respectively. After transfections and treatments, cells were fixed in 4% paraformaldehyde in PBS at room temperature or 100% ice- cold methanol at -20°C (for TAX1BP1 staining) for 20 min. For staining for endogenous UBE2QL1, cells were pre-extracted in PIPES solution for 3 min before fixation. For indirect

immunofluorescence, cells were permeabilized with 0.1% Triton X-100 in PBS for 10 min and blocked with blocking solution for 45 min. Incubation with primary antibodies at final concentrations was done in blocking solution for 90 min. Samples were washed three times with 0.1% Triton in PBS. Sondary fluorescently labeled antibodies were diluted in blocking solution and incubation was for 30 min. Staining with 1 µg/ml DAPI (AppliChem) and 1 µg/ml HSC CellMask™ Deep Red Stain (ThermoFisher Scientific) for recognition of cells for automated image analysis was done together with the sondary antibody incubation. Washing two times in 0.1% Triton in PBS, once in PBS and once in ultrapure water was followed by mounting in ProLong Gold (ThermoFisher Scientific) on object slides (Marienfeld). All antibodies are listed in tables 4.1 and 4.2.

4.5.2 Confocal laser-scanning microscopy

Confocal laser scanning microscopy was performed on a TCS SP5 Acousto Optical Beam Splitter (AOBS) system. Images were acquired using an HCX PL APO 63x/1.4NA oil immersion objective or an HC PL APO 20x/0.7NA dry objective. Fluorophores were excited with a helium-neon laser (for Alexa-633), a diode-pumped solid-state laser (for Alexa Fluor 568 and mCherry), an argon laser (for Alexa Fluor 488 and GFP) and a diode laser (for DAPI). Signals were detected with standard PMT detectors as well as sensitive Hybrid detectors (HyD) in a 1024x1024 px format with 1 or 1.5 x zoom for image quantification or 3 or 4 x zoom for exemplary images with a bit depth of 12 bit. Acquisition and hardware was controlled by LAS AF software (Leica Microsystems).

4.5.3 Image analysis

Images were processed using Fiji software (Schindelin et al. 2012), Adobe Photoshop and Illustrator CS5 (Adobe Systems). Automated quantifications were done with CellProfiler software versions 2.1, 2.2 and 3.0 (Carpenter et al. 2006). The pipelines were individual for the assays. In general, nuclei were detected in the DAPI channel with “IdentifyPrimaryObjects”. Based on the nuclei and using the signal of the HSC CellMask™ stain, whole cells were identified with the “IdentifySondaryObjects” module. Cells were filtered depending on their size or, in cases of overexpression based on the intensity of the signal of the transfected protein with “FilterObjects”. For colocalization measurements, vesicles (e.g. in the LAMP1 and FK2, K48 or K63 staining) were determined with the “IdentifyPrimaryObjects” module and identified vesicles of two channels were related using “MaskObjects” to determine their overlap. For correlation

studies, the Pearson's Correlation Coefficient of two signals (e.g. LAMP1 with K48, K63, p62, mTOR, p97-GFP or Gal3 with LC3) was measured in the whole cell or only on before determined LAMP1 vesicles with "MeasureCorrelation". For the TFEB localization assay, the cytoplasm was determined by subtracting the identified nuclei from cells with "IdentifyTertiaryObjects". "MeasureIntensity" was used to determine intensity of the TFEB staining in nuclei and cytoplasm and the ratio was calculated using the "CalculateMath" module. Graphs and statistical analysis were done using Excel 2016 (Microsoft Corporation) and GraphPad Prism 5 (GraphPad Software Inc.).

4.6 siRNA screen

The screen was performed in the lab of Christian Behrends in Frankfurt with the help of Mira Polajnar. siRNA libraries and single siRNAs for the sondary screen (Dharmacon) were a kind gift of Christian Behrends. Using a CyBi®-SELMA pipetting robot (Analytik Jena AG), a stock 96-well plate containing dilutions of all siRNAs was prepared, as well as 96-well plate containing RNAiMAX. The transfection reagent and the siRNAs were mixed in quadruplicates in CellCarrier-384 Black well plates (PerkinElmer), so that together with the culturing medium a final concentration of 20 nM of siRNAs was reached. HeLa cells were plated out manually using a multichannel pipette in a density of 700 cells in 40 µl medium per well. After 72 h, lysosomal damage was induced by treatment with 250 µM LLOMe for 3 h and cells were fixed and stained as described before (), except that DRAQ5 (CellSignalling) was used to stain nuclei. The 384-well plates were automatically imaged using an Opera automated spinning disk confocal microscope controlled by the EvoShell_OperaLX software and equipped with a UPLAPO 60x/1.2NA water objective. Images were acquired with a High QE CCD camera and analyzed with the Acapella 2.6 Studio software (PerkinElmer). Colocalizations were determined by Mira Polajnar. Statistical analysis was done using Excel 2016 (Microsoft Corporation). The percentage of LAMP1 vesicles that were positive for FK2 or K48 vesicles was calculated. From this, the robust z-scores of each sample against the whole plate were calculated.

Equation 1: Calculation of the median absolute deviation (MAD)

$$MAD\ (Sample_{all}) = 1.4826\ \times median\ (|Sample_{individual} - median(Sample_{all})|)$$

Equation 2: Calculation of the robust Z-score

$$Robust\ z - score = \frac{Sample_{indivdual} - \mathrm{median}(Sample_{all})}{\mathrm{MAD}(Sample_{all})}$$

4.7 Biochemical assays

4.7.1 Preparation of cell extracts

After depletions and treatments, cells were harvested for analysis by Western blotting. To preserve the proteins, all steps were performed on ice. Cells were washed twice in ice-cold PBS before addition of 70 µl lysis buffer per 6-well. All lysis buffers used for the different conditions (listed in buffers) were supplemented with 1 x protease and 1 x phosphatase inhibitors. Lysis was carried out for 10 min in the plates before scraping the cells with a cell scraper and transferring them to reaction tubes. Lysates were incubated rotating at 4°C for additional 10 min. Centrifugation was done at 13,000 rpm for 15 min at 4°C and the protein concentration of supernatants was measured with the Bicinchoninic Acid Assay (BCA) assay (Interchim) in 96-well plates at a SpectraMay plus plate reader (Molecular Devices). Lysates were either frozen in liquid nitrogen for storage at -80°C or processed for Western blot analysis. For this, extracts containing 20 µg protein were supplemented with 6 x SDS loading buffer and boiled at 95°C for 5 min.

4.7.2 SDS-PAGE and Western blotting

Cell lysates were separated by sodium dodecyl sulfate polyacrylamide gel electrophoresis (SDS-PAGE). Polyacrylamide gels were casted using the Mini-PROTEAN Tetra Handcast System (BioRad). The prepared cell extracts were loaded to gels with varying concentrations, depending on the proteins to be analyzed, and electrophoresis was done in the Mini-PROTEAN Tetra Cell in 1 x SDS running buffer at a current of 20 mA/gel at an EPS 601 power supply (GE Healthcare). The Mini Trans-Blot cell (BioRad) was used to transfer proteins to nitrocellulose membranes (Amersham Protan Premium 0.45 µm, GE Healthcare) in wet blot buffer at 800 mA for 3 h at 4°C. For visualization of the transferred proteins, the membrane was stained with Ponceau S and destained in 5% acetic acid. After complete destaining in PBS-T or Tris-Buffered Saline with Tween-20 (TBS-T) (for TFEB and p-S6 antibodies), the

membrane was blocked in 5% non-fat dry milk in PBS-T or TBS-T or 3% BSA in PBS-T (for UBE2QL1 antibody) for at least 30 min at room temperature. Primary antibodies were diluted to final concentrations (all antibodies are described in) in 3% BSA in PBS-T or TBS-T (or 5% milk and 3% BSA in PBS-T for UBE2QL1 antibody) and incubation was at 4°C over night (5% milk in TBS-T for at least 3 days for Gal8 antibody). After washing three times in PBS-T or TBS-T, incubation with horseradish peroxidase (HRP) coupled sondary antibodies was for 45 min at room temperature. After three times washing, detection of the signal was realized by incubating the membranes with SuperSignal West Pico ECL substrate (ThermoFisher Scientific) or ECL Prime Western Blotting detection reagent (GE Healthcare). Membranes were exposed to to Super RX film (Fujifilm) and developed with a Cawomat 2000 IR (Agfa-Gevaert Heathcare GmbH) or documented with a Chemostar ECL Imager (INTAS Science Imaging Instruments GmbH).

4.7.3 Affinity purification of UBE2QL1 antibody

The custom-made polyclonal rabbit antibody against UBE2QL1 (Eurogentec) was affinity purified against the C-terminal peptide that was also used for immunization (sent by Eurogentec). SulfoLink Coupling Gel (Pierce) was used in a 10 ml BioRad column to couple 5 mg of the peptide solved in 0.1 M sodium phosphate (pH 7.8) and 5 mM Ethylenediaminetetraacteic Acid (EDTA). The column was rotated slowly for 15 min and let stand for 30 min at room temperature. When coupling was complete the column was incubated with 0.1 mM sodium phosphate containing β-Mercaptoethanol (BME) first rotating and then standing for 30 min at room temperature each. It was washed with 0.1 mM $NaHCO_3$, with 1 mM $NaHCO_3$, 0.2 x PBs, 0.1 M glycine-HCl (pH 2.3) and lastly 1 x PBS.

The rabbit serum containing the antibody was filtered with a 0.4 µm filter and loaded on the column twice. The column was washed with 0.5 M NaCl and 0.1% Tween 20 in PBS and then 5 times in 0.2 x PBS. Elution of the antibody was done with 100 mM glycine-HCl (pH 2.3), which was collected in 2 M Tris-base for neutralization. The different fractions were pooled and dialyzed over night at 4°C in 40% glycerol in PBS. The protein concentration was determined photometrically (Eppendorf BioPhotometer) and the antibody was stored at -20°C.

5 References

Agop-Nersesian, Carolina, Livia Niklaus, Rahel Wacker, and Volker Theo Heussler. 2018. 'Host cell cytosolic immune response during Plasmodium liver stage development', *FEMS Microbiology Reviews*, 42: 324-34.

Aits, S., J. Kricker, B. Liu, A. M. Ellegaard, S. Hamalisto, S. Tvingsholm, E. Corcelle-Termeau, S. Hogh, T. Farkas, A. Holm Jonassen, I. Gromova, M. Mortensen, and M. Jaattela. 2015. 'Sensitive detection of lysosomal membrane permeabilization by lysosomal galectin puncta assay', *Autophagy*, 11: 1408-24.

Akutsu, M., I. Dikic, and A. Bremm. 2016. 'Ubiquitin chain diversity at a glance', *J Cell Sci*, 129: 875-80.

Alpi, A. F., V. Chaugule, and H. Walden. 2016. 'Mechanism and disease association of E2-conjugating enzymes: lessons from UBE2T and UBE2L3', *Biochem J*, 473: 3401-19.

Ambivero, C. T., L. Cilenti, S. Main, and A. S. Zervos. 2014. 'Mulan E3 ubiquitin ligase interacts with multiple E2-conjugating enzymes and participates in mitophagy by recruiting GABARAP', *Cell Signal*, 26: 2921-9.

Amerik, Alexander Y., and Mark Hochstrasser. 2004. 'Mechanism and function of deubiquitinating enzymes', *Biochimica et Biophysica Acta (BBA) - Molecular Cell Research*, 1695: 189-207.

Appelmans, F., R. Wattiaux, and C. De Duve. 1955. 'Tissue fractionation studies. 5. The association of acid phosphatase with a special class of cytoplasmic granules in rat liver', *Biochem J*, 59: 438-45.

Arhzaouy, K., C. Papadopoulos, N. Schulze, S. K. Pittman, H. Meyer, and C. C. Weihl. 2019. 'VCP maintains lysosomal homeostasis and TFEB activity in differentiated skeletal muscle', *Autophagy*: 1-18.

Ballabio, A., and J. S. Bonifacino. 2020. 'Lysosomes as dynamic regulators of cell and organismal homeostasis', *Nat Rev Mol Cell Biol*, 21: 101-18.

Banerjee, S., W. S. Brooks, and D. F. Crawford. 2007. 'Inactivation of the ubiquitin-conjugting enzyme UBE2Q2 causes a prophase arrest and enhanced apoptosis in response to microtubule inhibiting agents', *Oncogene*, 26: 6509-17.

Bell, J. L., A. Malyukova, J. K. Holien, J. Koach, M. W. Parker, M. Kavallaris, G. M. Marshall, and B. B. Cheung. 2012. 'TRIM16 acts as an E3 ubiquitin ligase and can heterodimerize with other TRIM family members', *PLoS One*, 7: e37470.

Birmingham, A., L. M. Selfors, T. Forster, D. Wrobel, C. J. Kennedy, E. Shanks, J. Santoyo-Lopez, D. J. Dunican, A. Long, D. Kelleher, Q. Smith, R. L. Beijersbergen, P. Ghazal, and C. E. Shamu. 2009. 'Statistical methods for analysis of high-throughput RNA interference screens', *Nat Methods*, 6: 569-75.

Blythe, E. E., K. C. Olson, V. Chau, and R. J. Deshaies. 2017. 'Ubiquitin- and ATP-dependent unfoldase activity of P97/VCP*NPLOC4*UFD1L is enhanced by a mutation that causes multisystem proteinopathy', *Proc Natl Acad Sci U S A*, 114: E4380-E88.

Bodnar, N. O., and T. A. Rapoport. 2017. 'Molecular Mechanism of Substrate Processing by the Cdc48 ATPase Complex', *Cell*, 169: 722-35 e9.

Bohannon, K. P., and P. I. Hanson. 2020. 'ESCRT puts its thumb on the nanoscale: Fixing tiny holes in endolysosomes', *Curr Opin Cell Biol*, 65: 122-30.

Boya, P., and G. Kroemer. 2008. 'Lysosomal membrane permeabilization in cell death', *Oncogene*, 27: 6434-51.

Buchberger, A., H. Schindelin, and P. Hanzelmann. 2015. 'Control of p97 function by cofactor binding', *FEBS Lett*, 589: 2578-89.

Bug, M., and H. Meyer. 2012. 'Expanding into new markets--VCP/p97 in endocytosis and autophagy', *J Struct Biol*, 179: 78-82.

Burr, M. L., D. J. van den Boomen, H. Bye, R. Antrobus, E. J. Wiertz, and P. J. Lehner. 2013. 'MHC class I molecules are preferentially ubiquitinated on endoplasmic reticulum luminal residues during HRD1 ubiquitin E3 ligase-mediated dislocation', *Proc Natl Acad Sci U S A*, 110: 14290-5.

Carpenter, A. E., T. R. Jones, M. R. Lamprecht, C. Clarke, I. H. Kang, O. Friman, D. A. Guertin, J. H. Chang, R. A. Lindquist, J. Moffat, P. Golland, and D. M. Sabatini. 2006. 'CellProfiler: image analysis software for identifying and quantifying cell phenotypes', *Genome Biol*, 7: R100.

Chau, V., J. W. Tobias, A. Bachmair, D. Marriot, D.J. Ecker, D.K. Gonda, and A. Varshavsky. 1989. 'A Multiubiquitin Chain Is Confined to Specific Lysine in a Targeted Short-Lived Protein', *Science*, 243: 1576-83.

Chauhan, S., S. Kumar, A. Jain, M. Ponpuak, M. H. Mudd, T. Kimura, S. W. Choi, R. Peters, M. Mandell, J. A. Bruun, T. Johansen, and V. Deretic. 2016. 'TRIMs and Galectins Globally Cooperate and TRIM16 and Galectin-3 Co-direct Autophagy in Endomembrane Damage Homeostasis', *Dev Cell*, 39: 13-27.

Clague, M. J., and S. Urbe. 2010. 'Ubiquitin: same molecule, different degradation pathways', *Cell*, 143: 682-5.

Clague, M. J., S. Urbe, and D. Komander. 2019. 'Breaking the chains: deubiquitylating enzyme specificity begets function', *Nat Rev Mol Cell Biol*.

Coccetti, P., F. Tripodi, G. Tedeschi, S. Nonnis, O. Marin, S. Fantinato, C. Cirulli, M. Vanoni, and L. Alberghina. 2008. 'The CK2 phosphorylation of catalytic domain of Cdc34 modulates its activity at the G1 to S transition in Saccharomyces cerevisiae', *Cell Cycle*, 7: 1391-401.

Cremer, T., M. L. M. Jongsma, F. Trulsson, A. C. O. Vertegaal, J. Neefjes, and I. Berlin. 2021. 'The ER-embedded UBE2J1/RNF26 ubiquitylation complex exerts spatiotemporal control over the endolysosomal pathway', *Cell Rep*, 34: 108659.

Das, R., Y. H. Liang, J. Mariano, J. Li, T. Huang, A. King, S. G. Tarasov, A. M. Weissman, X. Ji, and R. A. Byrd. 2013. 'Allosteric regulation of E2:E3 interactions promote a processive ubiquitination machine', *EMBO J*, 32: 2504-16.

Deshaies, R. J., and C. A. Joazeiro. 2009. 'RING domain E3 ubiquitin ligases', *Annu Rev Biochem*, 78: 399-434.

Dikic, I. 2017. 'Proteasomal and Autophagic Degradation Systems', *Annu Rev Biochem*, 86: 193-224.

Dove, K. K., and R. E. Klevit. 2017. 'RING-Between-RING E3 Ligases: Emerging Themes amid the Variations', *J Mol Biol*, 429: 3363-75.

Dove, K. K., J. L. Olszewski, L. Martino, D. M. Duda, X. S. Wu, D. J. Miller, K. H. Reiter, K. Rittinger, B. A. Schulman, and R. E. Klevit. 2017. 'Structural Studies of HHARI/UbcH7 approximately Ub Reveal Unique E2 approximately Ub Conformational Restriction by RBR RING1', *Structure*, 25: 890-900 e5.

Duncan, L. M., S. Piper, R. B. Dodd, M. K. Saville, C. M. Sanderson, J. P. Luzio, and P. J. Lehner. 2006. 'Lysine-63-linked ubiquitination is required for endolysosomal degradation of class I molecules', *EMBO J*, 25: 1635-45.

Echeverri, C.J., P.A. Beachy, B. Baum, M. Boutros, F. Bucholz, S.K. Chanda, Downwardm J., J. Ellenberg, A.G. Fraser, N. Hacohen, W.C. Han, A.L.

Jackson, A. Koger, P. S. Linsley, L. Lum, Y. Ma, B. Mathey-Prévot, D.E. Root, D. M. Sabatini, J. Taipale, N. Perrimin, and R. Bernards. 2006. 'Minimizing the risk of reporting false positives in large-scale RNAi screens', *Nat Methods*, 3: 777-79.

Eddins, M. J., C. M. Carlile, K. M. Gomez, C. M. Pickart, and C. Wolberger. 2006. 'Mms2-Ubc13 covalently bound to ubiquitin reveals the structural basis of linkage-specific polyubiquitin chain formation', *Nat Struct Mol Biol*, 13: 915-20.

Eden, E. R. 2016. 'The formation and function of ER-endosome membrane contact sites', *Biochim Biophys Acta*, 1861: 874-79.

Elton, L., I. Carpentier, K. Verhelst, J. Staal, and R. Bayaert. 2015. 'The multifaceted role of the E3 ubiquitin ligase HOIL-1: beyond linear ubiquitination', *Immunological Reviews*, 266: 208-21.

Emmerich, C. H., A. Ordureau, S. Strickson, J. S. Arthur, P. G. Pedrioli, D. Komander, and P. Cohen. 2013. 'Activation of the canonical IKK complex by K63/M1-linked hybrid ubiquitin chains', *Proc Natl Acad Sci U S A*, 110: 15247-52.

Ernst, R., B. Mueller, H. L. Ploegh, and C. Schlieker. 2009. 'The otubain YOD1 is a deubiquitinating enzyme that associates with p97 to facilitate protein dislocation from the ER', *Mol Cell*, 36: 28-38.

Escobar-Henriques, M., and V. Anton. 2020. 'Mitochondrial Surveillance by Cdc48/p97: MAD vs. Membrane Fusion', *Int J Mol Sci*, 21.

Evers, B., K. Jastrzebski, J. P. Heijmans, W. Grernrum, R. L. Beijersbergen, and R. Bernards. 2016. 'CRISPR knockout screening outperforms shRNA and CRISPRi in identifying essential genes', *Nat Biotechnol*, 34: 631-3.

Fiesel, F. C., E. L. Moussaud-Lamodiere, M. Ando, and W. Springer. 2014. 'A specific subset of E2 ubiquitin-conjugating enzymes regulate Parkin activation and mitophagy differently', *J Cell Sci*, 127: 3488-504.

Finley, D. 2009. 'Recognition and processing of ubiquitin-protein conjugates by the proteasome', *Annu Rev Biochem*, 78: 477-513.

Fujita, N., E. Morita, T. Itoh, A. Tanaka, M. Nakaoka, Y. Osada, T. Umemoto, T. Saitoh, H. Nakatogawa, S. Kobayashi, T. Haraguchi, J. L. Guan, K. Iwai, F. Tokunaga, K. Saito, K. Ishibashi, S. Akira, M. Fukuda, T. Noda, and T. Yoshimori. 2013. 'Recruitment of the autophagic machinery to endosomes during infection is mediated by ubiquitin', *J Cell Biol*, 203: 115-28.

Goktug, AN, SC Chai, and T Chen. 2013. 'Data Analysis Approaches in High Throughput Screening.' in, *Drug Discovery*.

Grice, G. L., I. T. Lobb, M. P. Weekes, S. P. Gygi, R. Antrobus, and J. A. Nathan. 2015. 'The Proteasome Distinguishes between Heterotypic and Homotypic Lysine-11-Linked Polyubiquitin Chains', *Cell Rep*, 12: 545-53.

Haakonsen, D. L., and M. Rape. 2019. 'Branching Out: Improved Signaling by Heterotypic Ubiquitin Chains', *Trends Cell Biol*, 29: 704-16.

Hannon, G.J. 2002. 'RNA interference', *Nature*, 418: 244-51.

Harper, J. W., and E. J. Bennett. 2016. 'Proteome complexity and the forces that drive proteome imbalance', *Nature*, 537: 328-38.

Herhaus, L., and I. Dikic. 2015. 'Expanding the ubiquitin code through post-translational modification', *EMBO Rep*, 16: 1071-83.

Hira, A., K. Yoshida, K. Sato, Y. Okuno, Y. Shiraishi, K. Chiba, H. Tanaka, S. Miyano, A. Shimamoto, H. Tahara, E. Ito, S. Kojima, H. Kurumizaka, S. Ogawa, M. Takata, H. Yabe, and M. Yabe. 2015. 'Mutations in the gene encoding the E2-conjugating enzyme UBE2T cause Fanconi anemia', *Am J Hum Genet*, 96: 1001-7.

Hormaechea-Agulla, D., Y. Kim, M. S. Song, and S. J. Song. 2018. 'New Insights into the Role of E2s in the Pathogenesis of Diseases: Lessons Learned from UBE2O', *Mol Cells*, 41: 168-78.

Huang, X., and V. M. Dixit. 2016. 'Drugging the undruggables: exploring the ubiquitin system for drug development', *Cell Res*, 26: 484-98.

Huett, A., R. J. Heath, J. Begun, S. O. Sassi, L. A. Baxt, J. M. Vyas, M. B. Goldberg, and R. J. Xavier. 2012a. 'The LRR and RING domain protein LRSAM1 is an E3 ligase crucial for ubiquitin-dependent autophagy of intracellular Salmonella Typhimurium', *Cell Host Microbe*, 12: 778-90.

Huett, Alan, Robert J Heath, Jakob Begun, Slim O Sassi, Leigh A Baxt, Jatin M Vyas, Marcia B Goldberg, and Ramnik J Xavier. 2012b. 'The LRR and RING Domain Protein LRSAM1 Is an E3 Ligase Crucial for Ubiquitin-Dependent Autophagy of Intracellular Salmonella Typhimurium', *Cell Host & Microbe*, 12: 778-90.

Hung, Y. H., L. M. Chen, J. Y. Yang, and W. Y. Yang. 2013. 'Spatiotemporally controlled induction of autophagy-mediated lysosome turnover', *Nat Commun*, 4: 2111.

Hurley, J. H. 2015. 'ESCRTs are everywhere', *EMBO J*, 34: 2398-407.

Jia, J., Y. P. Abudu, A. Claude-Taupin, Y. Gu, S. Kumar, S. W. Choi, R. Peters, M. H. Mudd, L. Allers, M. Salemi, B. Phinney, T. Johansen, and V. Deretic. 2018. 'Galectins Control mTOR in Response to Endomembrane Damage', *Mol Cell*, 70: 120-35 e8.

Jia, J., B. Bissa, L. Brecht, L. Allers, S. W. Choi, Y. Gu, M. Zbinden, M. R. Burge, G. Timmins, K. Hallows, C. Behrends, and V. Deretic. 2020. 'AMPK, a Regulator of Metabolism and Autophagy, Is Activated by Lysosomal Damage via a Novel Galectin-Directed Ubiquitin Signal Transduction System', *Mol Cell*, 77: 951-69.e9.

Jin, Jianping, Xue Li, Steven P. Gygi, and J. Wade Harper. 2007. 'Dual E1 activation systems for ubiquitin differentially regulate E2 enzyme charging', *Nature*, 447: 1135-38.

Johnson, A. E., H. Shu, A. G. Hauswirth, A. Tong, and G. W. Davis. 2015. 'VCP-dependent muscle degeneration is linked to defects in a dynamic tubular lysosomal network in vivo', *Elife*, 4.

Karanasios, E., E. Stapleton, M. Manifava, T. Kaizuka, N. Mizushima, S. A. Walker, and N. T. Ktistakis. 2013. 'Dynamic association of the ULK1 complex with omegasomes during autophagy induction', *J Cell Sci*, 126: 5224-38.

Karbowski, M., and R. J. Youle. 2011. 'Regulating mitochondrial outer membrane proteins by ubiquitination and proteasomal degradation', *Curr Opin Cell Biol*, 23: 476-82.

Kim, J., Y. C. Kim, C. Fang, R. C. Russell, J. H. Kim, W. Fan, R. Liu, Q. Zhong, and K. L. Guan. 2013. 'Differential regulation of distinct Vps34 complexes by AMPK in nutrient stress and autophagy', *Cell*, 152: 290-303.

Kimura, S. , T. Noda, and T. Yoshimori. 2008. 'Dynein-dependent Movement of Autophagosomes Mediates Efficient Encounters with Lysosomes', *CELL STRUCTURE AND FUNCTION*, 33: 109–22.

Kirkegaard, T., A. G. Roth, N. H. Petersen, A. K. Mahalka, O. D. Olsen, I. Moilanen, A. Zylicz, J. Knudsen, K. Sandhoff, C. Arenz, P. K. Kinnunen, J. Nylandsted, and M. Jaattela. 2010. 'Hsp70 stabilizes lysosomes and reverts Niemann-Pick disease-associated lysosomal pathology', *Nature*, 463: 549-53.

Koerver, L., C. Papadopoulos, B. Liu, B. Kravic, G. Rota, L. Brecht, T. Veenendaal, M. Polajnar, A. Bluemke, M. Ehrmann, J. Klumperman, M. Jäättelä, C. Behrends, and H. Meyer. 2019. 'The ubiquitin-conjugating enzyme UBE2QL1 coordinates lysophagy in response to endolysosomal damage', *EMBO reports*.

Komander, D., and M. Rape. 2012. 'The ubiquitin code', *Annu Rev Biochem*, 81: 203-29.

Lake, M. , M. M. Wuebbens, K. V. Rajagopalan, and H. Schindelin. 2001. 'Mechanism of ubiquitin activation revealed by the structure of a bacterial MoeB±MoaD complex', *Nature*, 414: 325-29.

Lenk, U., H. Yu, J. Walter, MS. Gelman, E. Hartmann, RR. Kopito, and T. Sommer. 2002. 'A role for mammalian Ubc6 homologues in ERassociated protein degradation', *Journal of Cell Science*, 115: 3007-14.

Li, Y., B. Chen, W. Zou, X. Wang, Y. Wu, D. Zhao, Y. Sun, Y. Liu, L. Chen, L. Miao, C. Yang, and X. Wang. 2016. 'The lysosomal membrane protein SCAV-3 maintains lysosome integrity and adult longevity', *J Cell Biol*, 215: 167-85.

Lystad, and Simonsen. 2019. 'Mechanisms and Pathophysiological Roles of the ATG8 Conjugation Machinery', *Cells*, 8.

Machida, Y. J., Y. Machida, Y. Chen, A. M. Gurtan, G. M. Kupfer, A. D. D'Andrea, and A. Dutta. 2006. 'UBE2T is the E2 in the Fanconi anemia pathway and undergoes negative autoregulation', *Mol Cell*, 23: 589-96.

Maejima, I., A. Takahashi, H. Omori, T. Kimura, Y. Takabatake, T. Saitoh, A. Yamamoto, M. Hamasaki, T. Noda, Y. Isaka, and T. Yoshimori. 2013. 'Autophagy sequesters damaged lysosomes to control lysosomal biogenesis and kidney injury', *EMBO J*, 32: 2336-47.

Mercer, T. J., A. Gubas, and S. A. Tooze. 2018. 'A molecular perspective of mammalian autophagosome biogenesis', *J Biol Chem*, 293: 5386-95.

Metzger, M. B., J. N. Pruneda, R. E. Klevit, and A. M. Weissman. 2014. 'RING-type E3 ligases: master manipulators of E2 ubiquitin-conjugating enzymes and ubiquitination', *Biochim Biophys Acta*, 1843: 47-60.

Meyer, H., and C. C. Weihl. 2014. 'The VCP/p97 system at a glance: connecting cellular function to disease pathogenesis', *J Cell Sci*, 127: 3877-83.

Mizushima, Noboru, and Masaaki Komatsu. 2011. 'Autophagy: Renovation of Cells and Tissues', *Cell*, 147: 728-41.

Mukhopadhyay, D., and H. Riezman. 2007. 'Proteasome-Independent Functions of Ubiquitin in Endocytosis and Signaling', *Science*, 315: 201-05.

Murakawa, T., A. A. Kiger, Y. Sakamaki, M. Fukuda, and N. Fujita. 2020. 'An autophagy-dependent tubular lysosomal network synchronizes degradative activity required for muscle remodeling', *J Cell Sci*, 133.

Nakamura, S., and T. Yoshimori. 2017. 'New insights into autophagosome-lysosome fusion', *J Cell Sci*, 130: 1209-16.

Napolitano, G., and A. Ballabio. 2016. 'TFEB at a glance', *J Cell Sci*, 129: 2475-81.

Pankiv, S., T. H. Clausen, T. Lamark, A. Brech, J. A. Bruun, H. Outzen, A. Overvatn, G. Bjorkoy, and T. Johansen. 2007. 'p62/SQSTM1 binds directly to Atg8/LC3 to facilitate degradation of ubiquitinated protein aggregates by autophagy', *J Biol Chem*, 282: 24131-45.

Papadopoulos, C., P. Kirchner, M. Bug, D. Grum, L. Koerver, N. Schulze, R. Poehler, A. Dressler, S. Fengler, K. Arhzaouy, V. Lux, M. Ehrmann, C. C. Weihl, and H. Meyer. 2017. 'VCP/p97 cooperates with YOD1, UBXD1 and PLAA to drive clearance of ruptured lysosomes by autophagy', *EMBO J*, 36: 135-50.

Papadopoulos, C., and H. Meyer. 2017. 'Detection and Clearance of Damaged Lysosomes by the Endo-Lysosomal Damage Response and Lysophagy', *Curr Biol*, 27: R1330-R41.

Papadopoulos, Chrisovalantis, Bojana Kravic, and Hemmo Meyer. 2019. 'Repair or Lysophagy: Dealing with Damaged Lysosomes', *Journal of Molecular Biology*.

Perera, R. M., and R. Zoncu. 2016. 'The Lysosome as a Regulatory Hub', *Annu Rev Cell Dev Biol*, 32: 223-53.

Pickart, C. M., and M. J. Eddins. 2004. 'Ubiquitin: structures, functions, mechanisms', *Biochim Biophys Acta*, 1695: 55-72.

Pruneda, J. N., P. J. Littlefield, S. E. Soss, K. A. Nordquist, W. J. Chazin, P. S. Brzovic, and R. E. Klevit. 2012. 'Structure of an E3:E2~Ub complex reveals an allosteric mechanism shared among RING/U-box ligases', *Mol Cell*, 47: 933-42.

Radulovic, M., K. O. Schink, E. M. Wenzel, V. Nahse, A. Bongiovanni, F. Lafont, and H. Stenmark. 2018. 'ESCRT-mediated lysosome repair precedes lysophagy and promotes cell survival', *EMBO J*, 37.

Rape, M. 2018. 'Ubiquitylation at the crossroads of development and disease', *Nat Rev Mol Cell Biol*, 19: 59-70.

Repnik, U., M. Borg Distefano, M. T. Speth, M. Y. W. Ng, C. Progida, B. Hoflack, J. Gruenberg, and G. Griffiths. 2017. 'L-leucyl-L-leucine methyl ester does not release cysteine cathepsins to the cytosol but inactivates them in transiently permeabilized lysosomes', *J Cell Sci*, 130: 3124-40.

Roczniak-Ferguson, A., C. S. Petit, F. Froehlich, S. Qian, J. Ky, B. Angarola, T. C. Walther, and S. M. Ferguson. 2012. 'The transcription factor TFEB links mTORC1 signaling to transcriptional control of lysosome homeostasis', *Sci Signal*, 5: ra42.

Rogov, V., V. Dotsch, T. Johansen, and V. Kirkin. 2014. 'Interactions between autophagy receptors and ubiquitin-like proteins form the molecular basis for selective autophagy', *Mol Cell*, 53: 167-78.

Rubinsztein, David C, Tomer Shpilka, and Zvulun Elazar. 2012. 'Mechanisms of Autophagosome Biogenesis', *Current Biology*, 22: R29-R34.

Sadowski, M., A. Mawson, R. Baker, and B. Sarcevic. 2007. 'Cdc34 C-terminal tail phosphorylation regulates Skp1/cullin/F-box (SCF)-mediated ubiquitination and cell cycle progression', *Biochem J*, 405: 569-81.

Scheffner, M., U. Nuber, and J. M. Huibregtse. 1995. 'Protein ubiquitination involving an E1-E2-E3 enzyme ubiquitin thioester cascade', *Nature*, 373: 81-83.

Schindelin, J., I. Arganda-Carreras, E. Frise, V. Kaynig, M. Longair, T. Pietzsch, S. Preibisch, C. Rueden, S. Saalfeld, B. Schmid, J. Y. Tinevez, D. J. White, V. Hartenstein, K. Eliceiri, P. Tomancak, and A. Cardona. 2012. 'Fiji: an open-source platform for biological-image analysis', *Nat Methods*, 9: 676-82.

Schneider, Jaime L., and Ana Maria Cuervo. 2014. 'Autophagy and human disease: emerging themes', *Current Opinion in Genetics & Development*, 26: 16-23.

Schulman, B. A., and J. W. Harper. 2009. 'Ubiquitin-like protein activation by E1 enzymes: the apex for downstream signalling pathways', *Nat Rev Mol Cell Biol*, 10: 319-31.

Schulze, Ekkehard, Maria E. Altmann, Ibrahim M. Adham, Bettina Schulze, Stephan Fröde, and Wolfgang Engel. 2003. 'The maintenance of neuromuscular function requires UBC-25 in Caenorhabditis elegans', *Biochemical and Biophysical Research Communications*, 305: 691-99.

Schwintzer, L., E. Aguado Roca, and M. Broemer. 2019. 'TRIAD3/RNF216 E3 ligase specifically synthesises K63-linked ubiquitin chains and is inactivated by mutations associated with Gordon Holmes syndrome', *Cell Death Discov*, 5: 75.

Seghatoleslam, A., A. Monabati, F. Bozorg-Ghalati, M. Nikseresht, MR. Bordbar, M. Rahvar, and AA. Owji. 2006. 'Expression of UBE2Q2, a Putative Member of the Ubiquitinconjugating Enzyme Family in Pediatric Acute Lymphoblastic Leukemia', *Archives of Iranian Medicine*, 15: 352-55.

Seibenhener, M. L., J. R. Babu, T. Geetha, H. C. Wong, N. R. Krishna, and M. W. Wooten. 2004. 'Sequestosome 1/p62 is a polyubiquitin chain binding protein involved in ubiquitin proteasome degradation', *Mol Cell Biol*, 24: 8055-68.

Settembre, C., A. Fraldi, D. L. Medina, and A. Ballabio. 2013. 'Signals from the lysosome: a control centre for cellular clearance and energy metabolism', *Nat Rev Mol Cell Biol*, 14: 283-96.

Settembre, C., R. Zoncu, D. L. Medina, F. Vetrini, S. Erdin, S. Erdin, T. Huynh, M. Ferron, G. Karsenty, M. C. Vellard, V. Facchinetti, D. M. Sabatini, and A. Ballabio. 2012. 'A lysosome-to-nucleus signalling mechanism senses and regulates the lysosome via mTOR and TFEB', *EMBO J*, 31: 1095-108.

Shafiee, SM., A. Seghatoleslam, M. Nikseresht, M. Alizadeh-Hosseini, A. Safaei, and AA. Owji. 2014. 'Expression Status of UBE2Q2 in Colorectal Primary Tumors and Cell Lines', *IJMS*, 39: 196-202.

Shaid, S., C. H. Brandts, H. Serve, and I. Dikic. 2013. 'Ubiquitination and selective autophagy', *Cell Death Differ*, 20: 21-30.

Sharma, Vartika, Surbhi Verma, Elena Seranova, Sovan Sarkar, and Dhiraj Kumar. 2018. 'Selective Autophagy and Xenophagy in Infection and Disease', *Frontiers in Cell and Developmental Biology*, 6.

Shiba-Fukushima, K., Y. Imai, S. Yoshida, Y. Ishihama, T. Kanao, S. Sato, and N. Hattori. 2012. 'PINK1-mediated phosphorylation of the Parkin ubiquitin-like domain primes mitochondrial translocation of Parkin and regulates mitophagy', *Sci Rep*, 2: 1002.

Skowyra, M. L., P. H. Schlesinger, T. V. Naismith, and P. I. Hanson. 2018. 'Triggered recruitment of ESCRT machinery promotes endolysosomal repair', *Science*, 360.

Sluimer, J., and B. Distel. 2018. 'Regulating the human HECT E3 ligases', *Cell Mol Life Sci*, 75: 3121-41.

Smit, J. J., D. Monteferrario, S. M. Noordermeer, W. J. van Dijk, B. A. van der Reijden, and T. K. Sixma. 2012. 'The E3 ligase HOIP specifies linear ubiquitin chain assembly through its RING-IBR-RING domain and the unique LDD extension', *EMBO J*, 31: 3833-44.

Stewart, M. D., T. Ritterhoff, R. E. Klevit, and P. S. Brzovic. 2016. 'E2 enzymes: more than just middle men', *Cell Res*, 26: 423-40.

Swatek, K. N., J. L. Usher, A. F. Kueck, C. Gladkova, T. E. T. Mevissen, J. N. Pruneda, T. Skern, and D. Komander. 2019. 'Insights into ubiquitin chain architecture using Ub-clipping', *Nature*, 572: 533-37.

Taylor, J. P. 2015. 'Multisystem proteinopathy: intersecting genetics in muscle, bone, and brain degeneration', *Neurology*, 85: 658-60.

Thiele, DW., and PE Lipsky. 1990. 'Mechanism of L-leucyl-L-leucine methyl ester-mediated killing of cytotoxic lymphocytes: Dependence on a lysosomal thiol protease, dipeptidyl peptidase I, that is enriched in these cells', *Proc Natl Acad Sci U S A*, 87: 83-87.

Thurston, T. L., M. P. Wandel, N. von Muhlinen, A. Foeglein, and F. Randow. 2012. 'Galectin 8 targets damaged vesicles for autophagy to defend cells against bacterial invasion', *Nature*, 482: 414-8.

Uchimoto, T., H. Nohara, R. Kamehara, M. Iwamura, N. Watanabe, and Y. Kobayashi. 1999. 'Mechanism of apoptosis induced by a lysosomotropic agent, L-Leucyl-L-Leucine methyl ester', *Apoptosis*, 4: 357-62.

Vadlamudi, R.K., I. Jooung, J.L. Strominger, and J. Shin. 1996. 'p62, a Phosphotyrosineindependent Ligand of the SH2 Domain of p56lck, Belongs to a New Class of Ubiquitin-binding Proteins', *The Journal of Biological Chemistry*, 271: 20235-37.

Vainshtein, A., and P. Grumati. 2020. 'Selective Autophagy by Close Encounters of the Ubiquitin Kind', *Cells*, 9.

van den Boom, J., and H. Meyer. 2018. 'VCP/p97-Mediated Unfolding as a Principle in Protein Homeostasis and Signaling', *Mol Cell*, 69: 182-94.

van der Veen, A. G., and H. L. Ploegh. 2012. 'Ubiquitin-like proteins', *Annu Rev Biochem*, 81: 323-57.

van Wijk, S. J., and H. T. Timmers. 2010. 'The family of ubiquitin-conjugating enzymes (E2s): deciding between life and death of proteins', *FASEB J*, 24: 981-93.

Vietri, M., M. Radulovic, and H. Stenmark. 2020. 'The many functions of ESCRTs', *Nat Rev Mol Cell Biol*, 21: 25-42.

Wake, N. C., C. J. Ricketts, M. R. Morris, E. Prigmore, S. M. Gribble, A. B. Skytte, M. Brown, N. Clarke, R. E. Banks, S. Hodgson, A. S. Turnell, E. R. Maher, and E. R. Woodward. 2013. 'UBE2QL1 is disrupted by a constitutional translocation associated with renal tumor predisposition and is a novel candidate renal tumor suppressor gene', *Hum Mutat*, 34: 1650-61.

Walden, H., and K. Rittinger. 2018. 'RBR ligase-mediated ubiquitin transfer: a tale with many twists and turns', *Nat Struct Mol Biol*, 25: 440-45.

Weber, J., S. Polo, and E. Maspero. 2019. 'HECT E3 Ligases: A Tale With Multiple Facets', *Front Physiol*, 10: 370.

Weidberg, H., E. Shvets, and Z. Elazar. 2011. 'Biogenesis and cargo selectivity of autophagosomes', *Annu Rev Biochem*, 80: 125-56.

Xu, P., D. M. Duong, N. T. Seyfried, D. Cheng, Y. Xie, J. Robert, J. Rush, M. Hochstrasser, D. Finley, and J. Peng. 2009. 'Quantitative proteomics reveals the function of unconventional ubiquitin chains in proteasomal degradation', *Cell*, 137: 133-45.

Yau, R., and M. Rape. 2016. 'The increasing complexity of the ubiquitin code', *Nat Cell Biol*, 18: 579-86.

Ye, Y., and M. Rape. 2009. 'Building ubiquitin chains: E2 enzymes at work', *Nat Rev Mol Cell Biol*, 10: 755-64.

Ye, Y., W. K. Tang, T. Zhang, and D. Xia. 2017. 'A Mighty "Protein Extractor" of the Cell: Structure and Function of the p97/CDC48 ATPase', *Front Mol Biosci*, 4: 39.

Yim, W. W., and N. Mizushima. 2020. 'Lysosome biology in autophagy', *Cell Discov*, 6: 6.

Yoshida, Y., S. Yasuda, T. Fujita, M. Hamasaki, A. Murakami, J. Kawawaki, K. Iwai, Y. Saeki, T. Yoshimori, N. Matsuda, and K. Tanaka. 2017. 'Ubiquitination of exposed glycoproteins by SCF(FBXO27) directs damaged lysosomes for autophagy', *Proc Natl Acad Sci U S A*, 114: 8574-79.

Yoshii, S. R., and N. Mizushima. 2017. 'Monitoring and Measuring Autophagy', *Int J Mol Sci*, 18.

Yuan, L., Z. Lv, J. H. Atkison, and S. K. Olsen. 2017. 'Structural insights into the mechanism and E2 specificity of the RBR E3 ubiquitin ligase HHARI', *Nat Commun*, 8: 211.

Zhitomirsky, B., A. Yunaev, R. Kreiserman, A. Kaplan, M. Stark, and Y. G. Assaraf. 2018. 'Lysosomotropic drugs activate TFEB via lysosomal membrane fluidization and consequent inhibition of mTORC1 activity', *Cell Death Dis*, 9: 1191.

Abbreviations

AAA	ATPases Associated with diverse cellular Activities
ADP	Adenosine Diphosphate
ALIX	ALG-2 Interacting Protein
ALS	Amyotrophic Lateral Sclerosis
AMP	Adenosine Monophosphate
AMPK	AMP activated Kinase
AOBS	Acousto Optical Beam Splitter
APC/C	Anaphase Promoting Complex/Cyclosome
APEX2	Ascorbate Peroxidase 2
ApoE4	Apolipoprotein E4
Arl8b	ADP Ribosylation Facto Like GTPase 8b
ASM	Acid Sphingomyelinase
ATG	autophagy-related genes
ATPase	Adenosine Triphosphatases
BCA	Bicinchoninic Acid Assay
BECN1	Beclin 1
BME	β-Mercaptoethanol
BRCA1	Breast Cancer Gene 1
CALCOCO2	Calcium-Binding And Coiled-Coil Domain-Containing Protein 2
Cas	CRISPR Associated Protein
CCCP	Carbonyl cyanide 3-chlorophenylhydrazone
CCNE1	CyclinE1
cDNA	coding DNA
CDS	Coding Sequence
CK2	Casein Kinase II
CLEAR	Coordinated Lysosomal Expression And Regulation
CLINT1	Clathrin Interactor 1
CRISPR	Clustered Regularly Interspaced Short Palindromic Repeats
CRL	Cullin RING ligase
CUL	Cullin
DMEM	Dulbecco’s modified Eagle’s medium
DNA	Deoxyribonucleic Acid
dNTP	deoxyribonucleotide triphosphate
DRIL	Double RING Finger Linked
Drp1	Dynamin-Related Protein 1
DUB	Deubiquitinating Enzymes
EDLR	endolysosomal damage response
EDTA	Ethylenediaminetetraacteic Acid
ERAD	Endoplasmatic Reticulum-Associated Degradation
ESCRT	Endosomal Sorting Complexes Required for Transport
EtOH	Ethanol
FAK	Focal Adhesion Kinase
FBS	Fetal Bovine Serum
FBX	F-Box protein

FIP200	FAK family-Interacting Protein of 200 kDa
FTD	Frontotemporal Dementia
Fwd	forward
G418	Genetecin
GABARAB	γ-aminobutyric Acid Receptor Associated Proteins
Gal	Galectin
GFP	Green Fluorescent Protein
GPN	Glycyl-L-Phenylalanine 2-Naphthylamide
GTP	Guanosine Triphosphate
HA	Human Influenza Hemagglutinin
HAT	Histone Acetyltransferases
HDAC	Histone Deacetylases
HECT	homologous to E6AP C-terminus
HERC	HECT and RLD Domain Containing E3 Ubiquitin Protein Ligase
HGS	Hepatocte Growth factor-regulated tyrosine kinase Substrate
HHARI	Human Homolog of Ariadne
HOIL	Heme-Oxidized IRP2 Ubiquitin Ligase
HOPS	Homotypic fusion and Protein Sorting
HRP	Horseraddish Peroxidase
Hsc70	Heat Shock Cognate 70 kDa
Hsp70	Heat Shock Protein 70
HyD	Hybrid Detectors
IBM	Inclusion Body Myopathy
IBMPFB/ALS	IBM PDB FTD/ALS
IBR	In-between-RING
IL-1	Interleukin
ILV	Intraluminal Vesicles
IRP2	Iron-Responsive Element-Binding Protein
JAMM	Jab1/Mov34/MPN+
LAMP	Lysosome-Associated Membrane Protein
LB	Lysogeny broth
LC3	Light Chain 3
LIMP2	Lysosomal Integral Membrane Protein 2
LIR	LC3-Interacting Region
LLOMe	L-leucyl-L-leucine methyl ester
LMP	Lysosomal membrane permeabilization
LRSAM1	Leucine Rich Repeat And Sterile Alpha Motif Containing 1
LUBAC	Linear Ubiquitin Chain Assembly Complex
MAD	Mitochondria-Associated Degradation
MEM	Minimal Essential Medium
Mfn	Mitofusin
MHC I HCs	Major Histocompatibility Complex Class I Heavy Chains
MOM	Mitochondrial Outer Membrane
MOMP	Mitochondrial Outer Membrane Permeabilization
MPN+	Mpr1 Pad1 N-terminal+
mRNA	messenger RNA
MS	Mass spectrometry
MSP1	Multisystem Proteinopathy 1

mTORC1	Mechanistic Target of Rapamycin Complex 1
MULAN	Mitochondrial Ubiquitin Ligase Activator of NF-κB
MVB	Multivesicular Bodies
NBR1	Neighbor of BRCA1 gene 1
NDP2	Nuclear Dot Protein 2
NEDD	Neural-precursor-cell-expressed developmentally down- regulated
NF-κB	Nuclear Factor 'kappa-light-chain-enhancer' of Activated B-Cells
NPC1	Niemann-Pick C1
NPC1L	NPC1-Like protein
Npl4	Nuclear Protein Localization 4
OPA1	Optic Atrophy 1
OPTN	Optineurin
OTU	Ovarian Tumor
P.C.C.	Pearson's Correlation Coefficient
P13P	Phosphatidylinositol 3-Phosphate
PB1	Phox and Bem1
PBS	Phosphate Buffered Saline
PCR	Polymerase Chain Reaction
PDB	Paget's Disease of the Bone
PE	Phosphatidylethanolamine
Pen/Strep	Penicillin/Streptomycin
PFA	Paraformaldehyde
PI3K	Phosphoinosite 3-Kinase
PINK1	PTEN-Induced Kinase 1
PIPES	Piperazine-N,N′-bis(2-Ethanesulfonic Acid)
PLAA	Phospholipase A-2-Activating Protein
PLEKHM1	Pleckstrin Homology And RUN Domain Containing M1
pS6	Phosphorylated S6
Rab7	Ras-related protein 7
RBR	RING-between-RING
RCC	Regulator of Chromatin Condensation
RCC	Renal Cell Carcinoma
Rev	Reverse
RING	Really Interesting New Gene
RIPA	Radioimmunoprecipitation assay
RLD	RCC like domain
RNA	Ribonucleic acid
RNAi	RNA Interference
RNF	RING-finger protein
RQC	Ribosome-Associated Quality Control
RSP5	Reverses SPT-phenotype Protein 5
SCAV3	Scavenger receptor (SD36 family) related
SCF	SKP1/CUL/F-box ligase
SDS-PAGE	Sodium Dodecyl Sulfate Polyacrylamide Gel Electrophoresis
SEL1L	Suppressor/Enhancer of LIN-12-Like
siRNA	Small Interfering RNA
SKP1	S-Phase Kinase-associated Protein 1

SNARE	with N-ethylmaleimide Sensitive factor Attachment protein Receptors
SPT	Suppressor of Ty
SQSTM1	Sequestome-1
STAM	Signal Transducing Adapter Molecule
Strep	Streptavidin
SUMO	Small-Ubiquitin-related Modifier
TAK1	Transforming growth factor beta-Activated Kinase 1
TANK	TRAF family member-associated NF-kappa-B activator
TAX1BP1	Tax1 binding protein 1
TBK	TANK Binding Kinase 1
TBS-T	Tris-Buffered Saline with Tween-20
TFEB	Transcription Factor EB
TNF	Tumor Necrosis Factors
TRAF	TNF Receptor Associated Factor
TRIAD	Two RING Fingers And DRIL
TRIM16	Tripartite Motif Family 16
UBA	Ubiquitin-like modifier-Activating enzyme
UBC	Ubiquitin-Conjugating Domain
UBC	Ubiquitin-Conjugating Enzyme
UBE	Ubiquitin-Conjugating Enzyme
UBLs	Ubiquitin-like proteins
UBXD	Ubiquitin Regulatory X Domain containing protein
UFD	Ubiquitin Fold Domain
Ufd1	Fusion Degradation 1
ULK1	Unc-51 Like Kinase
Unc-51	Uncoordinated
UPS	ubiquitin proteasome system
UTR	Untranslated Region
v-ATPase	vacuolar ATPase
VCP	Valosin Containing Protein
VPS34	Vacuolar Protein Sorting 34
WIPI	WD-repeat Domain phosphoinositide-Interacting Proteins

Acknowledgements

I am especially thankful to Hemmo Meyer for giving me the opportunity to work on this project and for supervising it with great knowledge, valuable advices, passion and patience. Thank you for helping me expanding my scientific horizon by suggesting me for the IMRPS-LM graduate school and sending me to international conferences.

Actually, all VCPs somehow contributed to this project. Firstly, thanks to Chris Papadopoulos for supervising the project in the lab. It was hard, instructive and fun to work with you.
I would also like to thank Sven Fengler, Monika Bug and especially Bojana Kravic for their postdoctoral support and advices and collaboration. Special thanks go to Johannes van den Boom who was always there to talk and explain and for critical reading of my thesis.
It was also a pleasure to work with Giulia Rota in the last years, thank you for helping me with the experiments! Also, we had a good time discussing, laughing, eating with Bojana in the “girl’s office”.
Without the organizational and technical support of especially Sabine Effenberger and also Cristina Hartmann-Fatu, Christina Kamp-Melzer and Miriam Schmidt I would have been lost, thank you!
Thanks to all current and former lab members who made life in the lab, the breaks and in the pub easy and enjoyable.
This thesis would look different without Nina Schulze, who always supported me with imaging and especially image analysis.

I would also like to thank all our internal and external collaboration partners. Especially Christian Behrends and his co-workers contributed a lot to the project. Thank you Mira Polajnar for helping me to start project in the first place by guiding and analyzing the screen.

Finally, I would like to thank my family and friends for always being there for me, during fun and hard times of this project. Thanks to my parents for your unconditional support. Thank you Kevin for always supporting me and tolerating all my moods.

Affidavits / Erklärungen

Erklärung:

Hiermit erkläre ich, gem. § 6 Abs. (2) g) der Promotionsordnung der Fakultät für Biologie zur Erlangung der Dr. rer. nat., dass ich das Arbeitsgebiet, dem das Thema „Identification and functional characterization of the E2-conjugating enzyme UBE2QL1 in endolysosomal damage response“ zuzuordnen ist, in Forschung und Lehre vertrete und den Antrag von Lisa Körver befürworte und die Betreuung auch im Falle eines Weggangs, wenn nicht wichtige Gründe dem entgegenstehen, weiterführen werde.

Essen, den _____ _____

Unterschrift des Betreuers (Prof. oder PD) an der Universität Duisburg-Essen

Erklärung:

Hiermit erkläre ich, gem. § 7 Abs. (2) d) + f) der Promotionsordnung der Fakultät für Biologie zur Erlangung des Dr. rer. nat., dass ich die vorliegende Dissertation selbständig verfasst und mich keiner anderen als der angegebenen Hilfsmittel bedient, bei der Abfassung der Dissertation nur die angegeben Hilfsmittel benutzt und alle wörtlich oder inhaltlich übernommenen Stellen als solche gekennzeichnet habe.

Essen, den _____ _____

Unterschrift des/r Doktoranden/in

Erklärung:

Hiermit erkläre ich, gem. § 7 Abs. (2) e) + g) der Promotionsordnung der Fakultät für Biologie zur Erlangung des Dr. rer. nat., dass ich keine anderen Promotionen bzw. Promotionsversuche in der Vergangenheit durchgeführt habe und dass diese Arbeit von keiner anderen Fakultät/Fachbereich abgelehnt worden ist.

Essen, den _____ _____

Unterschrift des/r Doktoranden/in